Negative hydrogen ions production in the tandem-type microwave plasma source

Michael J. Mozjetchkov

Department of Fusion Science

School of Mathematical and Physical Science

The Graduate University for Advanced Studies

1998

Keywords:

Microwave Plasma Source, Ion Source, Negative Hydrogen Ions, Negative Hydrogen Ion Beam, Neutral Beam Injection, NBI

Abstract

Neutral Beam Injection (NBI) systems have been considered the most reliable method for plasma heating and are prospected so in the future fusion devices. However, for the beam particle energies over 100 keV, the neutralization efficiency of the positive deuterium ion beam drops below 50% and gradually decrease to zero when ion beam energy approaches 1000 keV. At the same time the neutralization efficiency for the negative hydrogen ion beam drops to 60% at 100keV and then does not change with increase of the ion beam energy. Obviously, the only way to create high-energy neutral hydrogen beams for plasma heating in the future fusion machines is the neutralization of the negative deuterium ion beam.

Compared to positive hydrogen ion sources, negative hydrogen ions production is much more complicated. The efficiency of the negative ion production determines the efficiency of the whole NBI system. That is why the development of the negative hydrogen ion sources is so important.

At present hot cathode arc discharge plasma sources are used as a negative ion source for the negative ion beam-based NBI systems. Those plasma sources being very efficient and easy in construction still have some

problems including filament sputtering which leads to plasma contamination and short lifetime of filaments. Because of the short lifetime, frequent maintenance of the negative ion sources is necessary and it is practically impossible in the radioactive environment of the future fusion reactors.

In this thesis I propose a new concept of the Tandem Microwave Plasma Source for negative ion production, which should eliminate those problems. I separate plasma production chamber with high magnetic field and hot non-uniform plasma from the confinement chamber where negative ion production occurs. A special reversed-field coil is eliminating residual magnetic field of the production chamber in the negative ion production region of the confinement chamber.

In the production chamber high-electron-temperature plasma is ideal for the excitation of the rotational-vibrational levels of the hydrogen molecules. Those excited molecules diffuse into the confinement region. Confinement region has a low electron temperature and the process of the dissociative attachment results in the negative hydrogen ion production.

To investigate the possibility of using this new approach to the negative hydrogen ion production, I have constructed and tested a plasma source of the tandem type. Plasma source consists of two chambers: plasma

production chamber (cylindrical shape, 20 cm long and 6 cm in diameter) and confinement chamber (rectangular, 26x26 cm square crossection and 30 cm in depth). Production chamber is placed into the axial magnetic field of about 1800G and the microwaves (2.45GHz, 5kW) are introduced through the quartz window along the magnetic field lines. Confinement chamber is surrounded by the magnetic cusp field, which is providing field-free uniform plasma area of 20x20 cm near the extraction region.

Non-uniform high-temperature plasma is generated in the production chamber and expands into the confinement chamber where it gets uniform and electron temperature decreases through the diffusion process. Plasma flux is controlled by conditioning coil around the confinement chamber, which also eliminates magnetic field from the plasma production region in the area of negative ion production.

For the input microwave power of 5 kW uniform plasma was generated with the plasma density of $3x10^{12}cm^{-3}$ for argon and $3x10^{11}cm^{-3}$ for hydrogen in a wide rectangular area of 20x20 cm. Plasma parameters uniformity is within 3%. Electron temperature in the plasma grid region is reduced to 1 eV and with the help of the conditioning coil may be controlled in the range of 1-4 eV.

To confirm the negative ion production the negative ion beam was extracted at voltage of 5kV through a single-hole (diameter 1 cm) extraction system. To measure the negative hydrogen beam, 9-channel Faraday Cup array unit was designed and manufactured. Source adjustment with continuous monitoring of negative ion beam current was carried out. Pressure of 4 mTorr and B=0 at the extraction region were found optimal for the negative hydrogen ions production. Dependence of the H^- production on the magnetic field strength at the extraction grid area shows that the obtained H^- current is proportional to the plasma density when the electron temperature is constant and when the electron temperature becomes high, the H^- current decreases.

We extracted 1.0 mA negative hydrogen ion beam current from a single hole 1 cm in diameter and that corresponds to 1.3 mA/cm^2 of the negative hydrogen ion current density at the plasma grid area. Considering that we have a wide uniform plasma area of 20x20-cm and input power of 5kW, total power efficiency of this ion source is higher and the operation pressure is lower than that of the conventional arc discharge and RF ion sources. The new source may be considered as an alternative for the NBI system.

Table of Contents

1. Introduction

1.1 Neutral Beam Injection

Neutral Beam Injection (NBI) systems have been considered the most reliable method for plasma heating and are prospected so in the future fusion devices. NBI line consists of the ion source, beam extraction system, beam acceleration system and gas/plasma neutralizer. In the neutralizer the high-energy ion beam is converted to a neutral beam which can penetrate the strong magnetic field of the fusion device and heat the plasma. Future fusion devices will have plasma with a size of 3 meters in minor radius and plasma density of over 1020m-3. To heat the core of such plasma, high-energy beam is necessary to penetrate to the center.

Unfortunately at the energy over 100 keV neutralization efficiency for the positive deuterium ions drops dramatically (it goes below 50% at 100 keV and gradually decreases to zero at 1000 keV)[1]. On the contrary, neutralization efficiency for negative deuterium ions also drops, but stays at the reasonable value of 60% even after beam energy increases above 100 keV level. At this conditions NBI based on the negative ions is the only practical solution for the generation of high-energy neutral beams.

The first negative-ion-based injector was introduced at JT-60U. The specification of the system is 500keV 10MW deuterium injection. The negative-ion-based NBI is also used for LHD. The Large Helical Device (LHD)[2] is the world's biggest superconducting heliotron/torsatron device. The LHD is the main project of National Institute for Fusion Science. It requires 180keV, 15 MW, 10-sec negative-ion-biased neutral beam injection system. Positive-ion-based NBI systems can not provide this amount of energy[3]. That is why the negative-ion-based NBI system is designed for LHD[4]. As we see, the JT-60U approach and LHD approach are different. At JT-60U beam energy is mainly provided by high acceleration voltage, while at LHD it is provided by high beam current. To obtain the mentioned parameters, neutral beam current at LHD should be 4 times as big as that of JT-60U. That's why the development of high-current negative ion sources is of great importance for NBI group at LHD.

1.2 Negative ion source

Present negative ion sources for the NBI line are based on the arc discharge using hot filaments. Extensive studies of the large multicusp plasma source operating with cesium seeding are held at NIFS NBI group[5,6,7]. Several sources are operated to test different aspects of H^- production[8,9].

Those ion sources prove to be very efficient, but face several problems including the filaments burn out through the sputtering process and as a result of sputtering, plasma is contaminated with the material of filaments. Burning out of the filaments also leads to the maintenance problem. It is necessary to open the ion source and replace filaments. At present this is a general practice, but in the future fusion devices running on deuterium and tritium this is completely unacceptable.

Alternative way is to use non-filament methods such as Radio Frequency (RF) waves or MicroWaves (MW) for plasma production. As the part of the same program for development of alternative ion sources for the NBI line, a large RF-driven hydrogen negative ion source[10,11] has been developed at NIFS, Plasma heating laboratories. Principles of operation are described

elsewhere[12,13]. In this type of source (30x30 cm, 20 cm in depth, rectangular shape), RF antenna is immersed into the plasma. RF power of 20-30 kW is applied and with cesium injection 5.5mA (4mA without Cs) of negative ion current is extracted which corresponds to 4.1mA/cm^2 (3mA/cm^2 respectively) of negative ion current density. External magnetic filter is used to reduce electron temperature from 5eV in the driver region to 1 eV in the extraction region. Magnetic field of 100G is applied in front of the plasma grid.

In case of RF sources, power is introduced into the plasma using RF antenna, which is also exposed to direct plasma interaction. Microwaves can be introduced by means of antenna, which poses the same problem, and also directly through the dielectric window. In the later case we don't have any parts which need maintenance and as a result we can get a clean and stable plasma source for the NBI line.

Ion sources with microwave discharge plasma have the following advantages compared to the filament or RF sources: no short life components in the source, no cathode (antenna) sputtering and therefore plasma contamination and lower operation pressure.

At present microwave ion sources are used in many different plasma processing fields including ion implantation for semiconductor application[14,15], ion beam deposition for high purity film formation[16], microfabrication for magnetic devices[17], etc. Microwave ion sources were successfully used for these applications because of their maintenance-free operation advantage due to filamentless discharge [18]. This is exactly what we need for the future negative ion source.

Hellblom and Jacquot first applied microwaves for the H^- ions generation in 1986[19]. Later there were many attempts to use a mirror configuration microwave plasma source to generate negative helium, oxygen[20,21] and negative hydrogen ions [22]. Unfortunately, mirror machine configuration suggested in these works has some disadvantages, which does not allow it to be used as an effective and practical negative hydrogen ion source. Those disadvantages are localized plasma production region and therefore low plasma uniformity, strong magnetic field necessary for microwave absorption and high electron temperature.

As a solution to eliminate those disadvantages I propose a two-chamber tandem structure of the microwave plasma source in which plasma production region (plasma production chamber) with a strong magnetic field

is separated from plasma confinement region (confinement chamber). In the confinement chamber plasma gets uniform, electron temperature is reduced through the diffusion process and initial magnetic field is eliminated using special reversed-field conditioning coil, which create magnetic field opposite to that used in the plasma production region. As a result we have wide, magnetic field free, uniform plasma near the plasma grid (extraction region). In that way we can create conditions for the negative ions production. As a basis for the conceptual negative ion source design I use a volume production mechanism model which is described in the next chapter.

This work is dedicated to construction and development of the microwave negative hydrogen ion source for the NBI line, based on the original concept of spatial separation of the plasma production and negative hydrogen ion production areas by means of two-chamber tandem microwave plasma source structure.

2. Negative Hydrogen Ion Sources

2.1 Volume production mechanism for H^-

The main process responsible for the volume production of the negative hydrogen ions is the process of the electron attachment to vibrationally excited hydrogen molecules leading to the molecule dissociation, or dissociative attachment (DA)[23]. In this process vibrationally excited hydrogen molecule collides with a slow electron resulting in the molecule dissociation with generation of the negative hydrogen ion. For the vibrationally excited molecules with $v'' > 6$ (which is considered the best for the negative ion production) the reaction rate for the dissociative attachment is optimal when electron temperature is equal or more than 0.75 eV[24,25,26].

To create conditions for the volume negative hydrogen ion production we need two separate areas. In the first area hydrogen high-energy electrons would excite molecules and in the second area the excited molecules would dissociate by collisions with low-energy electrons. This concept is realized in the conventional tandem-type ion source first constructed for the negative

hydrogen ion production in Ecole Polytechnique[27,28]. The tandem source principle is illustrated on a schematical diagram (Fig.1).

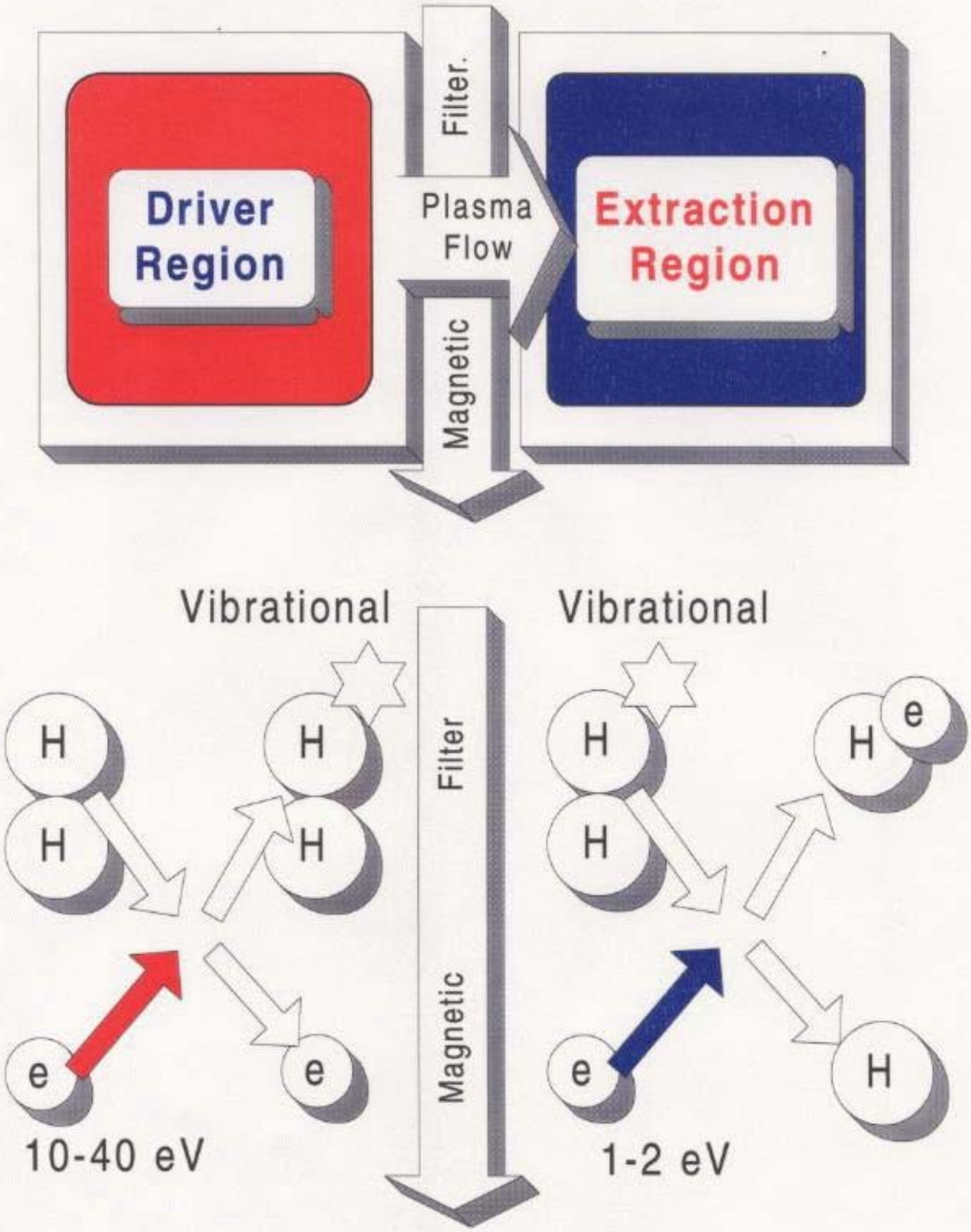

Fig 1. Two-chamber tandem ion source structure for the negative hydrogen ions generation. Production chamber (Driver Region) and Extraction chamber (Extraction Region) are separated by magnetic filter. In the driver region molecules are vibrationally excited by high-energy electrons and then drift to the extraction region. Electrons are cooled down and then negative ions are formed in the process of dissociative attachment.

In the first chamber high-energy (E>10eV with most efficiency at E~ 40eV) electron collisions provide for H_2 vibrational excitation according to the reaction

$$H_2 + e_{fast} = H_2 (v'' > 6) + e_{fast} \qquad (1)$$

Second chamber is separated from the first chamber by magnetic filter and is free of the high-energy electrons but contains low temperature thermal electrons. The electron temperature has to be chosen as to enhance the dissociative attachment process,

$$H_2 (v'' > 5) + e\ (slow) = H + H \qquad (2)$$

but to suppress electron and positive ion collisional detachment

$$H^- + e = H + 2e \qquad (3)$$

$$H^- + H^+ = 2H + e \qquad (4)$$

These conditions are satisfied for an electron temperature about 1 eV.

Tandem two-chamber negative ion source system has a lot in common with the tandem microwave plasma sources for industrial applications[29]. In both cases the goal is receiving the magnetic-field-free, low-temperature wide area uniform plasma.

Tandem model is also the main model for conventional hot filament plasma sources. Tandem design concepts of the Microwave and conventional hot-filament ion sources are compared on Fig. 2. In both cases we have plasma production area separated from negative ions production area. The only difference is that in case of the microwave source the coils field configuration and diffusion process play the role of magnetic filter.

Magnetic filter ordinary reduces plasma density 5-10 times, but in the case of diffusion instead of the magnetic filter, plasma is getting uniform and electrons are cooled down, but plasma losses are still within 20-30 % only.

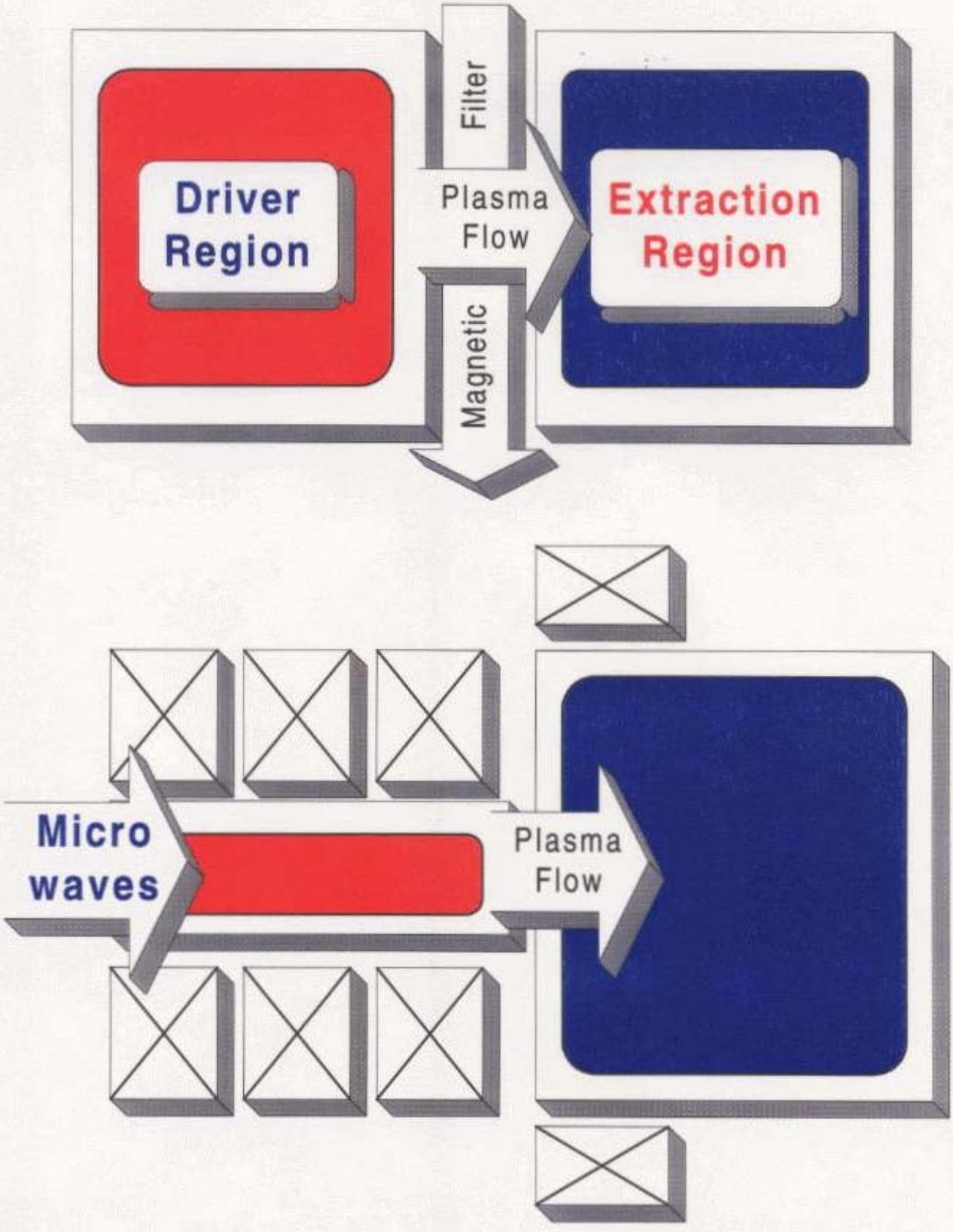

Fig. 2. Analogy between conventional tandem-type and Microwave tandem-type plasma source for H^- production. There is no magnetic filter in case of microwave plasma source.

Microwave discharge in the production chamber provides high-density plasma with very hot electrons. This is an ideal media for process (1). Actually measured plasma temperature distribution for the microwave plasma source is shown in color schematically on Fig. 3., where electron temperature gradient is shown as color gradient: red represents 10-40 eV plasma and blue represents 1-2 eV plasma. Plasma drifts to the confinement chamber where it gets uniform and electrons loose their energy through multiple collisions and reflections from the magnetic cusp field. Electron temperature in the vicinity of the plasma grid can be reduced as low as 1 eV using conditioning coil and that is providing necessary conditions for process (2). In this case conditioning coil plays a role of the magnetic filter to cut-off or cool down high-energy electron component. If this filtering proves to be sufficient to suppress the process (3), than the conventional magnetic filter would not be necessary.

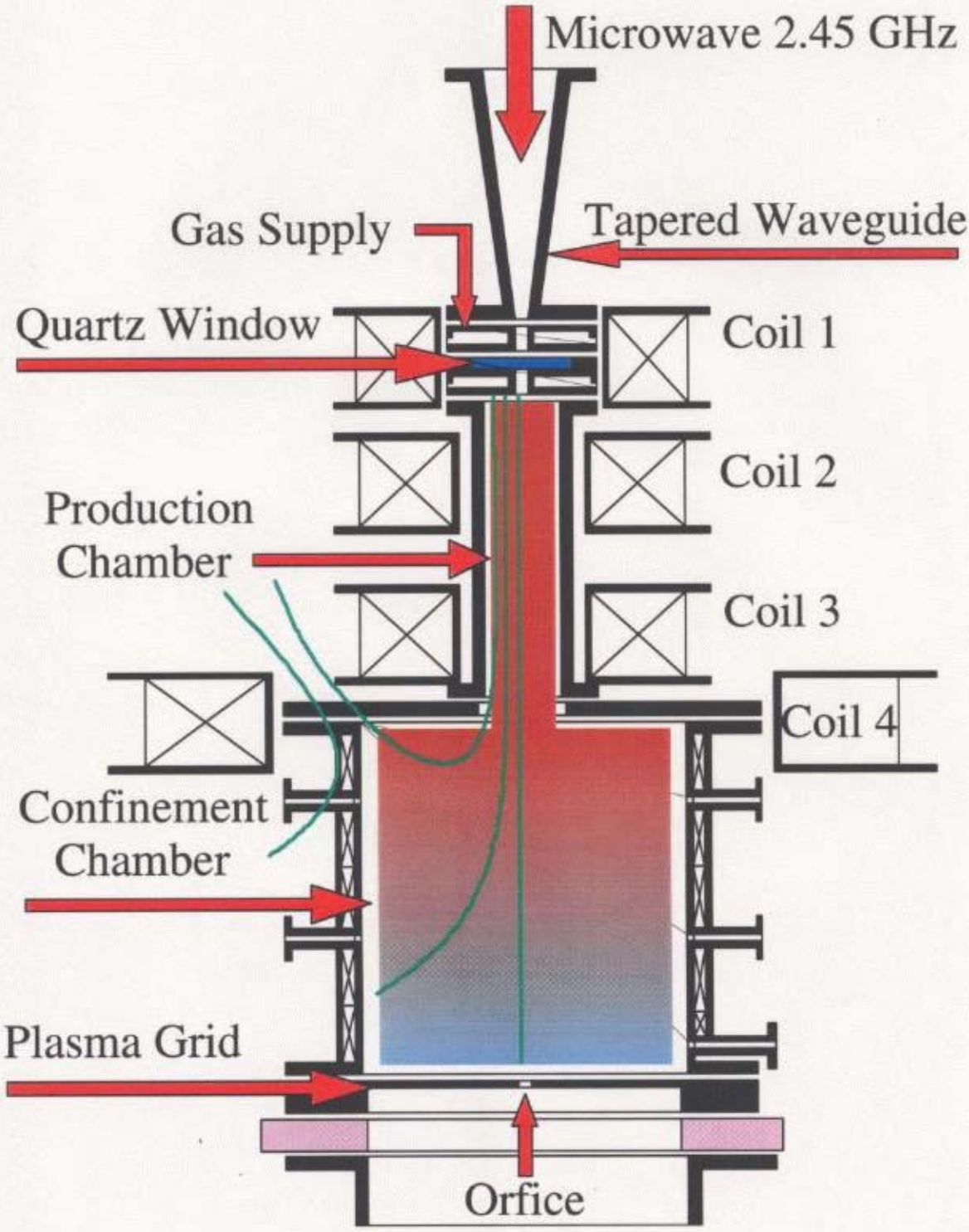

Fig. 3. General concept of the tandem microwave plasma source.

2.2 Design concept

I based the design of the microwave plasma source for the negative hydrogen ions production on the volume production mechanism. In this case we need two regions: 1) driver region, or the plasma production region and 2) extraction region, which is at the same time H^- production region. We compared conventional and microwave plasma sources on Fig. 2. The main difference is that there is no magnetic filter in the case of the microwave source.

I will explain the main principles of the microwave plasma source operation using Fig.3. Microwaves are absorbed in the production chamber and generated plasma drifts downstream along the magnetic field lines. Coils 1-3 generate strong magnetic field in the production region. Magnetic field structure created by three or more solenoid coils often resembles mirror machine to confine electrons and provide higher rate of ionization efficiency.

High-density, high-temperature plasma created in the first chamber flows to the second chamber along the field lines. Coil 4 has a magnetic field opposite to that of coils 1-3 and that makes it possible to control the

plasma flux. Plasma drifts along the field lines and reaches the walls of the confinement chamber, which are protected by cusp magnetic field. Plasma gets uniform through multiple collisions and wall reflections. Electron temperature decreases and we get a low-temperature uniform plasma in the plasma grid region.

This structure provides ideal conditions for the vibrational excitation of the hydrogen molecules in the production chamber and then necessary conditions for the H^- production can be provided in the plasma grid area by reducing electron temperature to the value of 1 eV.

2.3 Magnetic Filters

There are two types of magnetic filters used at present. First, the bar magnetic filter, when the cusp magnetic field is created by the rows of permanent magnets placed directly into the plasma volume in front of the plasma grid. Second, external magnetic filter, when the magnets are placed outside the plasma volume in the extraction area[30]. In both cases magnetic field of about 100G is necessary to cool down the hot electrons. In the case of the magnetic filter, plasma density after the filter may decrease up to 10 times. To avoid unnecessary plasma losses, it was proposed to separate the two steps of the negative hydrogen ion creation (the vibrational excitation of molecules and dissociative electron attachment to these molecules) in time rather than in space[31,32]. This is called the "temporal filter", when the discharge current is rapidly pulsed on and off. But this approach is not acceptable for powerful continuous operation (CW) machines.

I suggest an alternative filter based on the diffusion process when electrons are cooled down by multiple reflections from the walls shielded by cusp magnetic field. When the magnetic field is zero at the plasma grid, the magnetic lines from the production chamber end up at the walls of the

confinement chamber. Particles, which follow these magnetic lines, would be reflected by the cusp magnetic field and be drifting towards the plasma grid by multiple reflections from the cusp magnetic field and undergoing multiple collisions. If the cusp field is made appropriately, plasma losses on the wall are negligible. This method of hot electron cooling proved to be efficient in the case of our device. Electrons are cooled down from 10 to 1 eV without significant plasma losses.

Preliminary experiments to test if the parameters necessary for the negative hydrogen ion production may be obtained for the hydrogen discharge in this type of plasma source were held at The University of Tokyo, Professor Inoue lab. We used MIXT-3 experimental setup[33,34] to test a new production chamber, which I designed and manufactured at NIFS. Possibility to reduce the electron temperature to the value of 1 eV in the Plasma Grid region without using a magnetic filter was confirmed. Based on these preliminary results I started to build a plasma source which would be described in details in the next chapter.

3. Experimental Device

3.1 General description

The microwave plasma source, shown in Fig. 4, consists of two chambers. First chamber or the production chamber, is the place where microwaves are absorbed and plasma is generated. Production chamber is cylindrical shape, 6 cm in diameter and 20 cm long. Chamber diameter has been chosen as a result of the optimization process and chamber length is based on the absorption length for the microwaves in plasma. Second chamber or the confinement chamber, is the place where plasma is confined and gets uniform. Confinement chamber has rectangular crossection 26 x 26 cm and is 30 cm in depth. It is surrounded by 28 vertical rows of samarium-cobalt magnets, which create cusp field for plasma confinement. Production chamber is designed to be distinctively spatially separated from the confinement chamber. Production chamber is placed into a strong axial magnetic field (Fig. 5.), necessary to support microwave discharge.

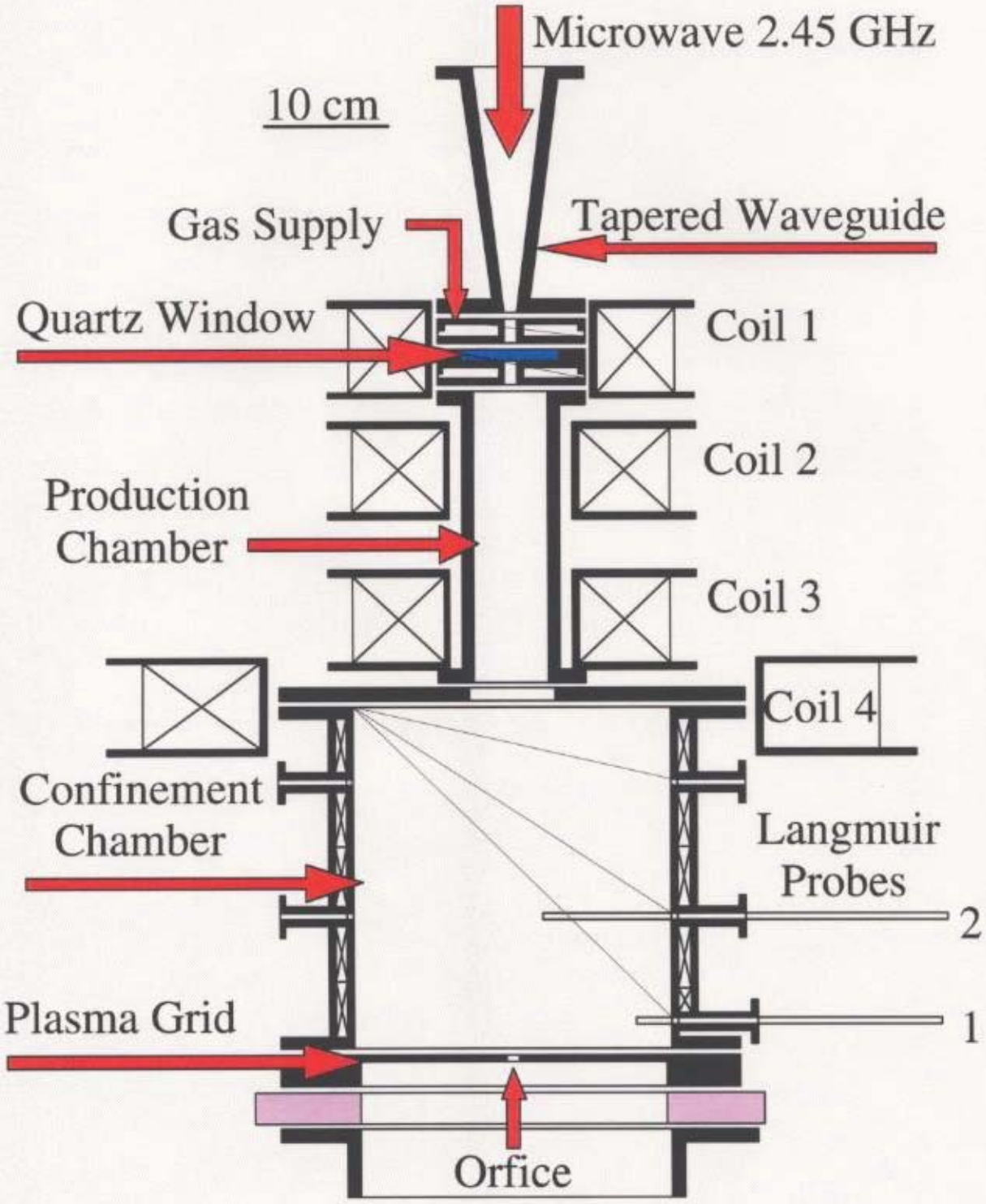

Fig. 4. Microwave Tandem Plasma Source diagram.

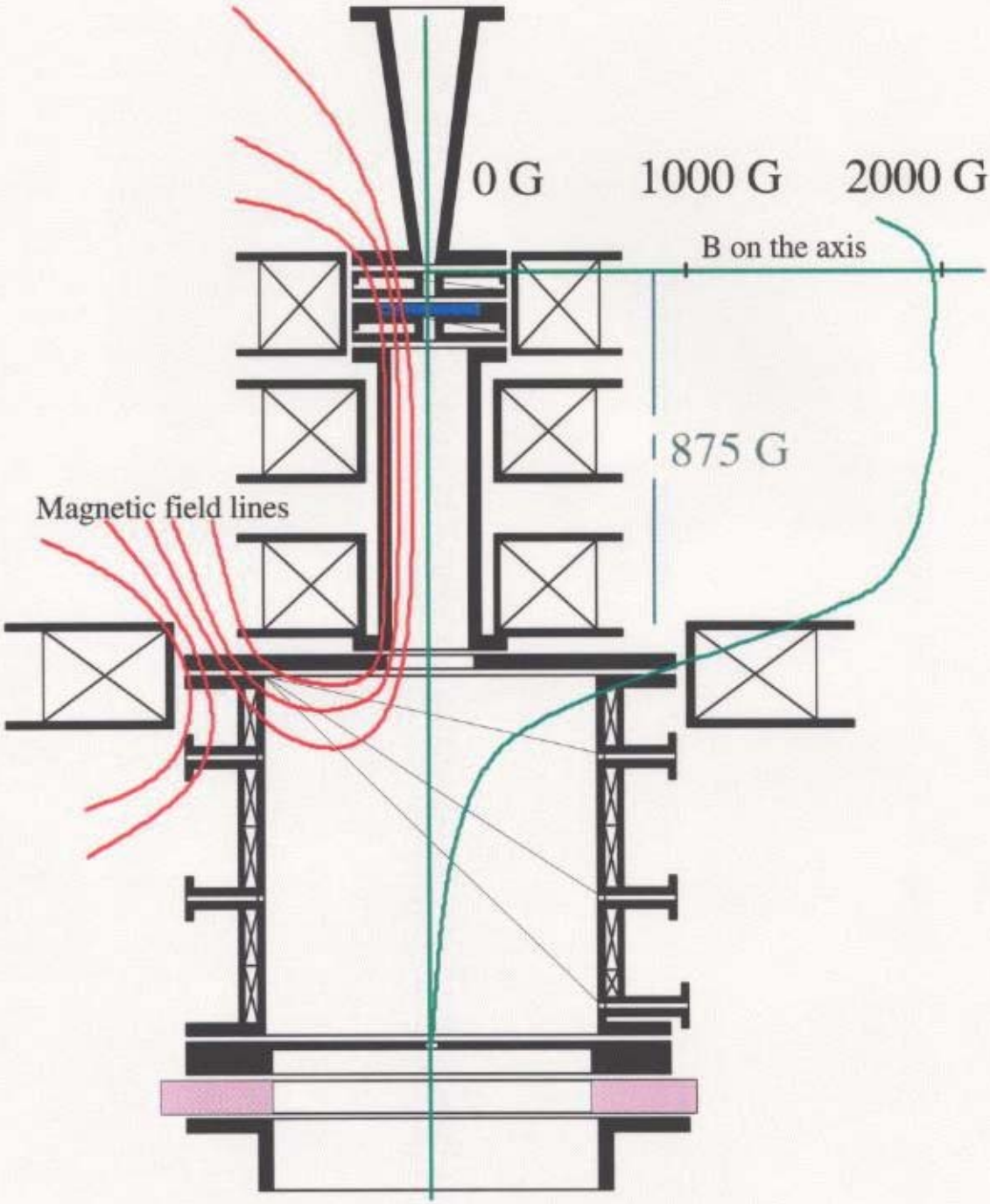

Fig. 5. Magnetic Field configuration : magnetic field lines structure (left side of the picture) and the magnetic field strength in Gauss on the axis of the plasma source (right side of the picture).

Three solenoid coils 1-3 are arranged outside the production chamber, generating a magnetic field equal to or larger than the ECR condition (875 G) and up to 2000 Gs. Produced high-density plasma then flows along the magnetic field lines downstream to the confinement chamber, where it is confined and made uniform. Changing of the Coil 4 magnetic field strength defines the plasma flux deviation and provides an effective control mechanism over the plasma uniformity and electron temperature.

Total Diagram of the experimental setup is shown on Fig. 6 and the actual picture is on Fig. 7. I will describe in detail main setup components.

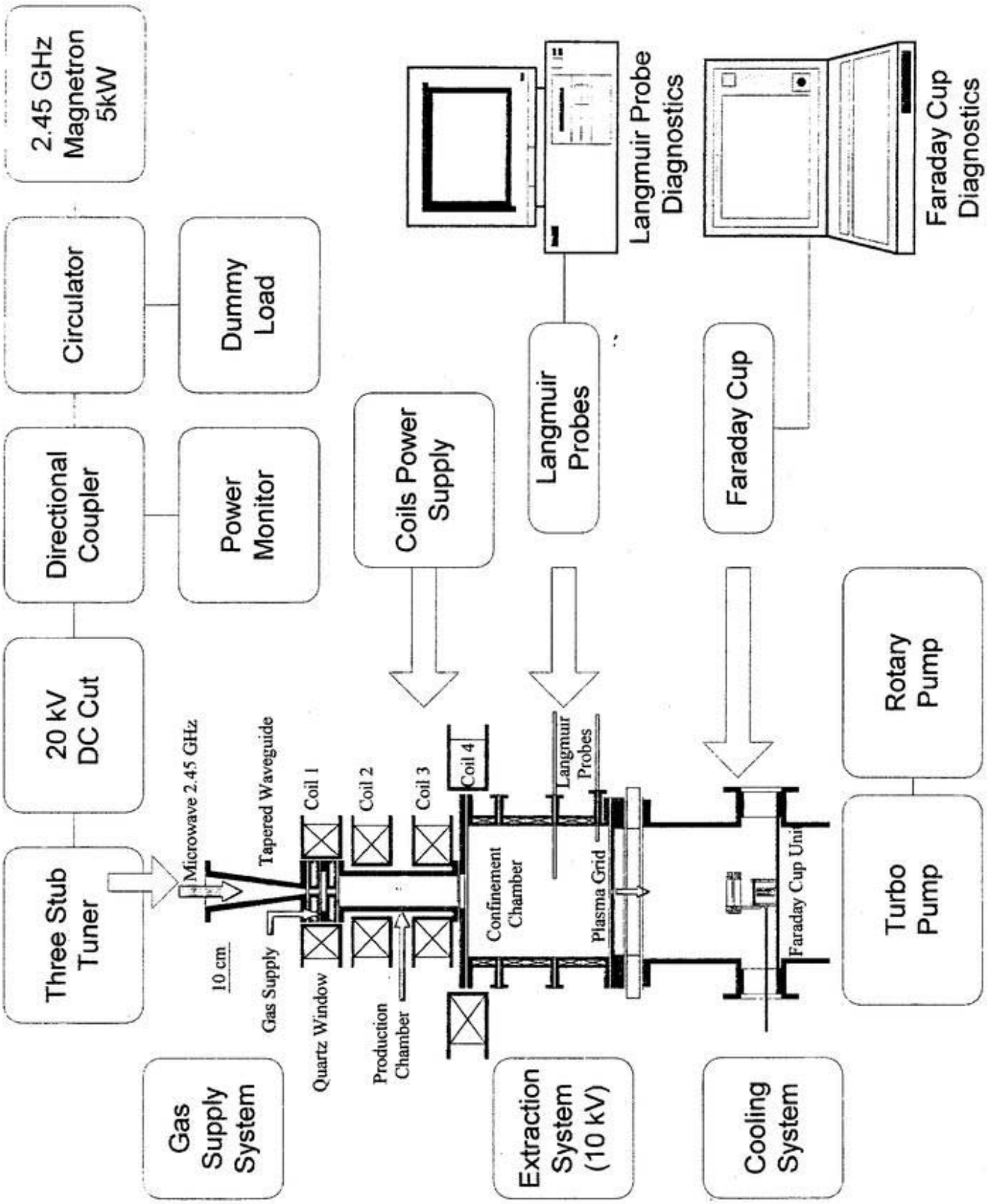

Figure 6. Total Device Diagram

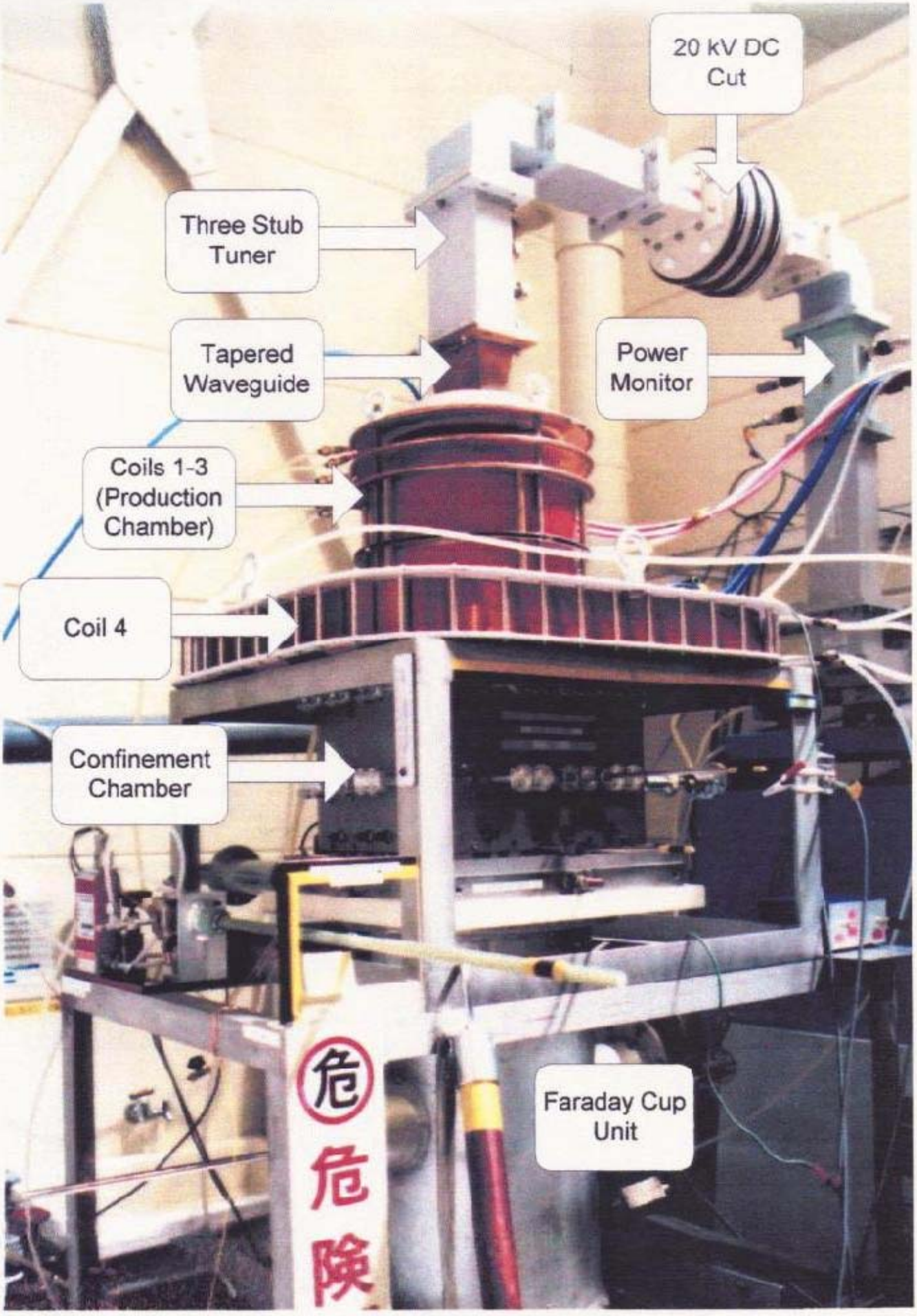

Fig. 7. Total experimental setup picture.

Gas supply system: hydrogen (argon) is supplied through a thin channel at the quartz window holder. The piezoelectric flow controller defines flow rate, which can be varied in the range of 0-20 ccm calibrated for hydrogen. Plasma grid is acting as a membrane with an orifice 1 cm in diameter, separating the high pressure area of the plasma source (pressure about 4mTorr) from the buffer chamber below where the extracted beam propagates and is measured by the Faraday cup unit (pressure about 0.04 mTorr). Gas is evacuated from the system by the turbo-molecular pump (2000 l/s) which is backed up by two rotary pumps 250 l/min each. Water cooling system is providing separate cooling circuits for plasma source, magnetron, turbo pump and magnetic coils system. High voltage pulse operation power supply is providing voltage up to 10 kV.

Microwaves are generated by the pulse operation magnetron (2.45 GHz, 5kW). Microwaves are passing through circulator (used to redirect reflected microwaves to the dummy load), directional coupler (used for power monitoring with crystal diodes system) and a Three stub tuner. Three stubs tuner system is used to adjust the impedance matching of the waveguide and the plasma source to provide minimum wave reflection. The

20kV DC cut unit is placed to insulate magnetron power supply system from the high voltage of the plasma source during the beam extraction.

Directional coupler's crystal-diode system has been calibrated using water calorymetry with a dummy load of the fixed water flow. Calibration in the range of 0-5 kW allows us to measure incident and reflected power with reasonable resolution within 5%.

Magnetron generated microwaves (2.45 GHz, power up to 5 kW) are introduced to the plasma through the rectangular tapered waveguide and a quartz window (Fig. 8). In the area of the quartz window TE_{01} mode from the rectangular waveguide is converted into TE_{11} mode of the cylindrical waveguide. By cylindrical waveguide I mean the production chamber itself. Production chamber has diameter of 6 cm, which is already small enough to be below the cut-off size of the cylindrical waveguide (which is the diameter of 7.2 cm for 2.45 GHz microwaves).

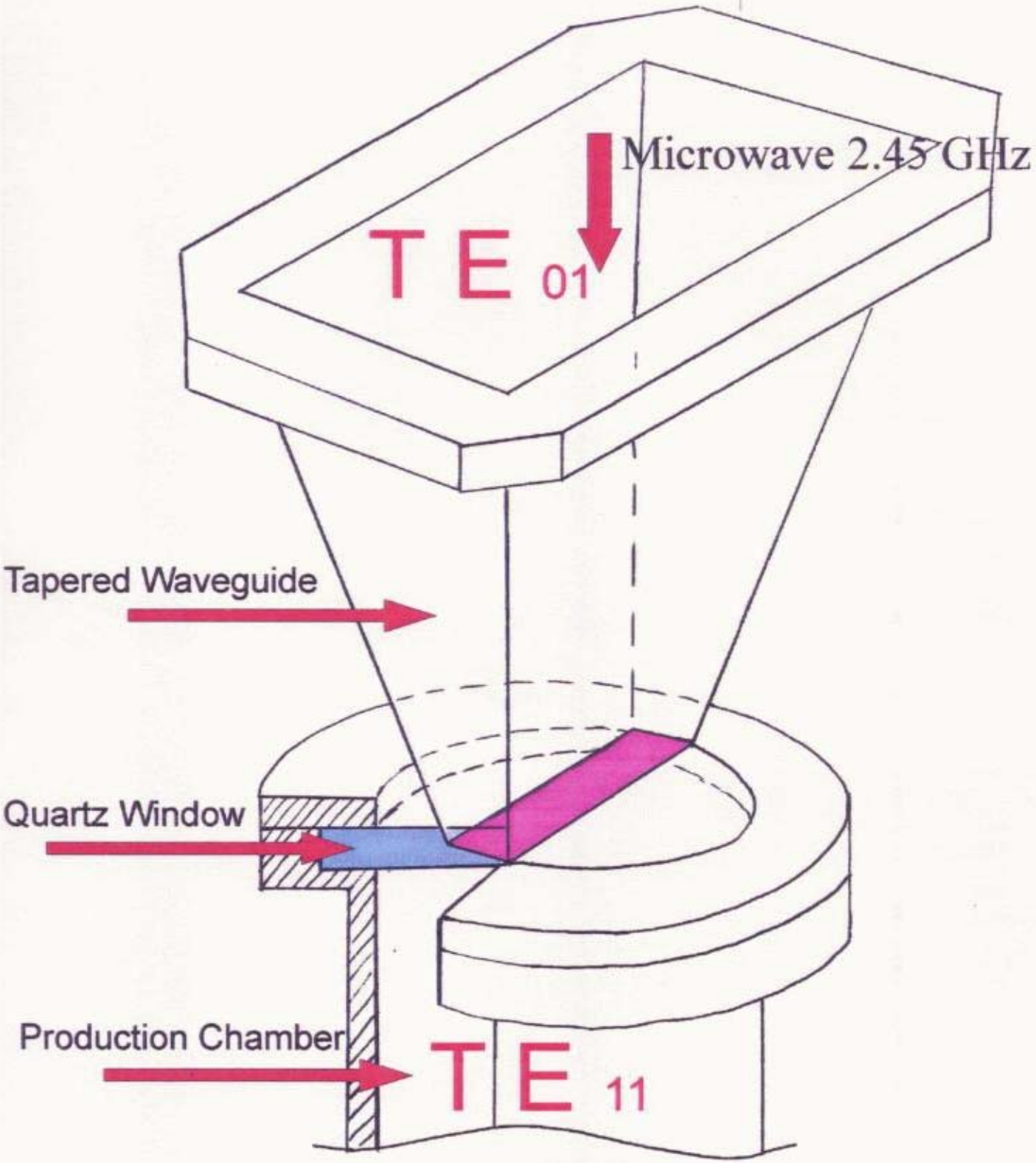

Fig. 8. Microwave is introduced through the tapered waveguide of rectangular crossection into the circular waveguide of the production chamber. TE_{01} mode is changed to TE_{11} mode in the area of the quartz window.

In ordinary conditions it is impossible to introduce 2.45GHz microwave into the cylindrical waveguide 6 cm in diameter. However, the cut-off diameter of the waveguide is defined by the wavelength of the wave propagating. The wavelength in dielectric material is proportional to one over the square root of the dielectric constant. Plasma may be considered as a dielectric with dielectric constant more than 1. Initial plasma ignition in the quartz window vicinity makes the wavelength shorter and the introduction of the microwaves into the below-the-cutoff size cylinder becomes possible. The wavelength of the microwaves is decreasing with the growth of the dielectric constant of the plasma (with the growth of plasma density). As a result, waves becomes shorter and the cut-off condition changes allowing waves to be introduced to the smaller waveguide filled with plasma (See Appendix 1 for details).

The confinement chamber is rectangular shape, 26x26 cm, and 30 cm in depth. A magnetic multipole line-cusp field produced by 28 vertical rows of samarium-cobalt permanent magnets surrounds it. The magnetic strength at the inner wall is 2.0 kG and it exponentially decreases to 20 G on the distance approximately 3 cm from the wall providing magnetically undisturbed plasma 20x20-cm rectangular crossection in the plasma grid

region. Solenoid coil 4 with the magnetic field reversed in respect to that of the coils 1,2,3 is located outside confinement chamber. It is reducing the magnetic field from the coils 1,2,3 and gradually eliminates it in the region near the plasma grid to match one of the main conditions for the creation of uniform plasma which is the absence of magnetic field.

3.2 Magnetic coils system field measurements and calculation

Magnetic system consists of 4 coils. Coils 1-3 have cylindrical shapes and coil 4 has rectangular shape to fit the shape of the confinement chamber. The specifications of the coils are summarized in Table 1.

Table 1. Specifications of magnetic coils

Coil	Inner diameter	Outer diameter	Thickness	Number of turns	Current
1	166	236	75	700	5 A
2,3	92	270	75	120	200 A
4	396	614	60	1000	5 A

All coils were designed for continuos operation. Coils 1 and 4 has external water cooling and coils 2 and 3 are made from the hollow conductor of the rectangular shape 6x6 mm with an inner water carrying duct of 3x3 mm.

Magnetic field of this system was calculated using BROWN - FLAX method for circular coils 1-3 and "Turns" method for frame-coil 4. High-accuracy computation of the integrals Lobatto' s quadrature formula, using Chebyshev`s polynomials was performed. Resulting magnetic field structure is shown on Fig. 9 and the field strength on the axis is shown on Fig. 10.

For the current of coils 2-3 equal to 200A, the current of 5 A in the conditioning coil 4 reduces magnetic field in the plasma grid area to zero.

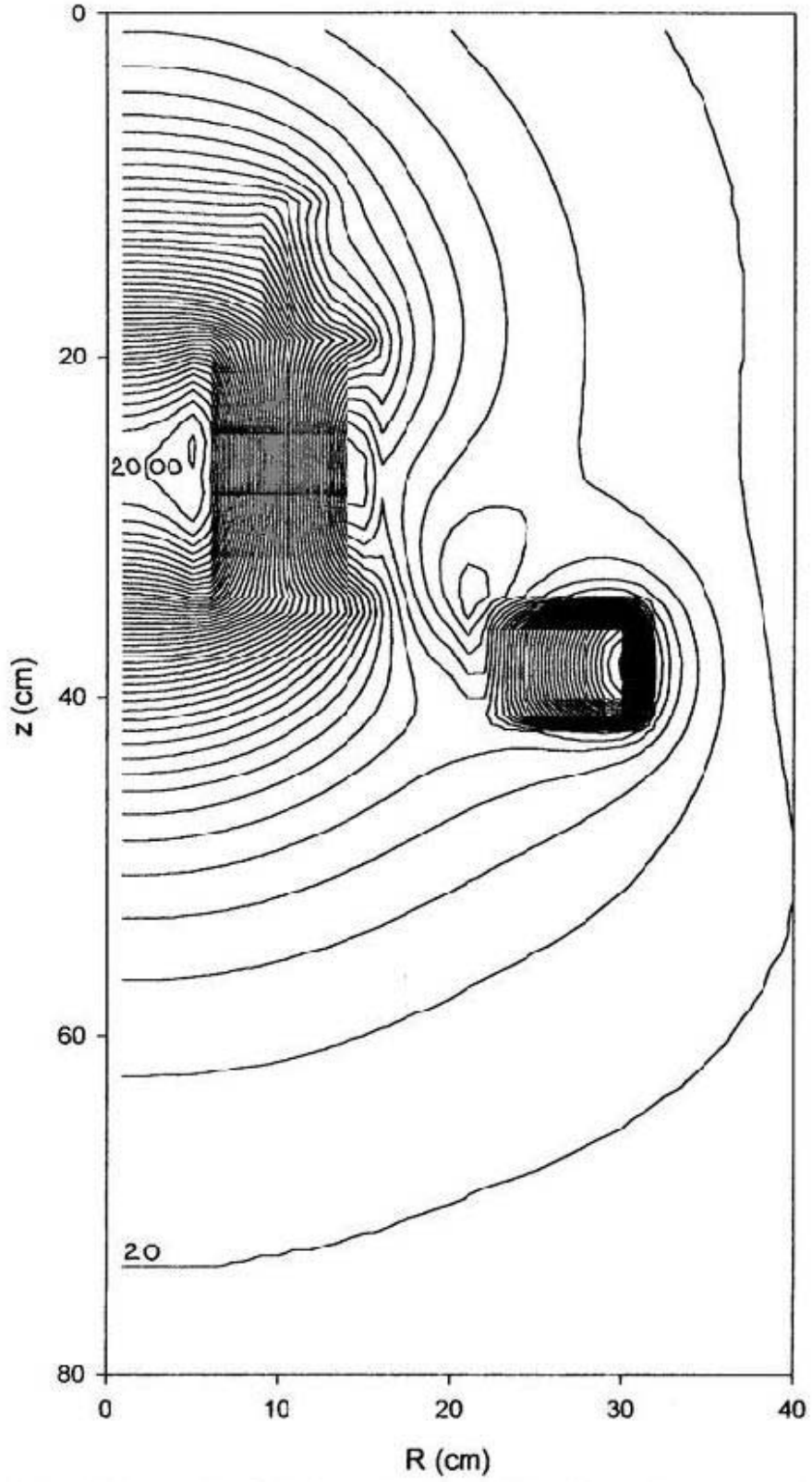

Fig. 9. Magnetic field contour profile for coils current of coils 1-4, 5-170-170-5 A respectively. (z = 0 corresponds to the point 15 cm above the quartz window)

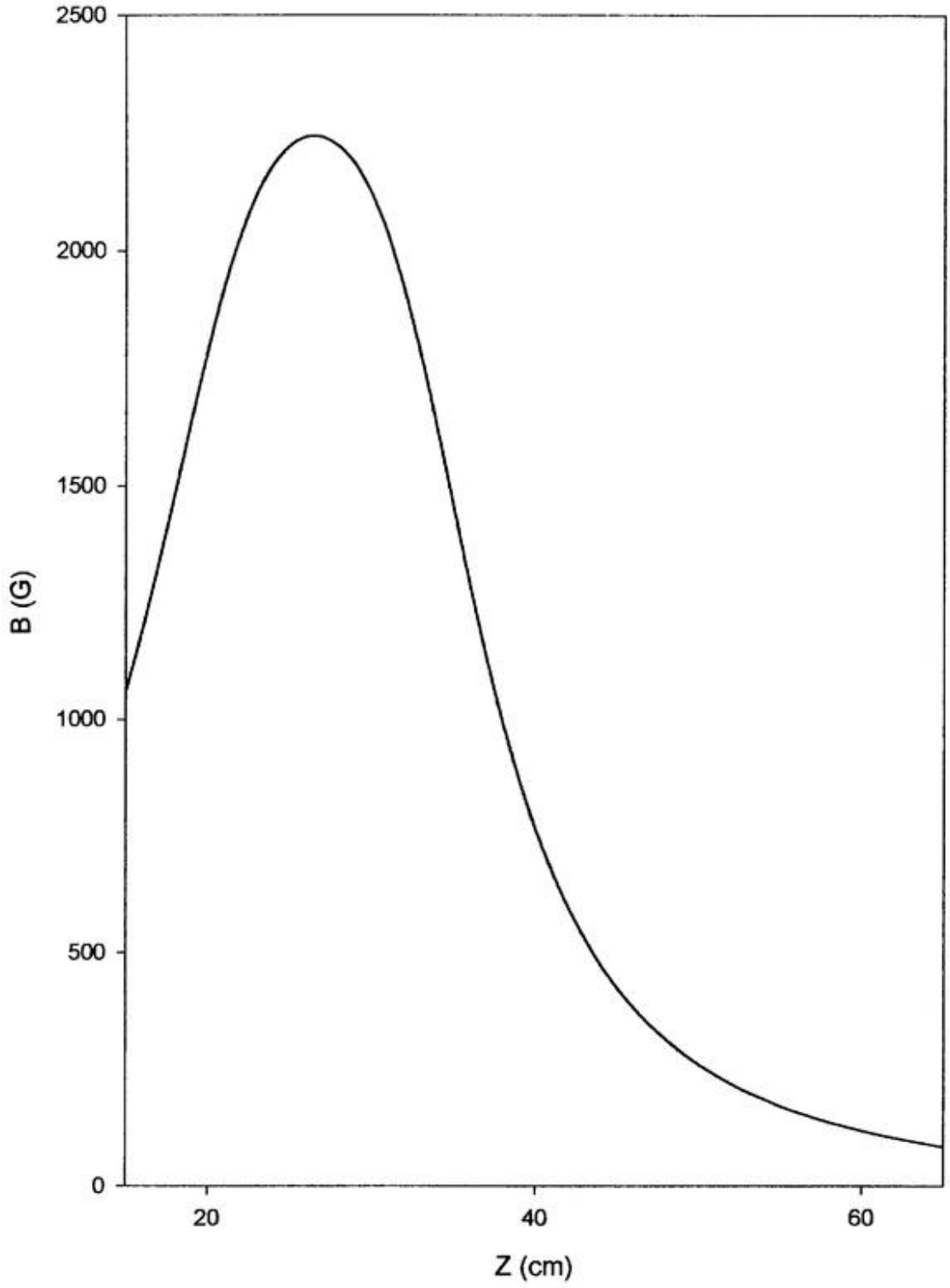

Fig. 10. Magnetic field on the axis for coils current of coils 1-4, 5-170-170-5 A respectively. (z = 0 corresponds to the point 15 cm above the quartz window)

3.3 Operation Parameters

For the continuos operation a powerful cooling system is necessary. On the development stage we used simple cooling system to reduce expenses and the plasma source was operated in a pulse mode. The discharge pulse duration was 200ms with 2 seconds rest and the probe measurements were conducted 100ms after the plasma ignition. Plasma density fluctuation during discharge was within 5%. Increasing the pulse time to 10 seconds does not change discharge and plasma parameters. One can consider that during the continuos operation plasma would have the same parameters as at the pulse operation mode.

Operational pressure is varied from 0.5 to 20mTorr with optimal hydrogen discharge conditions at the pressure of 4 mTorr. (That is less than for RF Ion sources, which is about 11 mTorr). Microwave Power is changed in the range of 1-5 kW. Operation pulse mode is 200 msec operation and 2 sec rest.

Extraction voltage in the range of 1-10kV was supplied continuously. Dark current through the water cooling pipes was about 300 μA.

3.4 Plasma Diagnostics

Plasma parameters (electron temperature, plasma density and plasma potential) in the confinement chamber were measured with radially moveable Langmuir probes 1 and 2 (Fig. 4). Langmuir probes are introduced to the confinement chamber through ports 1 and 2, which are 1 cm and 11 cm above the plasma grid respectively.

There are two methods to measure H^- production that are used at present. First method is measurement (by means of calorymetry or Faraday cup) of the extracted negative ion beam. It is widely used in present NBI negative ion sources R&D experiments[35] because it gives reliable quantitative approximation of the negative hydrogen ion production rate. Second method is photodetachment[36,37,38,39], which is more of the qualitative than quantitative nature. It allows measuring qualitatively a dynamic plasma behavior[40], but at present stage does not give exact value of H^- concentration.

The ion source described in this paper is constructed as a part of the R&D program and we need reliable evaluation of the negative hydrogen ions production. I have chosen the extracted beam intensity measurements.

However, at present R&D stage the plasma source input power is low and extracted beam was initially expected to be weak. At the same time we need to measure beam profile because the beam is extracted from the area with changeable (because of a conditioning coil 4), magnetic field and the beam deviation is unpredictable. To measure the profile of a beam of low intensity, I have chosen Faraday cup method, not calorymetry. The array of Faraday cups allow to measure beam profile and by Gaussian approximation to evaluate total beam current.

To confirm the H^- production we used extraction method. Simple extraction system consists of two grids: plasma grid and extraction grid. The plasma grid is electrically connected to the plasma chamber and biased to the voltage of 1-10 kV (actual operation value is 5 kV). Extraction grid is at the ground potential. Negative hydrogen ion beam is extracted from the plasma chamber through a 10mm diameter aperture. A pair of filter bar magnets is installed into the extraction grid. The filter magnets provide a transverse magnetic field (B=200G at the center). This magnetic filter is used to remove the electrons extracted together with negative hydrogen ions. Electron component of the extracted beam is bent in the magnetic field and the extraction grid itself absorbs electrons.

The extracted H^- beam is collected with Faraday cup unit. The unit has 9 channels placed in a row with a distance between two Faraday cups of 12 mm. Faraday cup array can be moved in the direction, perpendicular to the Faraday cup row. We can scan the actual 2-dimensional profile. Faraday cup unit would be described in details later.

4. Microwave Plasma Source Parameters

4.1 High energy transmitting quartz window holder

To provide high-density hydrogen plasma in the plasma grid region we need to inject high power microwaves through a quartz window directly into the plasma production chamber, which is 6 cm in diameter. In present experiments we inject up to 5kW of the microwave power. All parts of the plasma source were designed for the continuous operation except the quartz window, which is under double impact from microwave absorption during microwave pass-through and from the plasma bombardment. To reduce thermal load on the window, a special window holder has been designed (Fig. 11-a). In this design window is imbedded into the sandwich-type copper holder which is composed by two plates with intensive water-cooling. Microwaves pass through a rectangular waveguide 10x70 mm in crossection. The lower plate also cuts off the thermal flux from plasma. Using this cooling system operation at 5 kW power is possible during 30 second without any damage to packing and window itself.

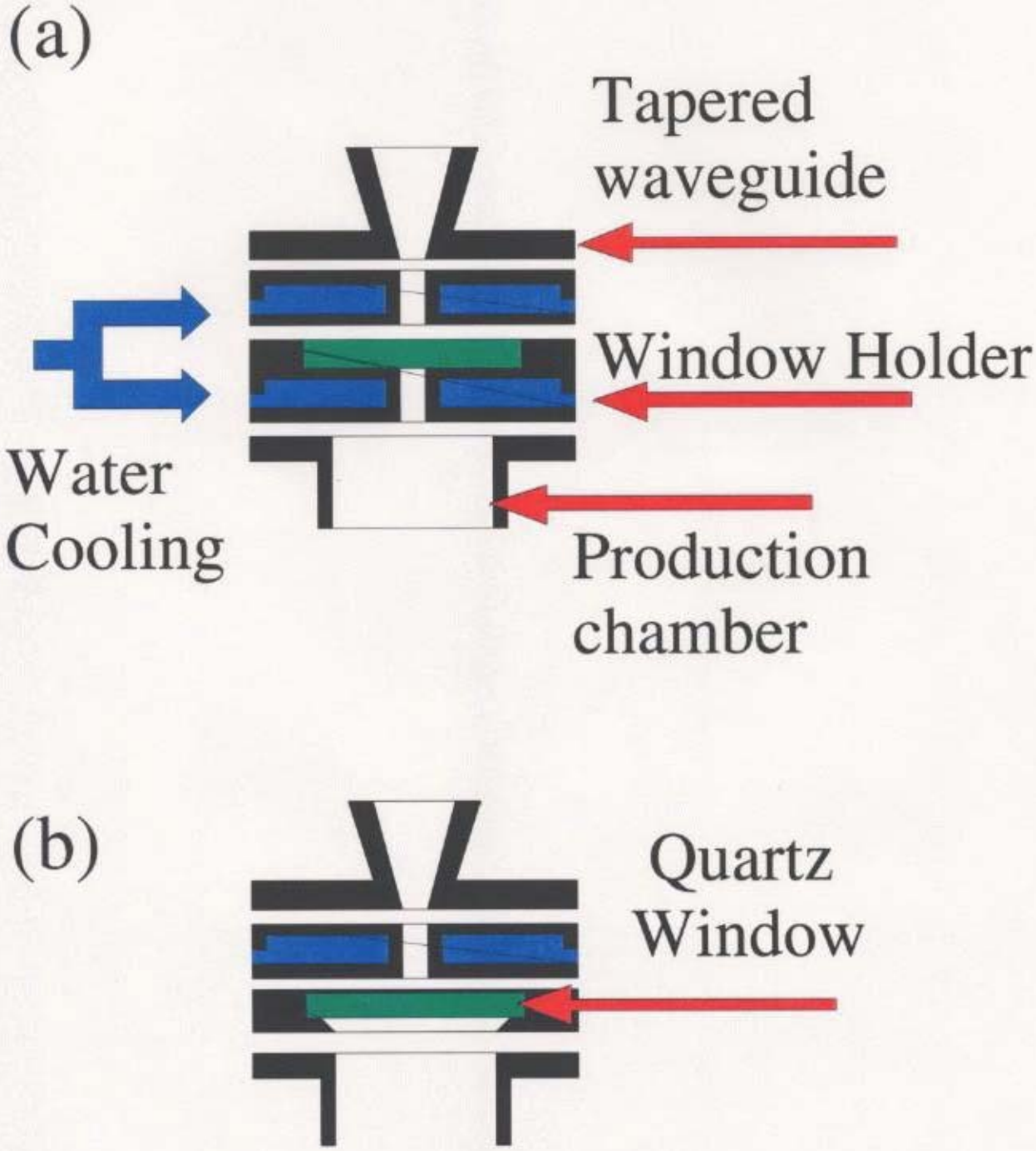

Fig. 11. Two window holders: (a) with metal surface facing plasma and (b) with quartz window facing plasma.

4.2 Reduction of the plasma potential

Although the window holder (Fig. 11-a) works well in case of the argon discharge, some unexpected problems appeared for the hydrogen discharge. During first set of experiments plasma potential was around 15 V for argon and 25-40 volts for hydrogen. Hydrogen discharge plasma potential was too high compared to conventional filament plasma sources and increased plasma losses to the wall. The reason was escape of the electrons from production chamber to the conducting surface of the copper quartz window holder along the magnetic field lines.

One of the possible solutions might be biasing of the window holder or covering it with the dielectric material. At present stage we removed the lower cooling plate and quartz window is exposed to plasma. For the pulse operation that does not pose any problems, but for the continuous operation in the future ion source Fig 11-a with extra dielectric coating have to be used. Plasma potential for hydrogen in a new configuration (Fig. 11-b) dropped to 12-15 V (Fig. 12) and plasma density in the plasma grid region (as measured with the Langmuir probe 1, increased more than 4 times from $0.7 \times 10^{11} cm^{-3}$ to $3 \times 10^{11} cm^{-3}$.

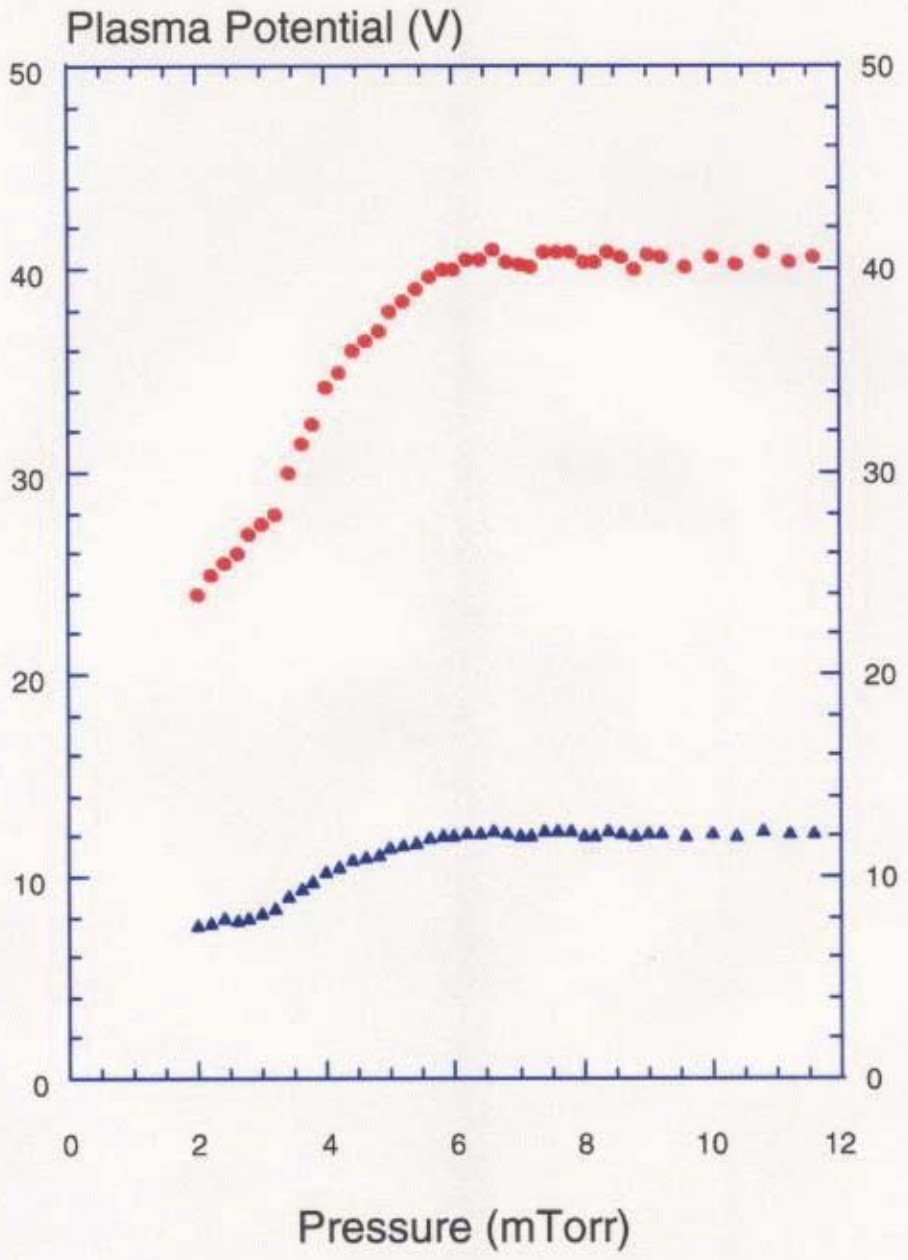

Fig. 12. Plasma potential in the confinement chamber for two windows configurations: metal surface (a) - (circles) and quarts surface (b) - (triangles).

4.3 Input Power Dependence

Microwave power can be varied in the range of 1-5 kW. We have measured power dependence (Fig. 13). At present power dependence data are limited by the magnetron power (5kW), but as we can see, the plasma density is linearly increasing with power. If the linear dependence on input power will preserve for higher energies, we can expect further increase of the plasma density and consequently H^- production, which as we will see later, is proportional to plasma density at fixed temperature.

For the pressure of 4 mTorr gas density is 1.4×10^{14} [cm^{-3}]

For the hydrogen discharge plasma density in the production chamber was measured to be about 2×10^{12} cm^{-3} and therefore the ionization rate is only 1,5%. At the same time for argon the plasma density in the production chamber for the same gas pressure and input microwave power is 10 times higher than that for hydrogen and ionization rate reaches 15%. One can suppose that in case of hydrogen further microwave power increase will result in the further linear plasma density growth at least until ionization rate for hydrogen reaches 15% as it was in case of argon.

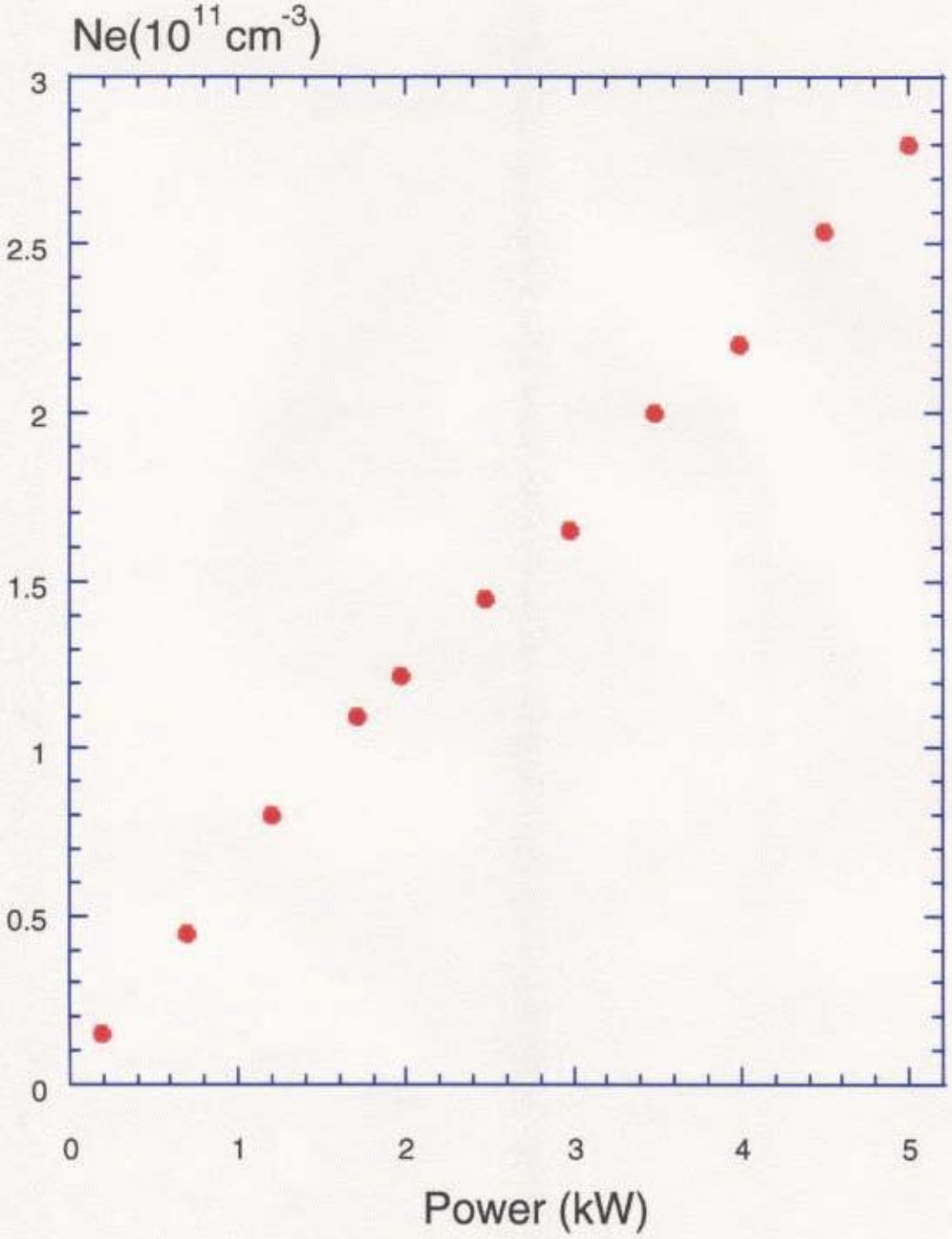

Fig. 13. Plasma density at the plasma grid area dependence on the microwave power injected.

4.4 Gas pressure dependence

Gas pressure dependence of plasma density and electron temperature for hydrogen is shown in Fig.14. Plasma density in the plasma grid region increases with the increase of pressure, because ionization efficiency of the hot electrons in the production region increases (electrons make more collisions before they escape to the walls). With further pressure increase all the energy is absorbed closer to the quartz window and less plasma can reach the bottom of the production chamber. Electron temperature is gradually decreasing with pressure due to collisional processes.

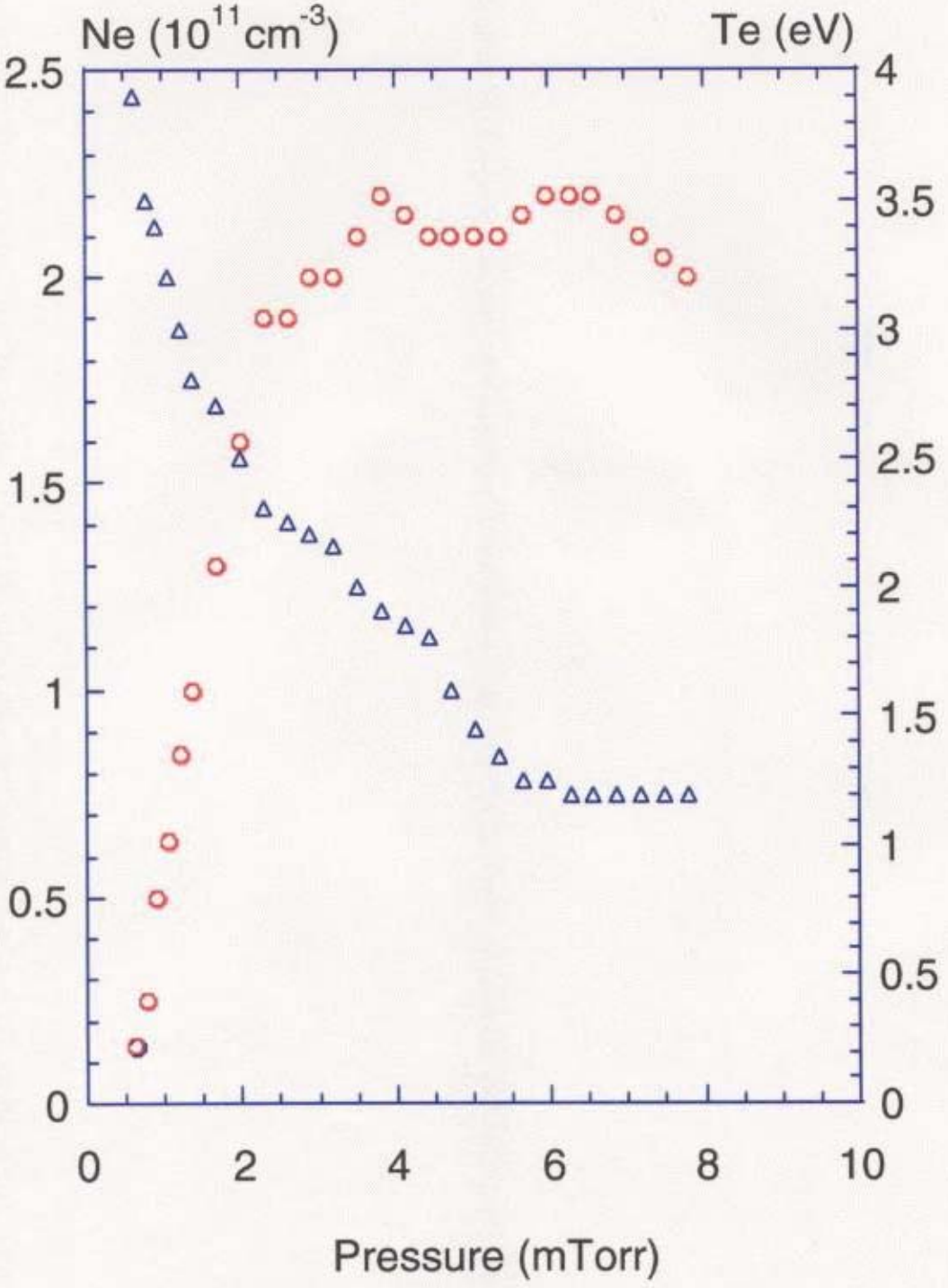

Fig. 14. Plasma density and electron temperature at the plasma grid area dependence on the gas pressure.

4.5 Magnetic field strength in the production chamber dependence

Magnetic field necessary for the microwave penetration into magnetized plasma is 875G for the 2.45GHz microwaves. Magnetic field value was increased more then twice over ECR condition. Results of the magnetic field strength scan are presented on Fig. 15. Plasma parameters used to characterize this process are measured near the plasma grid, not inside the production chamber itself. Before the value of 875G (corresponding to electron cyclotron resonance - ECR) is reached, no significant plasma is produced. There is still some plasma generation, because before being reflected microwaves penetrate to some skin depth in the quartz window region and inside this boundary layer they are partially absorbed. After the value of 875G is reached, microwaves easily penetrate into the plasma volume and are completely absorbed inside the production chamber. The reflected power is less than 5 % at the condition that B exceeds the threshold value of 845G. With the further increase of the magnetic field, plasma density gradually increases.

At the magnetic field value of 2000 G, T_e = 10 eV and T_i =0.5 eV, electron and ion cyclotron radii are:

r_e [cm] = v T_e / w_{ce} = 2.38 $T_e^{1/2}$ [eV] / B [G] = 3.8×10^{-3} cm

r_i [cm] = v T_i / w_{ci} = 102 $(T_i \mu)^{1/2}$ [eV] / B [G]

r_i (Ar^+) = 5.3×10^{-3} cm

r_i (H^+) = 8.4×10^{-4} cm

Plasma is strongly magnetized and linear plasma density dependence on the magnetic field strength in the production chamber may not be explained simply by the improvement of the plasma confinement. We need to look deeply into microwave absorption mechanism.

The mechanism of the microwave absorption was studied in detail by M. Tanaka et al.[41,42,43,44]. In those papers the difference between TE_{11} and TE_{01} modes in the cylindrical waveguide and the propagation mode influence on the plasma uniformity in the plasma grid region is studied in details. In our case the TE_{01} mode is supplied from the magnetron through the waveguide of rectangular crossection and is converted to the TE_{11} mode when the wave enters the production chamber (cylindrical waveguide).

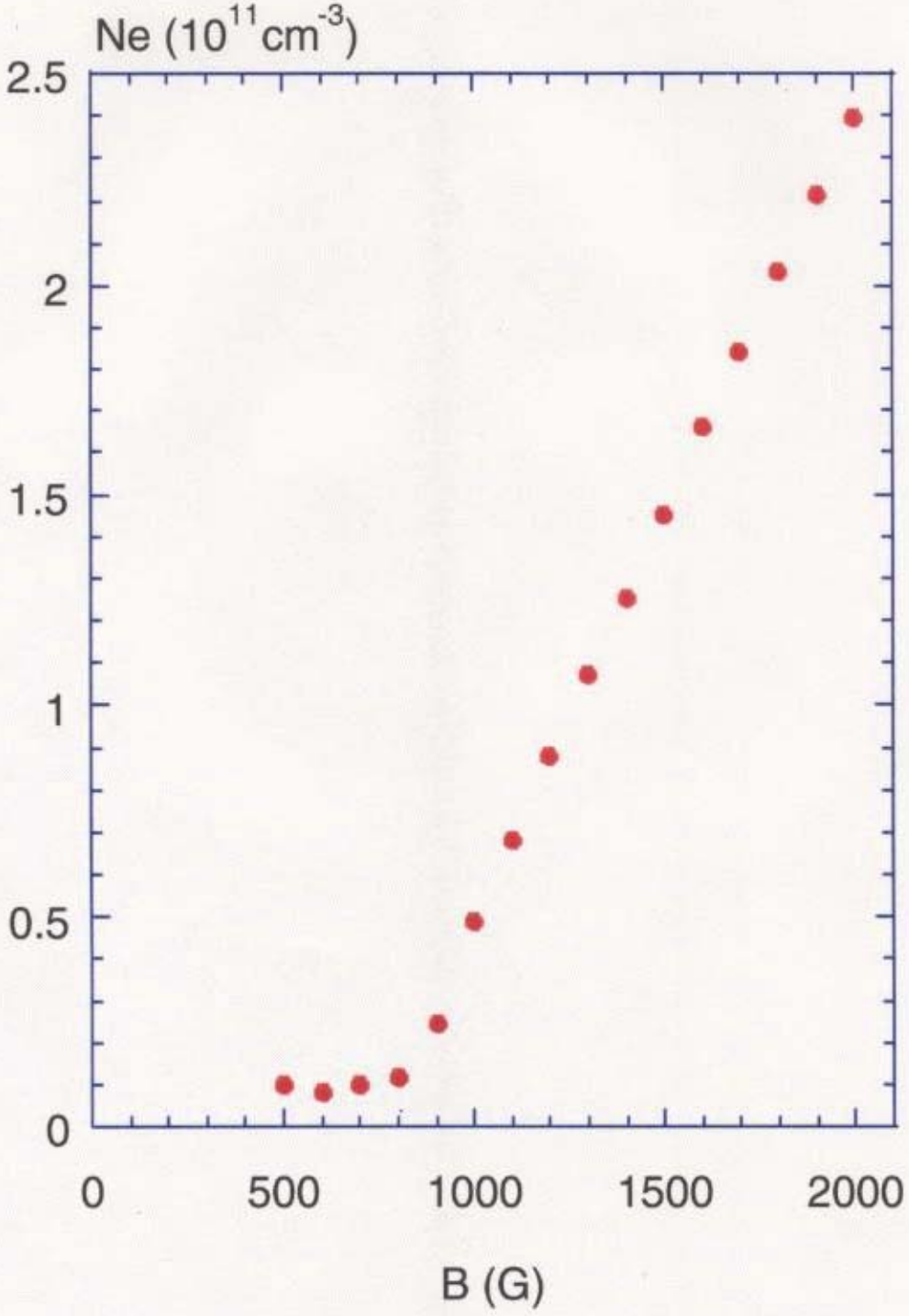

Fig. 15. Plasma density at the plasma grid area dependence on the magnetic field strength in the production region.

In the work of M. Tanaka, microwaves are injected from the side of the strong magnetic field and completely absorbed before reaching the Electron Cyclotron Resonance (ECR) region. There are several possible explanations to that: 1) Doppler shifted ECR 2) Generation of the whistler wave, which is later absorbed through the collisional processes, 3) collisional damping and 4) Landau damping.

In our case magnetic field is twice higher than ECR and therefore I consider that the microwave absorption mechanism is the generation of the whistler wave in the vicinity of the quartz window at the point of passing the critical plasma density. After that the whistler wave is damped in the plasma volume due to the electron cyclotron resonance and collisional damping. (For the choice of the magnetic field for the specified plasma parameters it is recommended to take into consideration the microwave rejection band, which is described in details elsewhere[45]).

K. Ohkubo et al. studied the Whistler wave generation and spatial damping in details[46,47,48]. In the similar microwave injection configuration for the same plasma densities and magnetic field values, the microwaves

were injected into the cylindrical plasma volume along the field lines. Microwaves were converted to the whistler waves and absorbed. In the described case microwave absorption is most effective for the value of the wave frequency equal 0.7 of the cyclotron frequency. In this situation microwave is absorbed mostly as a result of the collisional damping.

For B= 1800 G, the ratio of the wave frequency to the cyclotron frequency $w/w_c = 0.5$. According to K. Ohkubo, for the $w/w_c = 0.5$ the wave damping is ascribed totally to the (Coulomb) collisional damping.

Mathematical foundation of the whistler wave generation and collisional damping mechanism is given in Appendix 2.

4.6 Conditioning coil magnetic field dependence

Conditioning coil 4 is controlling the magnetic field strength at the plasma grid region. Magnetic field strength dependence on coil 4 current for the levels 1 and 2 of the Langmuir probes ports is shown on Fig. 16. These data were measured using Hall probe inserted into the confinement chamber through the Langmuir probe ports 1 and 2. As we can see, without coil 4 there is residual field of coils 1-3 which is about 30 G at point 2 and 15 G at point 3. In fact, it is the magnetic field lines configuration, not the actual value of B that strongly affects the plasma source parameters. The stronger the field of coil 4 - the stronger magnetic field lines bends and stretches against the cusp-field-shielded walls of the confinement chamber. That results in a longer path for the electrons before they reach the plasma grid region and as a result with increase of Coil 4 magnetic field, electron temperature steadily decreases (Fig. 17). Plasma density reaches some maximum value and then also decreases, because longer drifting path also means the increase of wall losses.

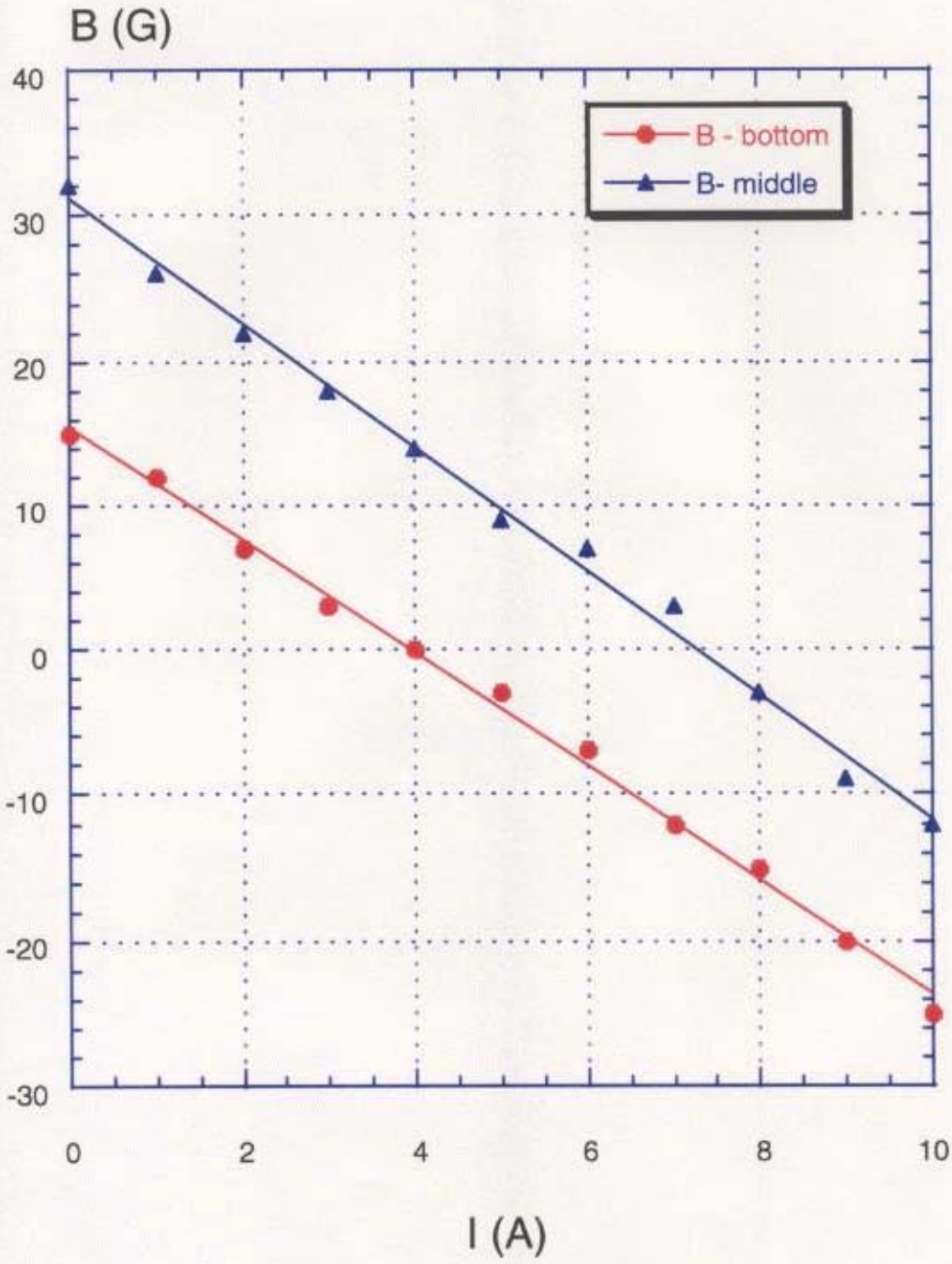

Fig. 16. Residual magnetic field dependence at the bottom of confinement chamber, near plasma grid (measured through port 1) and in the middle off the confinement chamber (measured through port 2) dependence on the current I(A) of the conditioning coil 4.

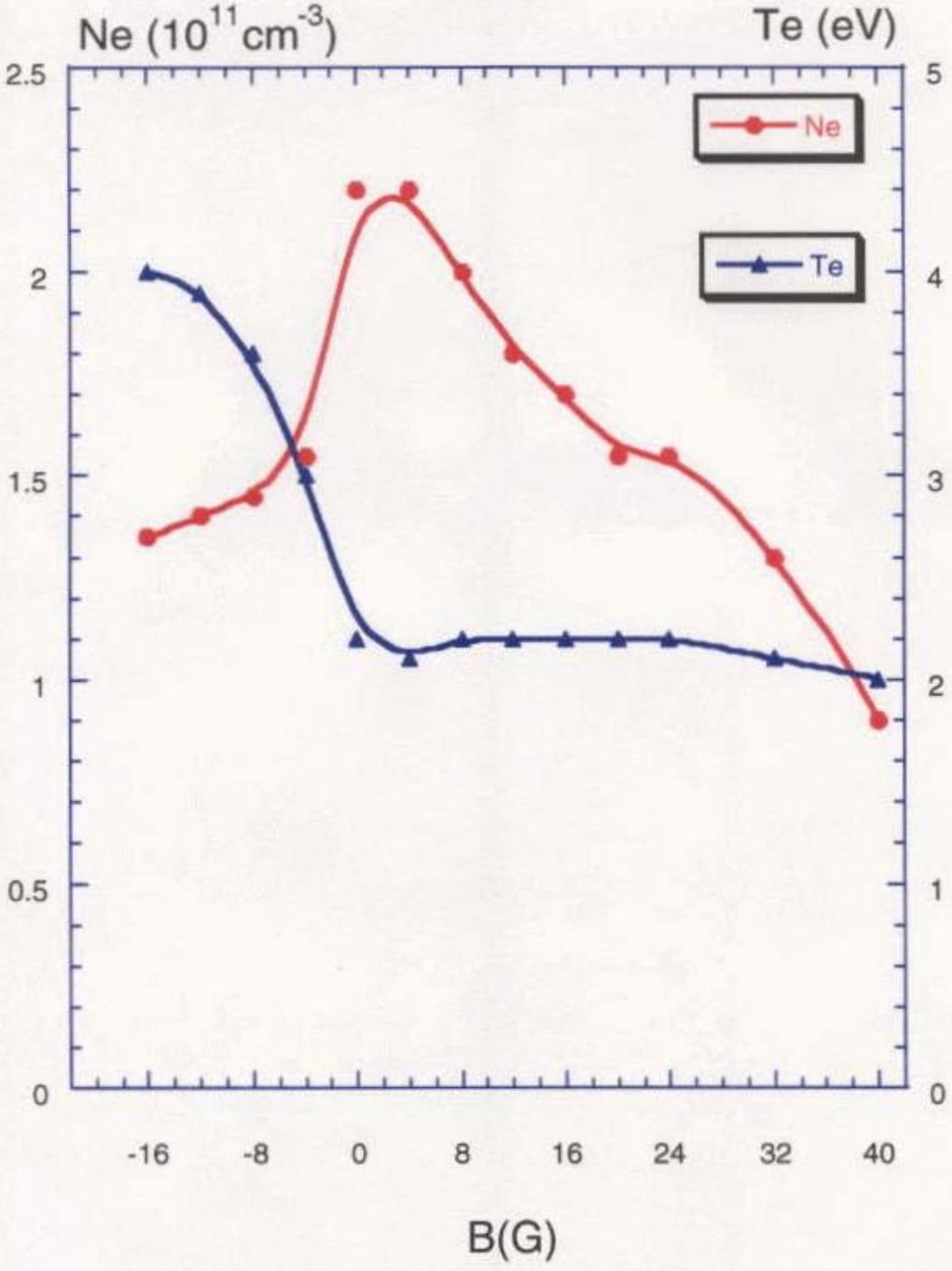

Fig. 17. Hydrogen plasma density in the confinement chamber at the plasma grid region in dependence on the magnetic field strength at that region.

Even for the residual field of 30 G and $T_e = 2$ eV,

r_e [cm] = 0.11 cm, r_i [cm] = 2.4 cm

We can consider that at these values charged particles follow magnetic field lines all the way to the bottom of the confinement chamber. Conditioning coil is a really powerful plasma flux control tool.

After magnetic field reaches zero value, further increase of the reverse field does not result in the decrease of the electron temperature and it stops at the value of 2 eV. At the B = 0 value at the bottom, all magnetic lines end up on the chamber walls and electrons are at least once reflected from the cusp magnetic field.

After all the plasma flow practically gets reflected from the cusp magnetic field of the confinement chamber walls, plasma gets uniform at the bottom of the confinement chamber.

Uniform radial profile at the plasma grid area guarantees uniform extracted beam density for the multi-hole ion beam extraction. In our plasma source the same negative ion density is obtained over a wide area of 20x20cm. Basically this type of plasma source is used for the plasma processing where plasma uniformity within 5% is a necessary condition.

Varying magnetic field of the coil 4, the most uniform profile was achieved for the coil 4 current of 4-5 A which corresponds to the zero magnetic field in the plasma grid area. Resulting radial distributions of plasma density and electron temperature are shown on Fig. 18. As we see, not only plasma density, but also electron temperature is uniform all over the plasma region.

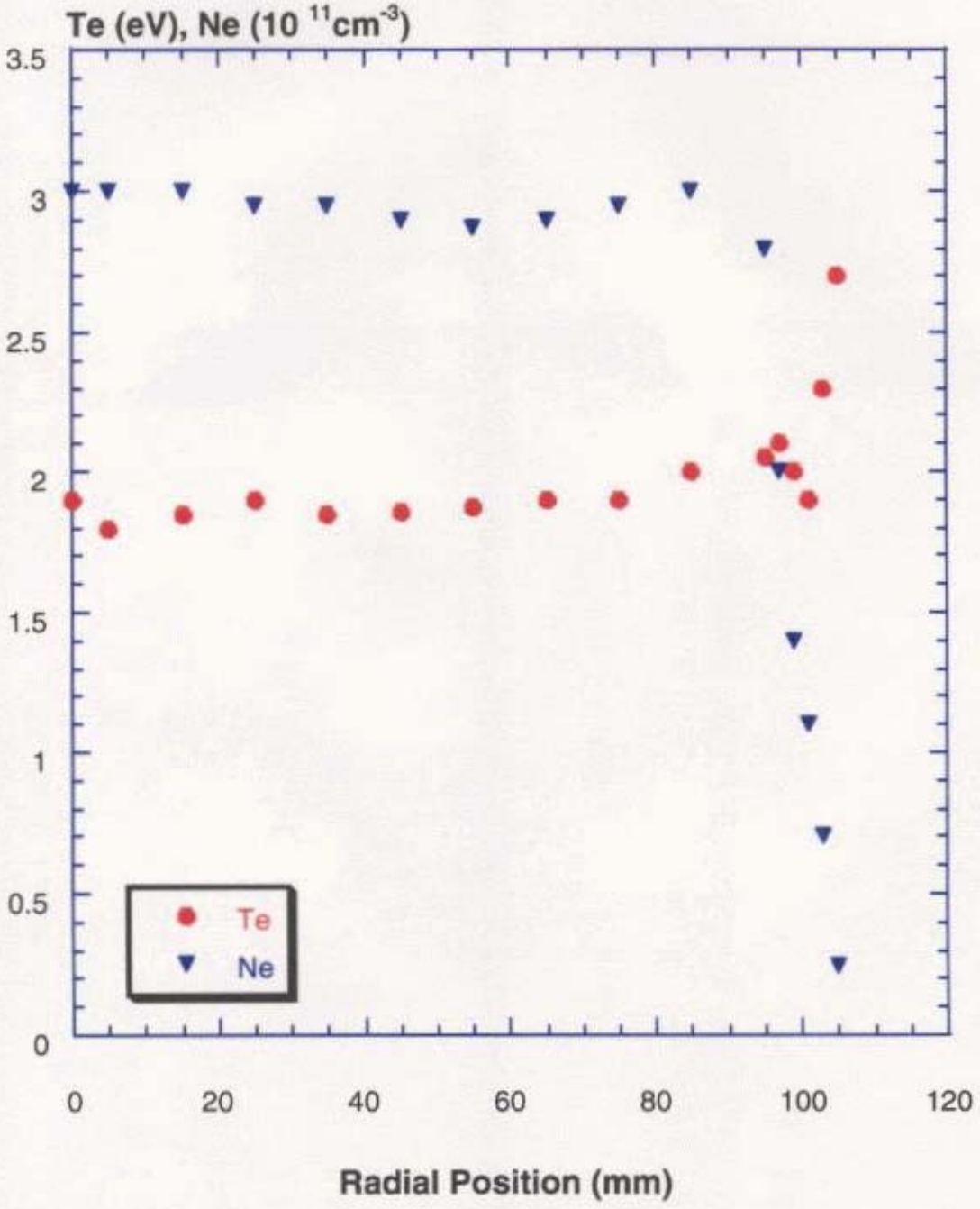

Fig18. Radial distribution of the plasma density N_e and electron temperature T_e in the plasma grid region for the hydrogen discharge, Pressure 4mTorr, input power 5 kW

4.7 U-probe and L-probe

To measure radial profiles on different levels of the plasma chamber and also plasma parameters within production chamber, two probes of complex construction were created. I call them L-probe and U-probe according to their shape (Fig. 19-1).

These probes can be installed from the top of the confinement chamber and move in the axial direction. They also can rotate around the input axis. A special precision dial was made to measure radial profiles. For the fixed position on the plasma source axis, radial profile was obtained by rotation of the probe and radial coordinate was recalculated from the rotation angle of the probe (Fig. 19-2).

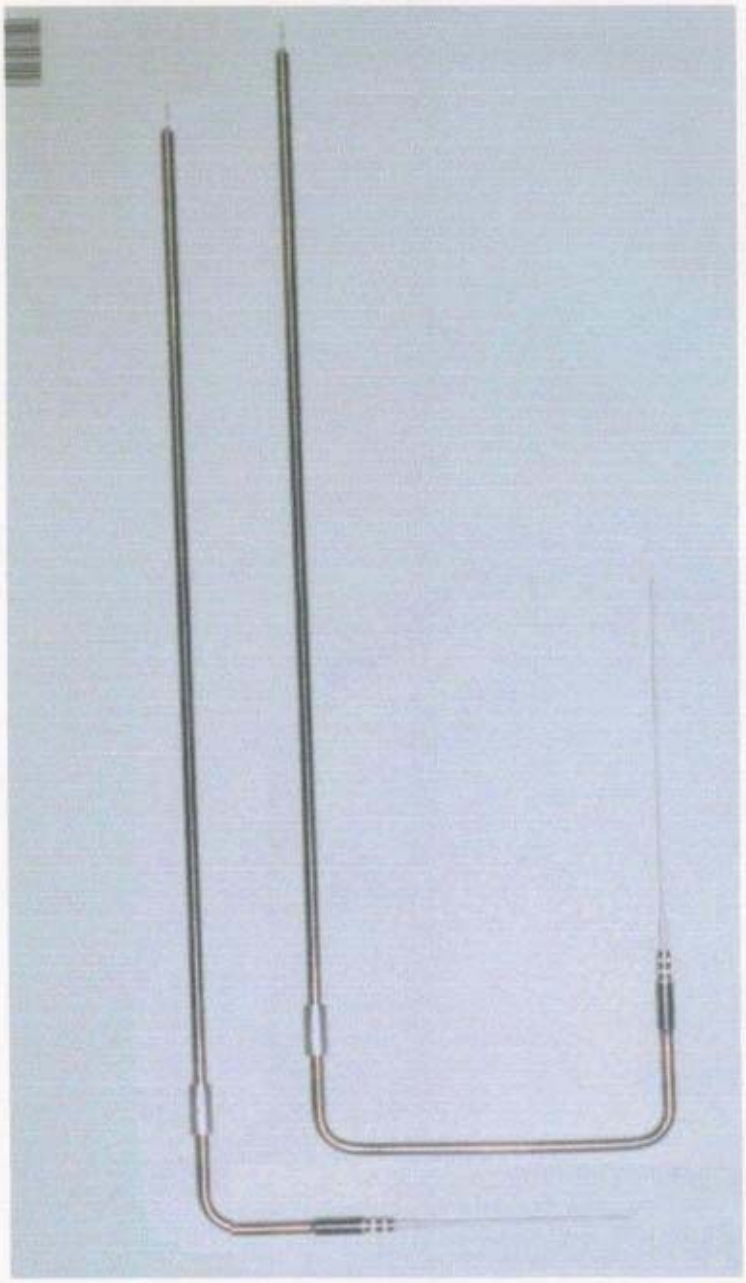

Fig. 19-1. Picture of L-probe and U-probe.

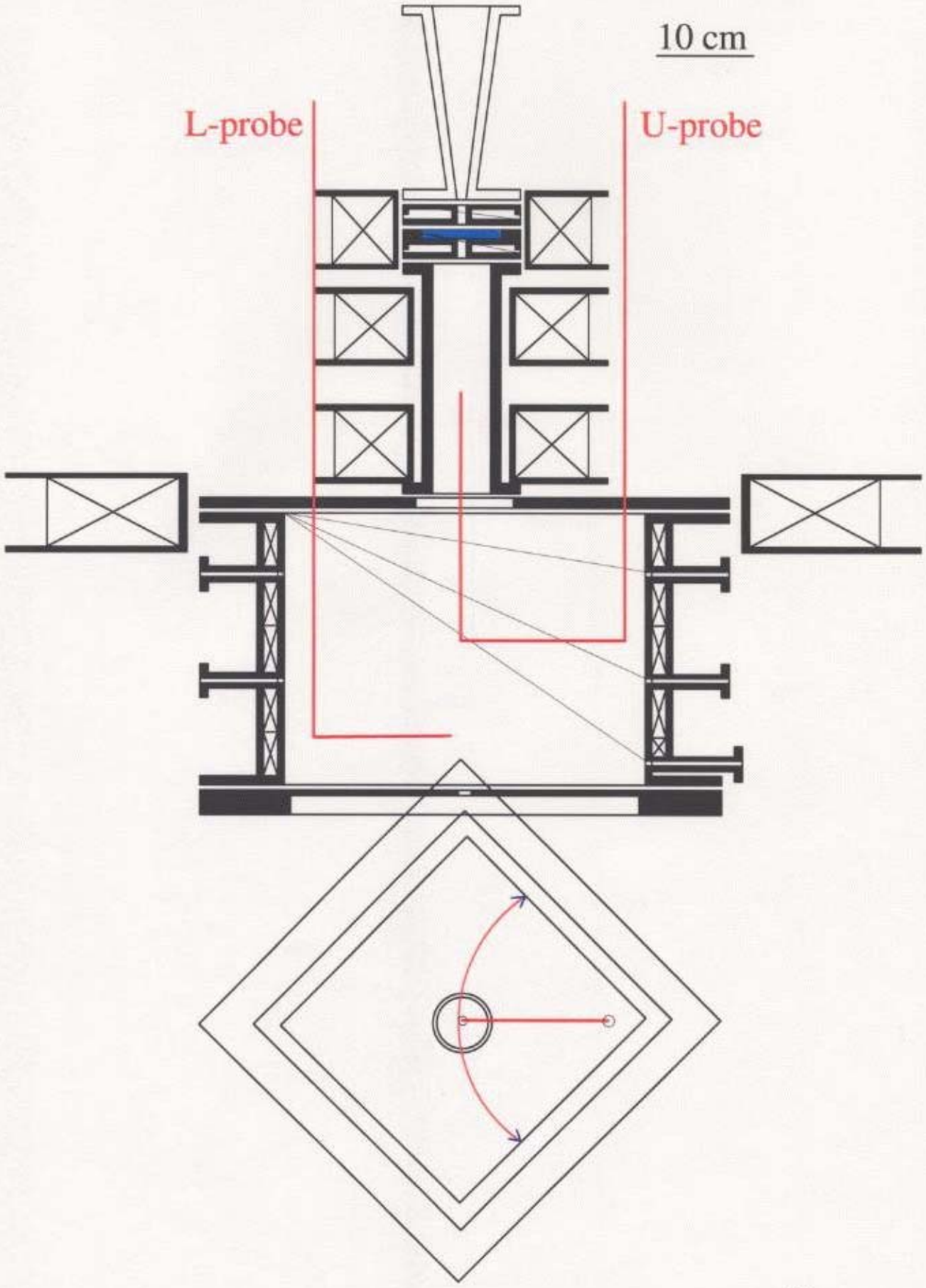

Fig. 19-2. L and U probes

L-probe is used to measure radial and axial distributions in the confinement chamber. U-probe is used to measure axial profile in the production chamber. Axial profiles of both probes were joined in the general axial profile describing plasma parameters along the z-axis from the quartz window at the top to the plasma grid at the bottom. Both probes are cylindrical shape, length 5 mm and diameter 0.3 mm. They are oriented perpendicular to z-axis. Probe s tips are embedded in ceramic tubes. There is no other insulation material except ceramics, because even glass melts in the plasma production region and Teflon wire insulation is affected by non-absorbed microwaves.

Results of the probe measurements are presented on the following graphs. On Fig. 19-3we can see axial plasma parameters distribution on a full range from the quartz window to the plasma grid. In the strongly magnetized plasma J_i and T_e are the most reliable parameters, while n_e data are practically incorrect in the strong magnetic field area.

$$J_i\,[mA/cm^2] = 9.52\, n_e\,[10^{11}cm^{-3}]\,(T_e[eV])^{1/2}$$

$$n_e\,[10^{11}cm^{-3}] = J_i\,[mA/cm^2] / 9.52\,(T_e[eV])^{1/2}$$

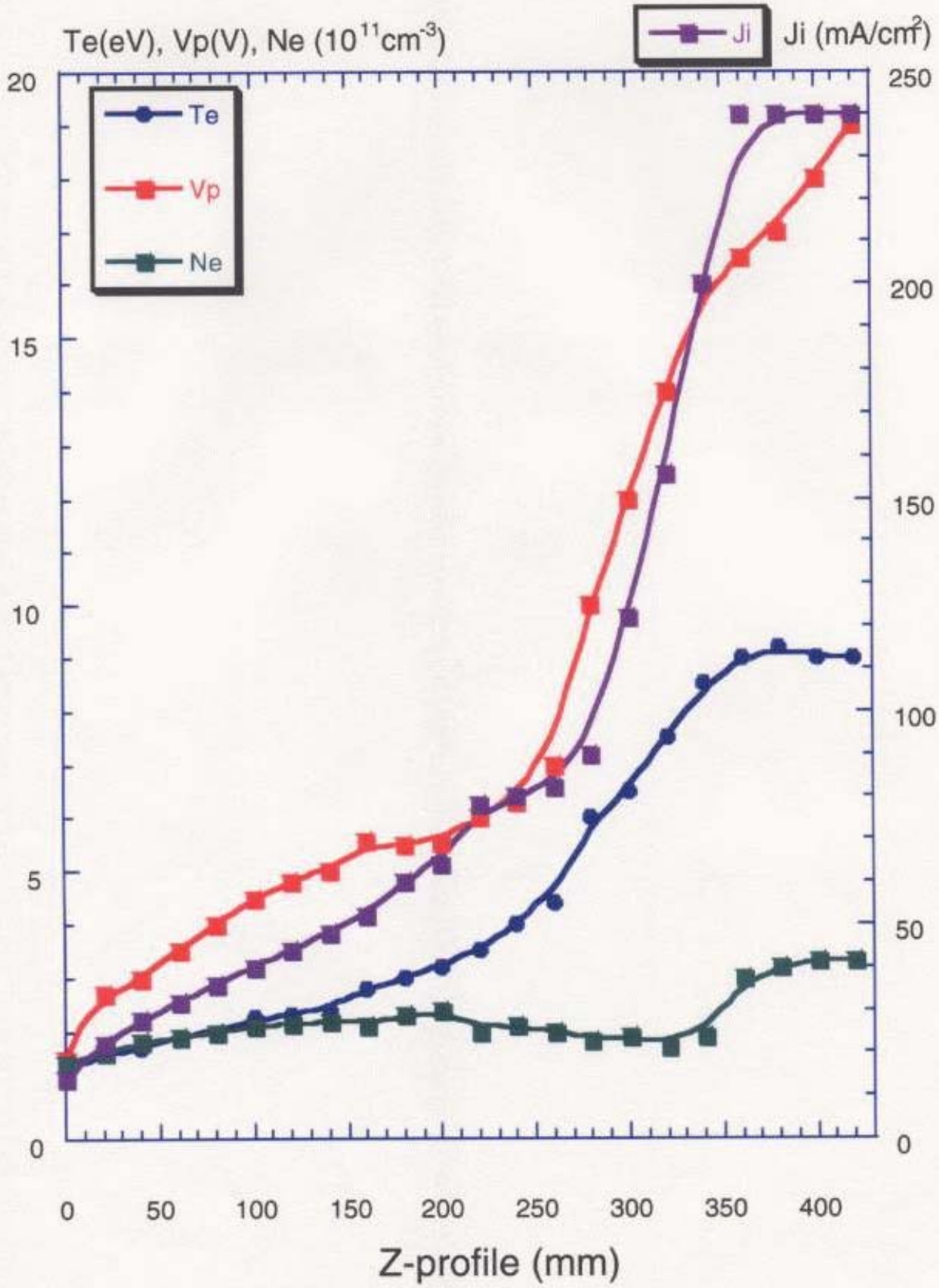

Fig. 19-3 Axial plasma parameters of the plasma source.
z=0 -plasma grid, z=300 chamber1/2 connection,
z=500 - quartz window

Evaluating plasma density near the plasma grid and in the production chamber, we can write:

J_i [mA/cm^2] = 20 mA/cm^2 ?? plasma grid Te = 1-2 eV

n_e [10^{11}cm^{-3}] = 20 [mA/cm^2] / 9.52 x (1-2[eV])$^{1/2}$ = 2.1-1.5 10^{11}cm^{-3}

This value is equal to the actually measured plasma density.

At the same time strongly magnetized plasma in the first chamber is efficiently bombarding 1-dimensionally only the double crossection of the probe, which is:

$S_{magnetized}$ =2 D L = 0.03 cm^2, while

$S_0 = \pi$ D L = 0.047 cm^2, $S_0/S_{magnetized} = \pi/2$.

In the production chamber:

J_i [mA/cm^2] = 240 x $\pi/2$ = 375 mA/cm^2, Te = 10 eV

n_e [10^{11}cm^{-3}] = 375 [mA/cm^2] / 9.52 x (10[eV])$^{1/2}$ = 1.25 x 10^{12}cm^{-3}

Total number of particles in 1 cm along z is:

N = n_e [10^{11}cm^{-3}] x S [cm^2] x 1 cm

$N_{production}$ = 1.25 x 10^{12} x 28 = 3.5 x 10^{13}

N_{grid} = 1.5 x 10^{11} x 400 = 6 x 10^{13}

We can see that there is a consistency between plasma flux leaving production chamber and plasma flux reaching plasma grid at the bottom of

confinement chamber. Plasma is cooled down and is getting uniform with considerably small losses.

Next I will present radial distribution measured at different levels of the confinement chamber for different current of the conditioning coil. On Fig. 19-4, 19-5, 19-6 we can see evolution of radial profile along Z.

Without conditioning coil the plasma density profile has a bell-shape with strongly expressed maximum in the middle, which is slowly deviating, but still preserving it' s bell-shape. Next graph for the B=0 at the plasma grid region shows, that coil 4 help to spread the flux and achieve uniform plasma density at the z-level, where B=0. Further increase of the conditioning coil current is also no good for the uniformity at the level of the plasma grid, where the value of B is passing the zero-mark and continue to increase. But at the same we see, that uniformity is obtained in the higher region (closer to the production chamber). Varying the current of conditioning coil 4 we can efficiently vary the z-coordinate where radial plasma profile gets uniform. That means, present magnetic field configuration allows us to vary in the wide range of Z the position where plasma becomes uniform and electrons are cooled down. That poses the question of the z scaling of the device. Considering the main processes happening in plasma, where along z

is it reasonable to place plasma grid and extract negative ion beam? Answer on this question is in the next chapter.

If we look on the profiles along the z-axis we can see that flux is preserved and plasma losses in the process of expansion are small.

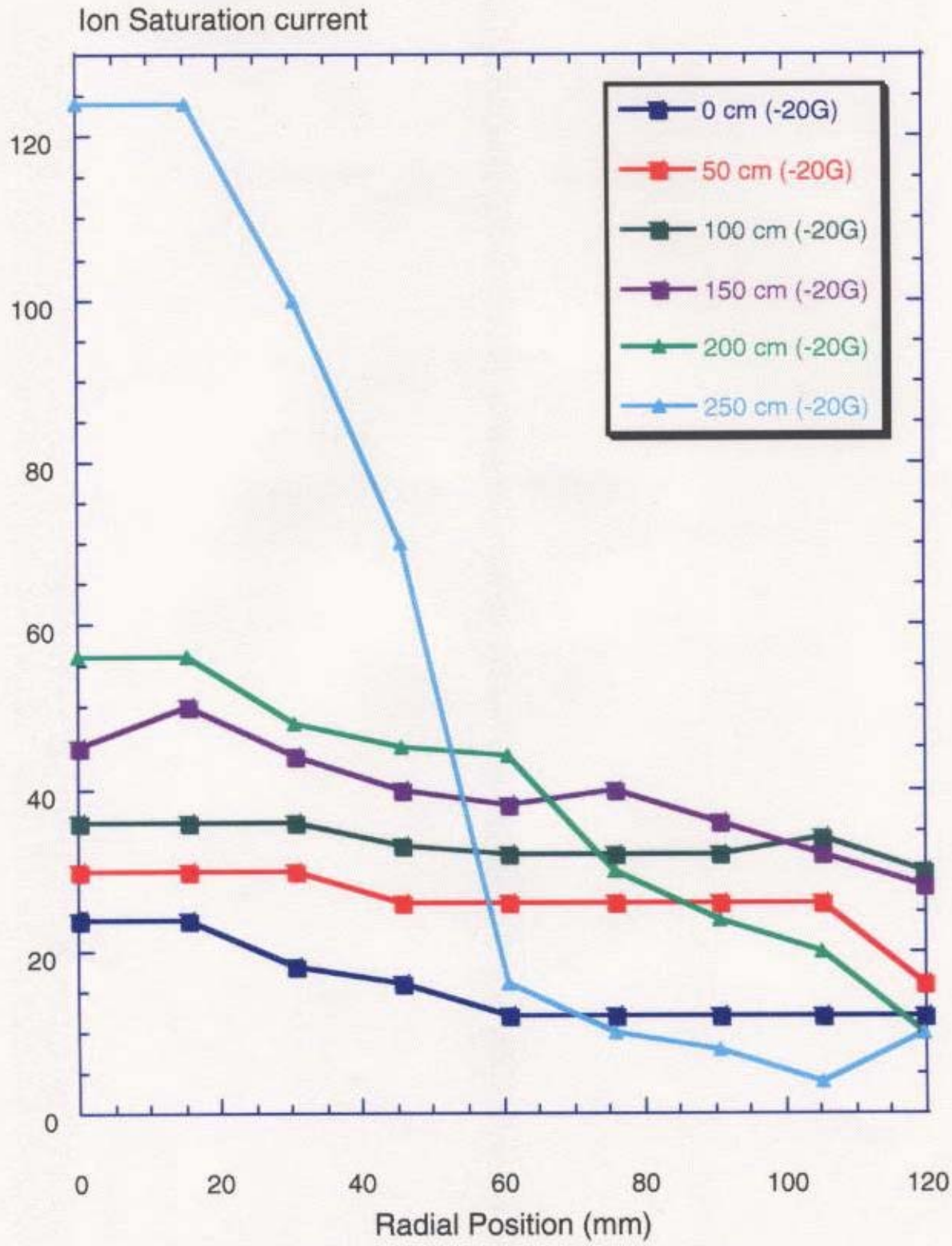

Fig. 19-4 Plasma flux deviation along the z-axis.
B=-20G, conditioning coil does not operate.
0 cm- profile near the plasma grid
250 cm - profile near the production chamber

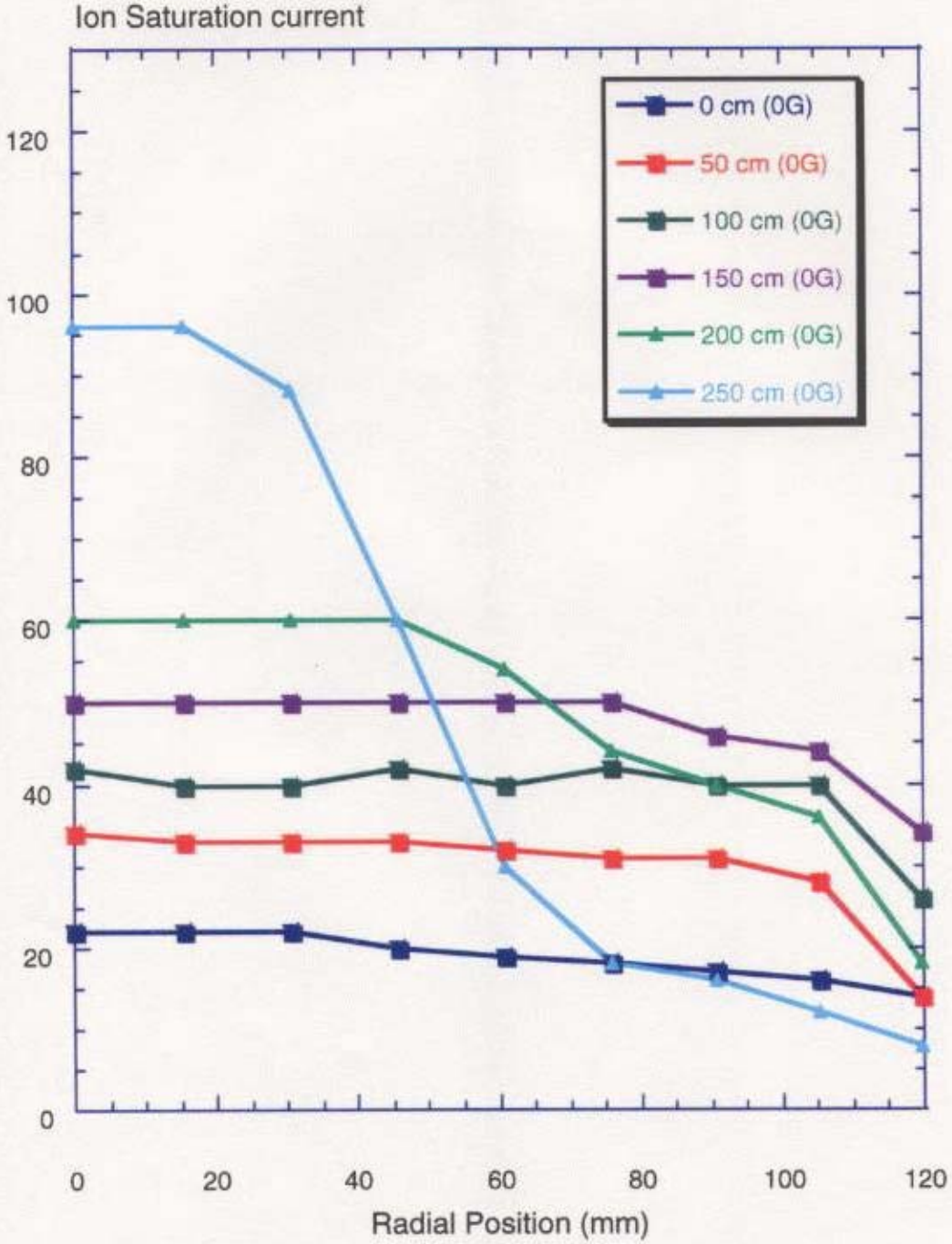

Fig. 19-5 Plasma flux deviation along the z-axis.
B=0G, conditioning coil operate.
0 cm- profile near the plasma grid
250 cm - profile near the production chamber

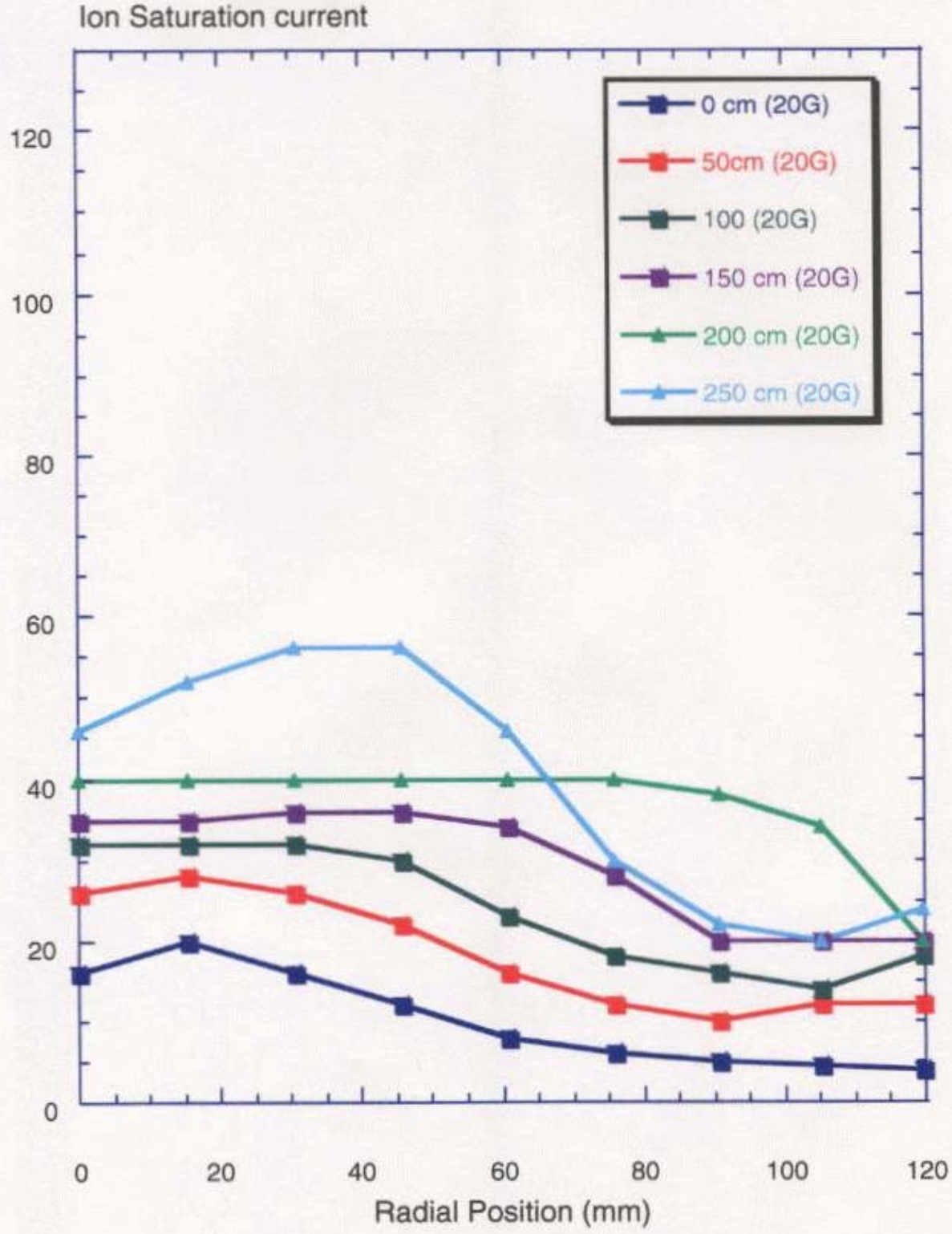

Fig. 19-6 Plasma flux deviation along the z-axis.
B=0G, conditioning coil operate.
0 cm- profile near the plasma grid
250 cm - profile near the production chamber

4.8 Optimized operation parameters of the plasma source

The purpose of plasma source optimization was to provide plasma parameters suitable for negative hydrogen ion source. That is: low electron temperature, high plasma density and uniformity. Electron temperature has been reduced to 2 eV. Plasma confinement improved by eliminating quartz window-side losses reducing plasma potential from 40 to 4-8 V and as a result increasing of the plasma density. Uniformity is within 3% and that is a good result for the industrial standard for plasma processing plasma sources.

We can summarize in this chapter optimal operation parameters of the microwave plasma source. These parameters were reported elsewhere[49].

Microwaves 2.45 GHz, Power 5 kW

Magnetic field in the production chamber 1800 G

Magnetic field at the plasma grid 0 G

Operation pressure 4 mTorr

20x20cm square crossection uniform (within 3%) plasma region

Argon: Ne=3x1012cm-3, Te=2eV

Hydrogen: Ne=3x1012cm-3, Te=2eV, reducible to 1 eV.

5. Negative hydrogen ion beam extraction and measurement system

5.1 Electric scheme and insulation diagram

To extract and measure the negative hydrogen beam the following biasing scheme was applied (Fig. 20). Confinement chamber, plasma grid and production chamber with the waveguide up to DC-cut unit were biased negatively. Extraction grid, magnetic coils system, magnetron with a waveguide before the DC-cut unit and Faraday cup measurement system are grounded.

Total electric scheme is presented on Fig. 21. Plasma Chamber and the plasma grid respectively are biased negatively (0-10 kV) in respect to the ground. Extraction grid is grounded. Biasing plasma grid, not extraction grid allows us to keep the diagnostics system at ground potential.

Magnetic filter installed inside the extraction grid creates magnetic field of 200 G and deflects the electrons extracted together with negative hydrogen ions.

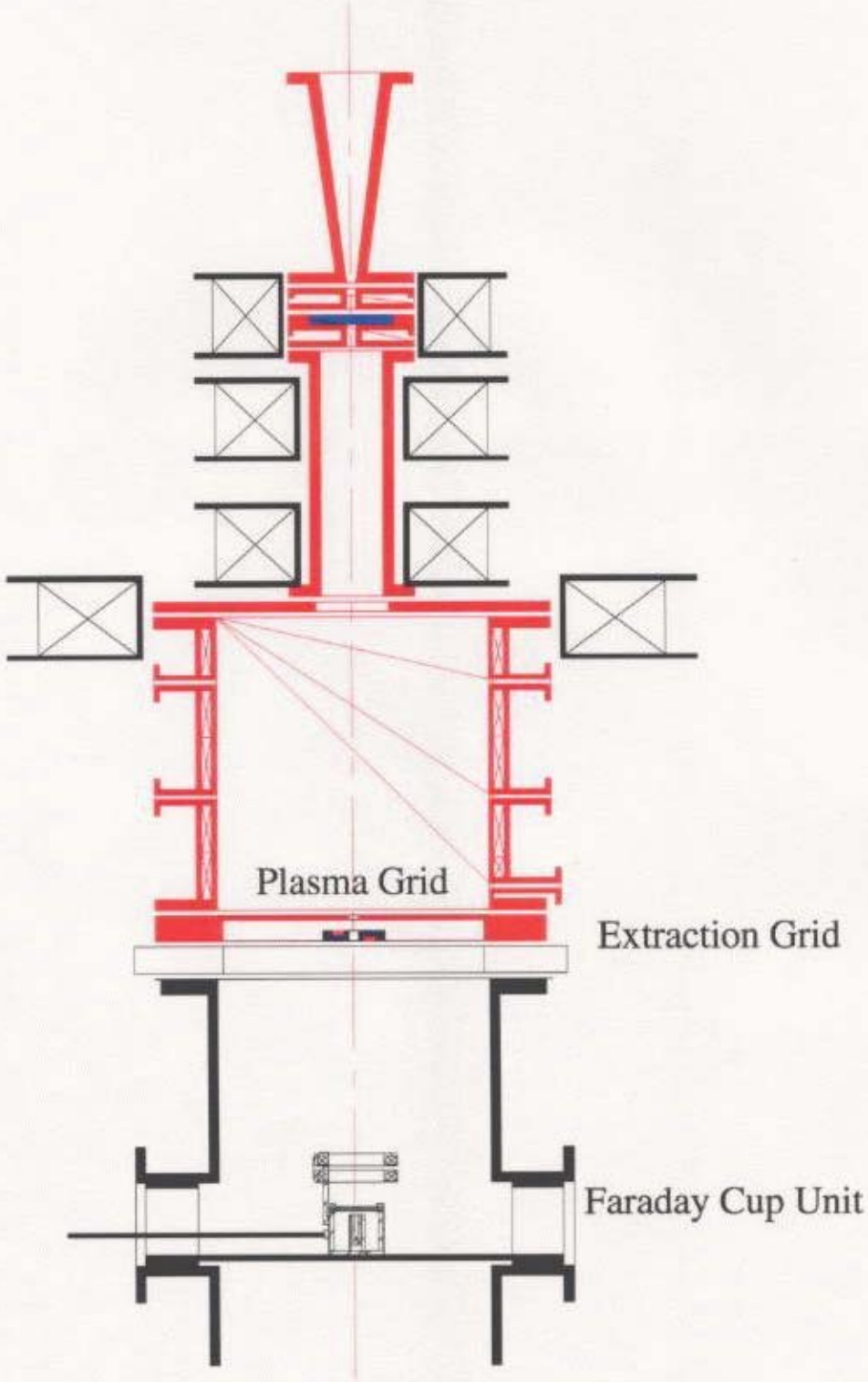

Fig. 20. Extraction system diagram: red color depicts high-voltage biased parts of the device. Coils are insulated from the plasma source by teflon shielding.

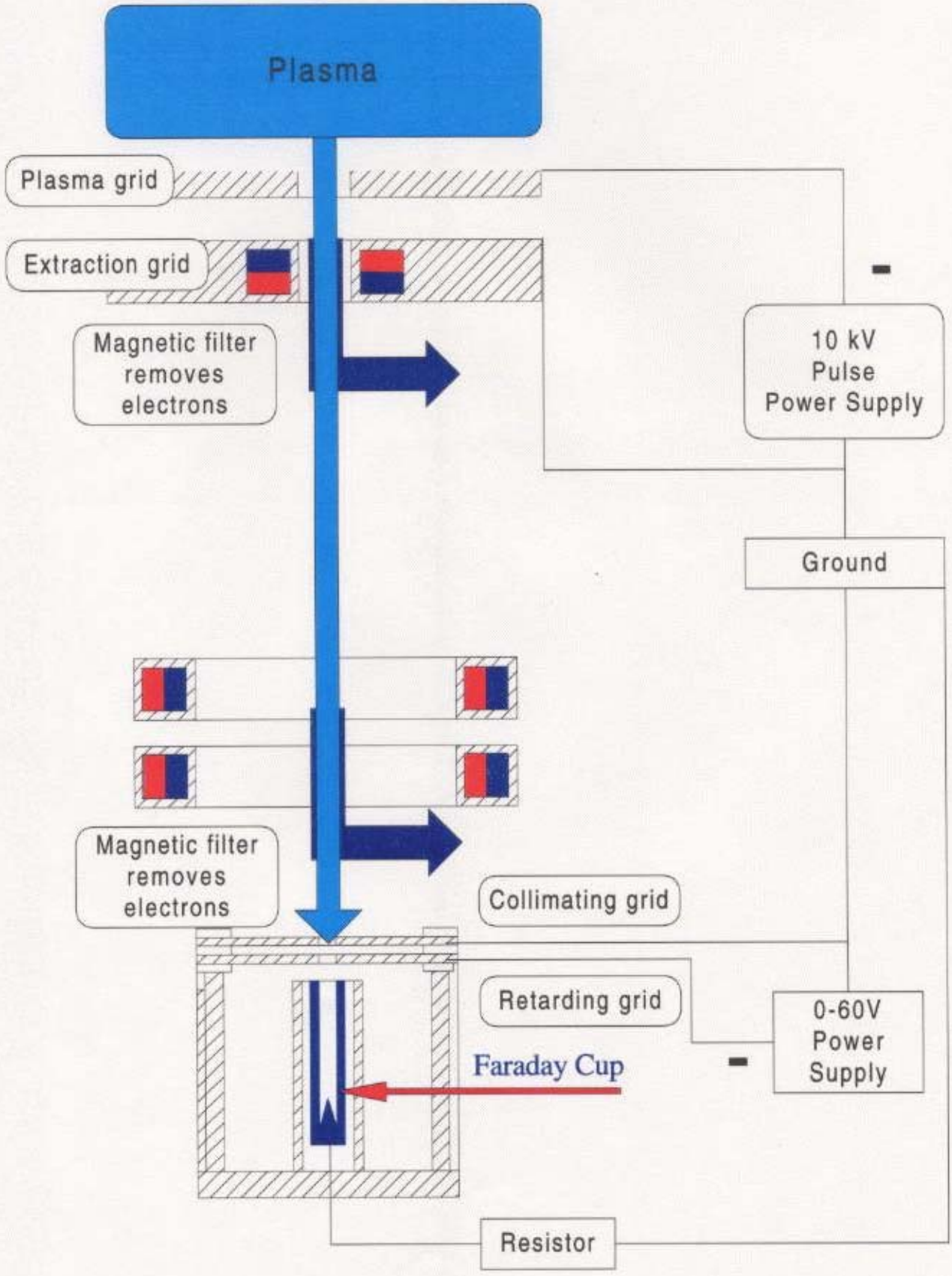

Fig. 21. Electric scheme of the beam extraction and measurement system

5.2 Faraday cup system design

A Faraday Cup Unit (a row of 9 Faraday cups) is used to measure the extracted beam radial distribution. Each Faraday cup is placed in the shielding case and connected to the ground through resistor. Voltage from this resistor is used to measure the total current coming to each Faraday cup. Each Faraday Cup has an independent RC circuit to reduce the noise.

Faraday cup has a characteristic cone structure at the bottom to reduce secondary electrons output. System of collimating and retarding grids placed in front of the Faraday cup serves to collimate incoming beam and reflect secondary electrons trying to escape the Faraday cup. It is found experimentally, that retarding grid potential over 20 V is sufficient to keep secondary electrons from escaping the Faraday cup.

Faraday cup unit (Fig. 22, 23, 24) has 9-channels arranged along the x-axis and the unit can be moved in the perpendicular y-direction to provide extra flexibility in the beam center position detection. Depending on the extraction voltage and the residual magnetic field value in the plasma grid region, beam center may deviate from the geometrical center of the device. X-Y scan also allows measuring 2-dimensional beam profile.

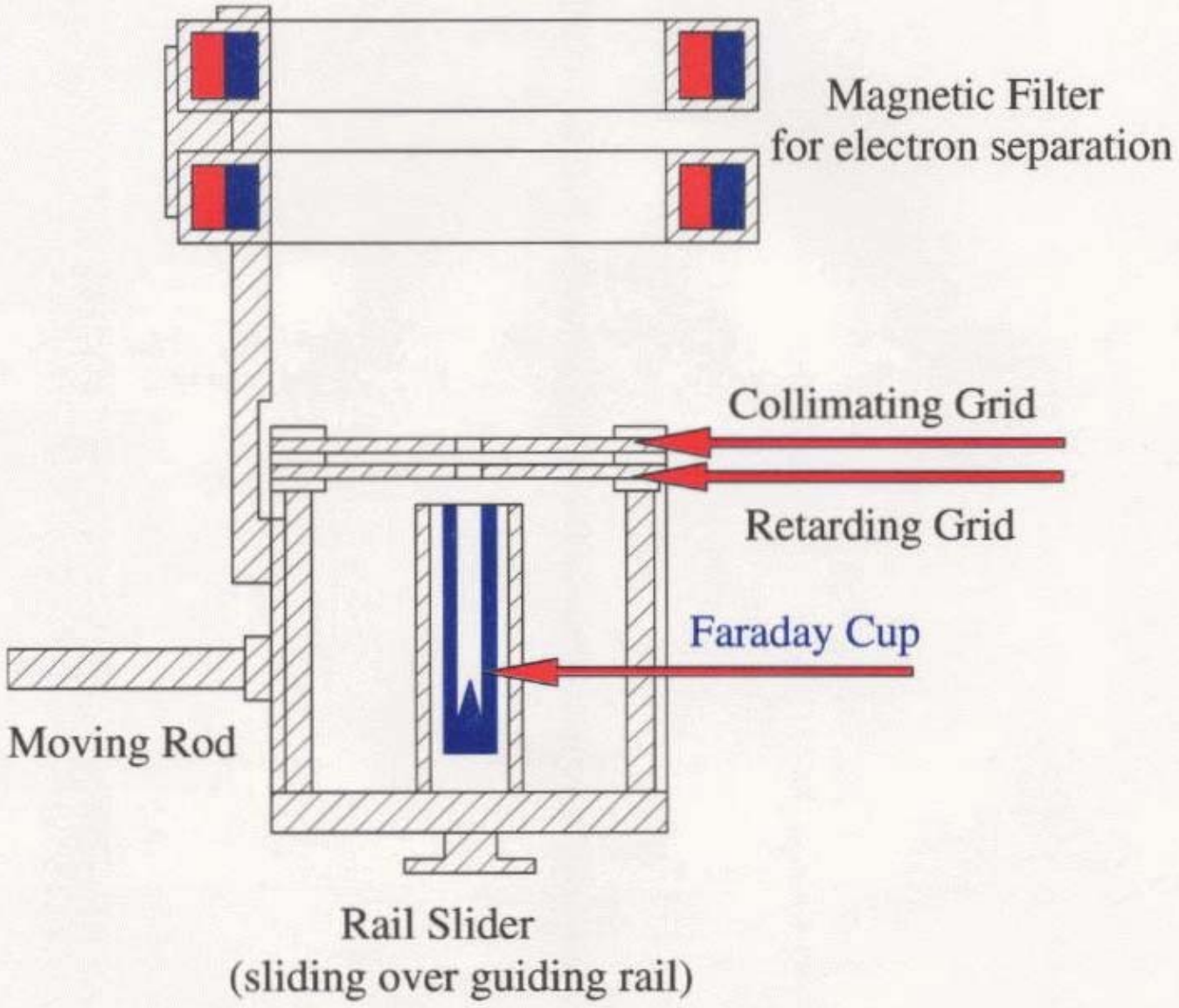

Fig 22. Faraday Cup Unit with the magnetic filter installed.

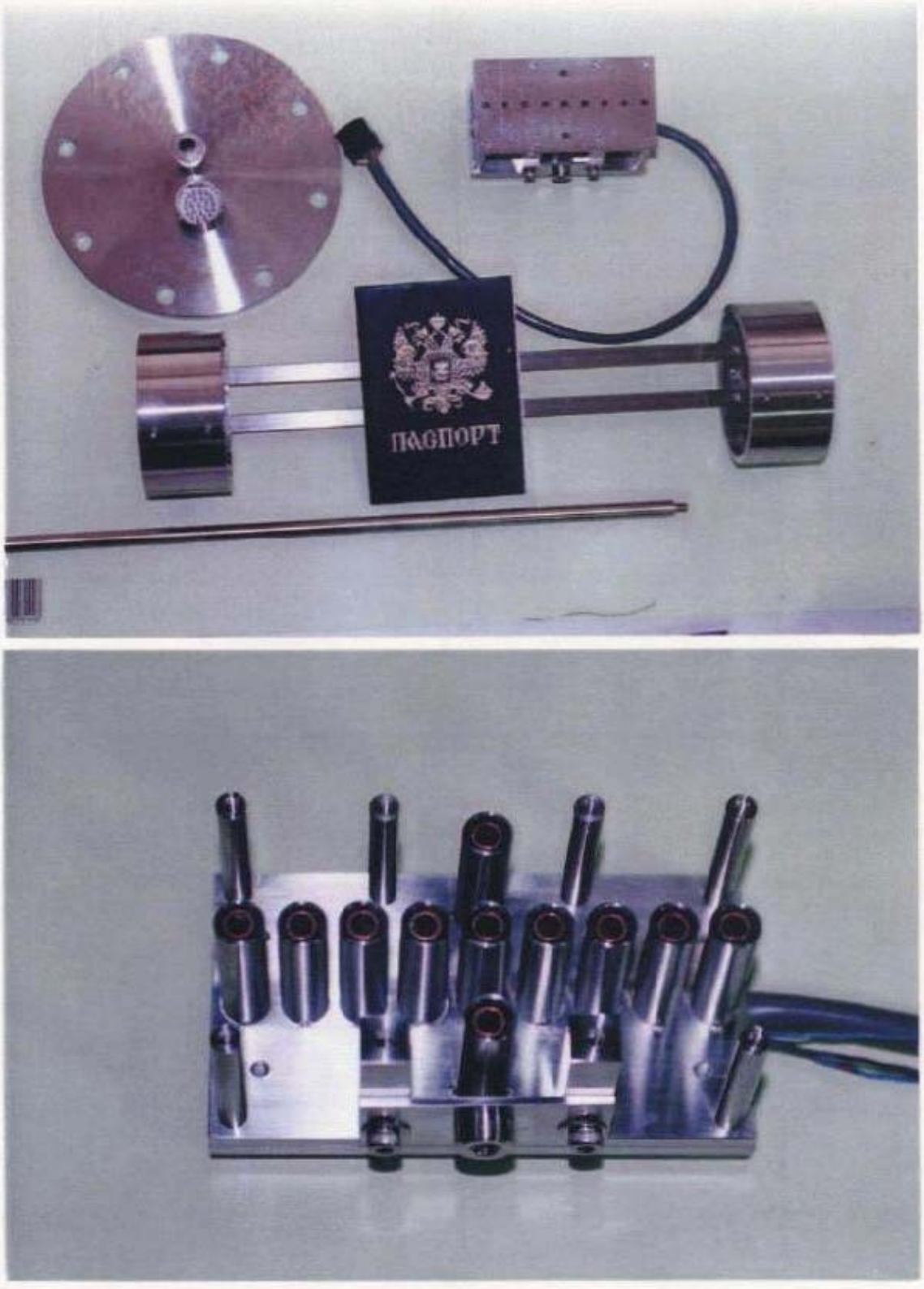

Fig. 23 Faraday cup unit

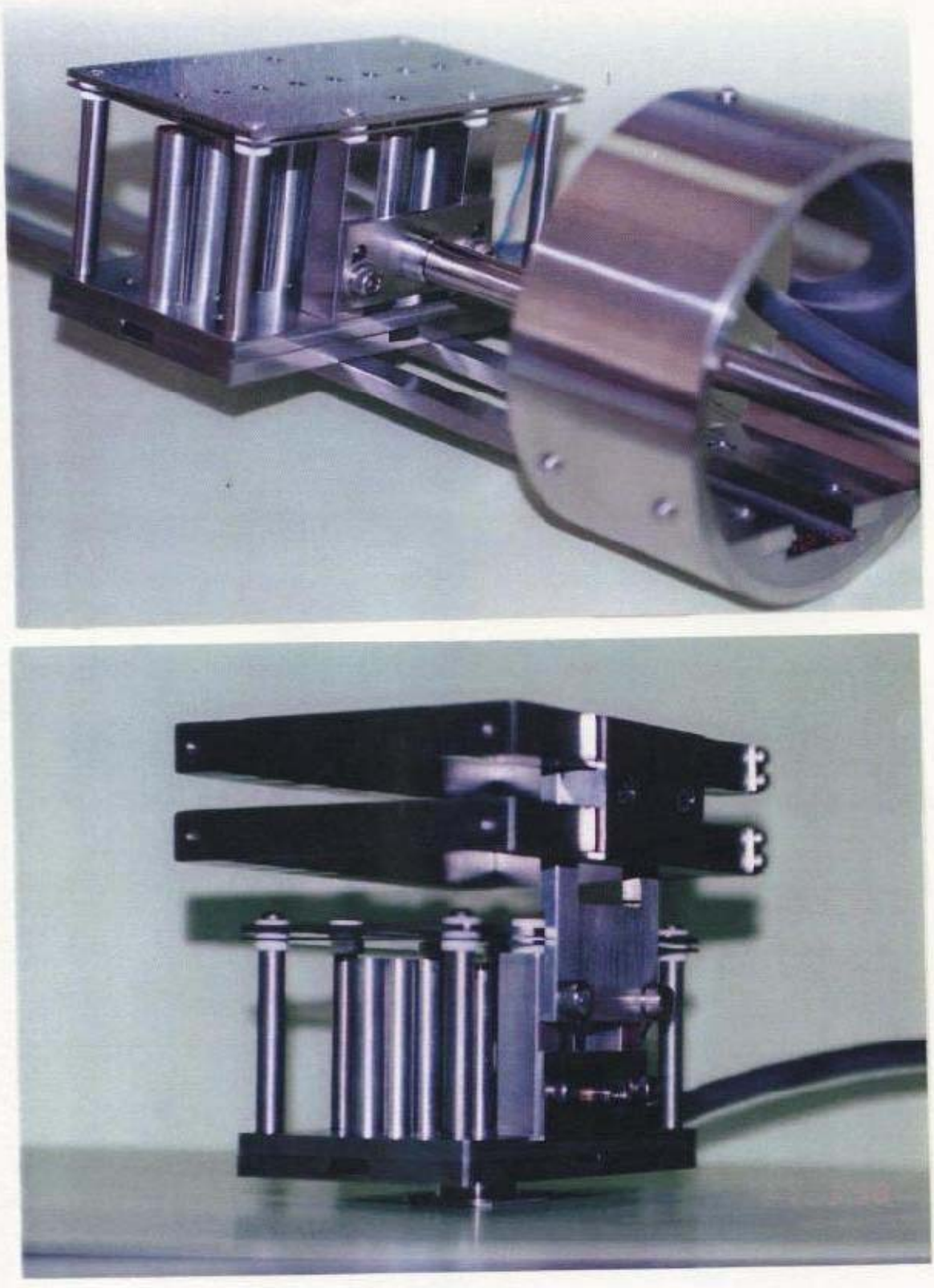

Fig. 24 Faraday cup unit with magnetic filter

On the first stage of experiments residual electron beam was passing the magnetic filter of the extraction grid and reaching the Faraday cup unit. To remove residual electrons two steps were made: 1) magnetic filter of the extraction grid strength was increased from 60 to 200G, 2) extra magnetic filter was manufactured and placed above the Faraday cup unit (Fig. 22, 24). After applying the extra magnetic filter which was placed on the special holder 5 cm above the Faraday cups row, the residual electron beam was eliminated.

To test if all the electrons are removed before the negative ion beam reaches the Faraday cup unit, experiments with argon and helium were held. In case of argon and helium there are no negative ions and only electrons are extracted. Absence of the signal on the Faraday cup unit should be the proof that magnetic filters are working well and no electrons reach the Faraday cup unit. At the same plasma parameters and extraction voltage of 5kV no signal was observed from the Faraday cups for argon and helium. Faraday cup measurement system was tested to be reliable and hydrogen data presented below- trustworthy.

National Instruments © Data Acquisition (DAQ) board AT-MIO-16E-1 have been used for simultaneous acquisition of 16 channels (including 9 Faraday cup channels, dark current, extraction grid current and high voltage). DAQ board was operated using LabView 4.0 © software. Example of 9-channel beam data is presented on Fig. 25. We can see that during operation extracted beam is very stable. Beam shape and intensity are unstable when plasma is unstable. Microwave plasma source presented in this paper can be characterized by high level of operational stability.

Data obtained using this Faraday cup unit are used for the estimation of the negative ion production. Measurement of the extracted negative ion beam density is typical in R&D of negative ion sources and allows us to compare the efficiency of this ion source with others.

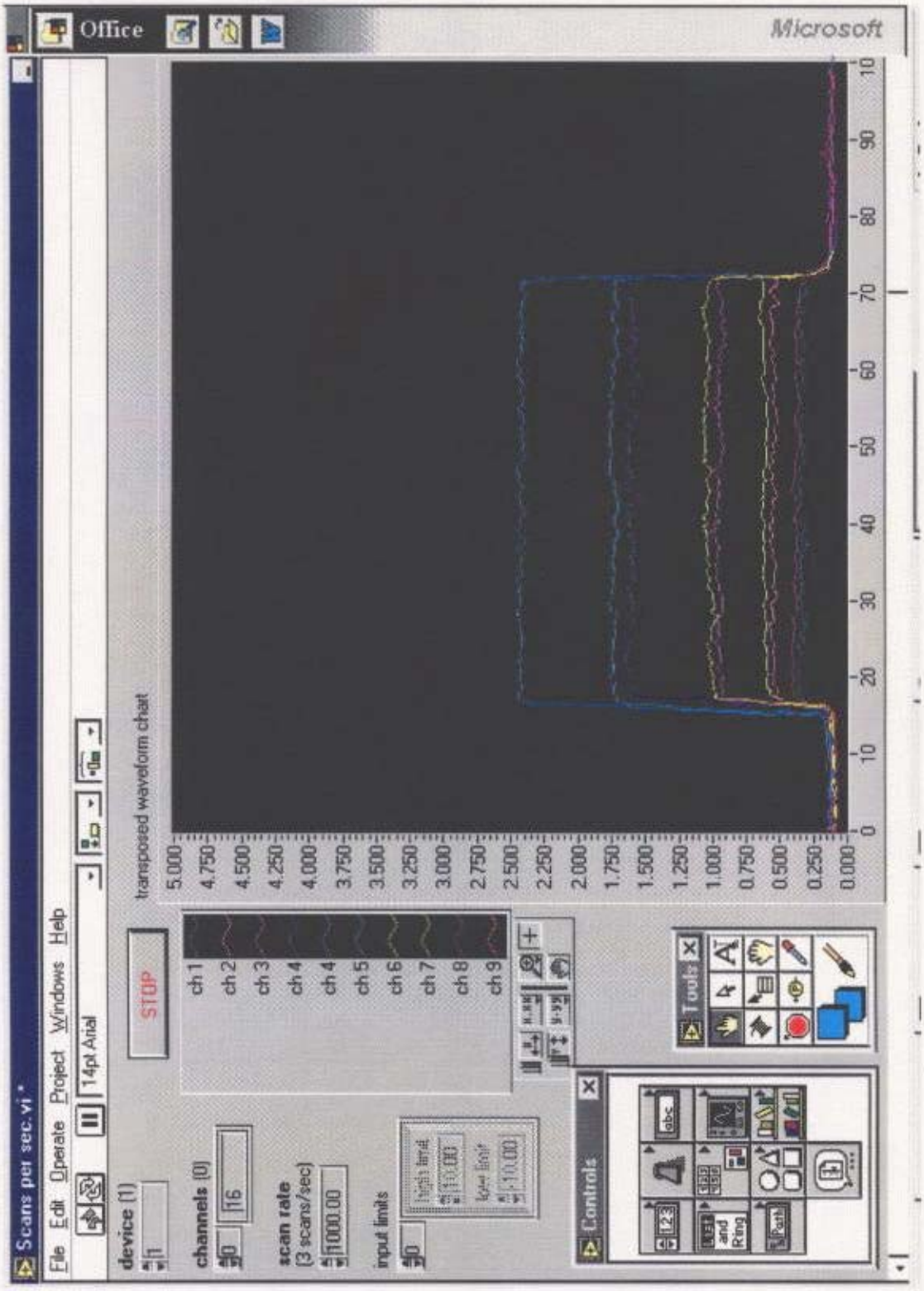

Fig. 25. 9-channel Faraday Cup system DAQ by LabView

6. Negative Hydrogen Ion Beam Parameters

6.1 Negative Ion Stripping

The stripping loss estimation[50] is important for evaluation of actual beam parameters. As far as the Faraday cup unit is located 30 cm below the extraction grid, it is necessary to take into account the negative ion stripping losses in the beam. I assume that the negative ion fraction goes down exponentially with the gas target thickness and calculations are made based on the stripping loss crossections[51]. This work also reports that actual beam losses exceed the losses directly calculated using only the H^- - H_2 collisional crossection and increase due to the secondary low-energy particles generated by the beam. We can assume that the beam current density reported here might be slightly underestimated.

$$I_{H^-} = I^0{}_{H^-} \exp(-n_{H2}\, \sigma\, z),$$

where z is a coordinate along the beam, and σ is a crossection of H^- and H_2 collisions. This formula would be used in the next chapter to reconstruct the actual value of the extracted H^- current.

6.2 Beam Profile

For the effective measurement of the total beam current, negative hydrogen beam has to be appropriately focused. We can not change extraction system parameters and beam focusing in our case totally depends on the extraction voltage. Extraction voltage dependence of the beam profile has been taken (Fig. 26) and on the basis of this measurements the acceleration voltage of 5 kV has been chosen for the beam measurement experiments.

By scanning in the y-direction, perpendicular to the x-direction along which the Faraday cup array is aligned, the 2 - dimensional beam profile was obtained (Fig. 27). The contour profile of the beam (Fig. 28) shows that the beam is slightly elongated in the y-direction as a result of the applying of the magnetic filter at the extraction grid. This fact has been taken into consideration when the total beam intensity was calculated. To calculate the total H- flux Gauss fitting of the collected data was applied.

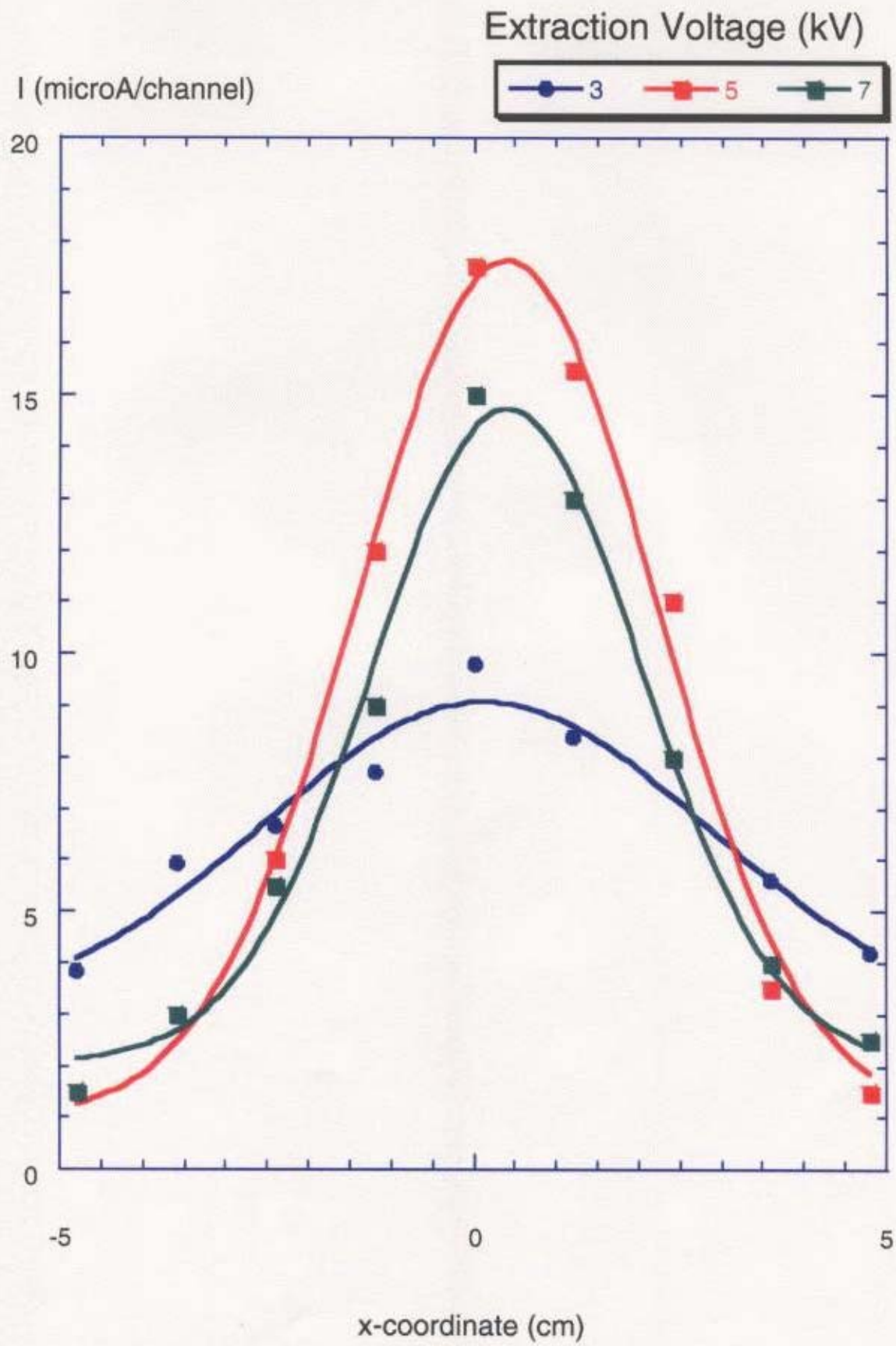

Fig. 26 Beam Focusing - beam profile
for the extraction voltage values of 3, 5, and 7 kV respectively.

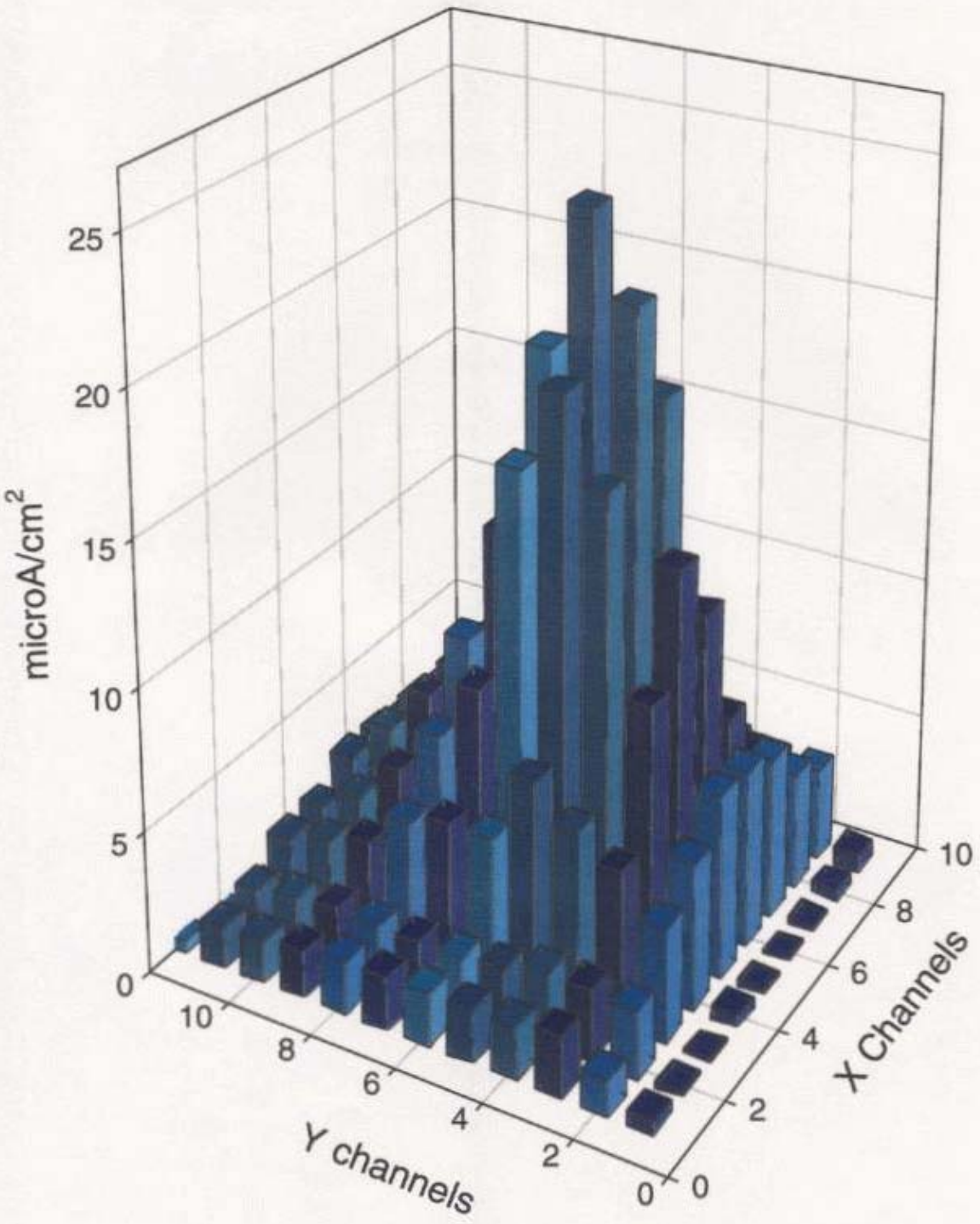

Fig. 27. Two-dimensional negative hydrogen ion beam profile for the extraction voltage of 5kV, microwaves power 5kW.

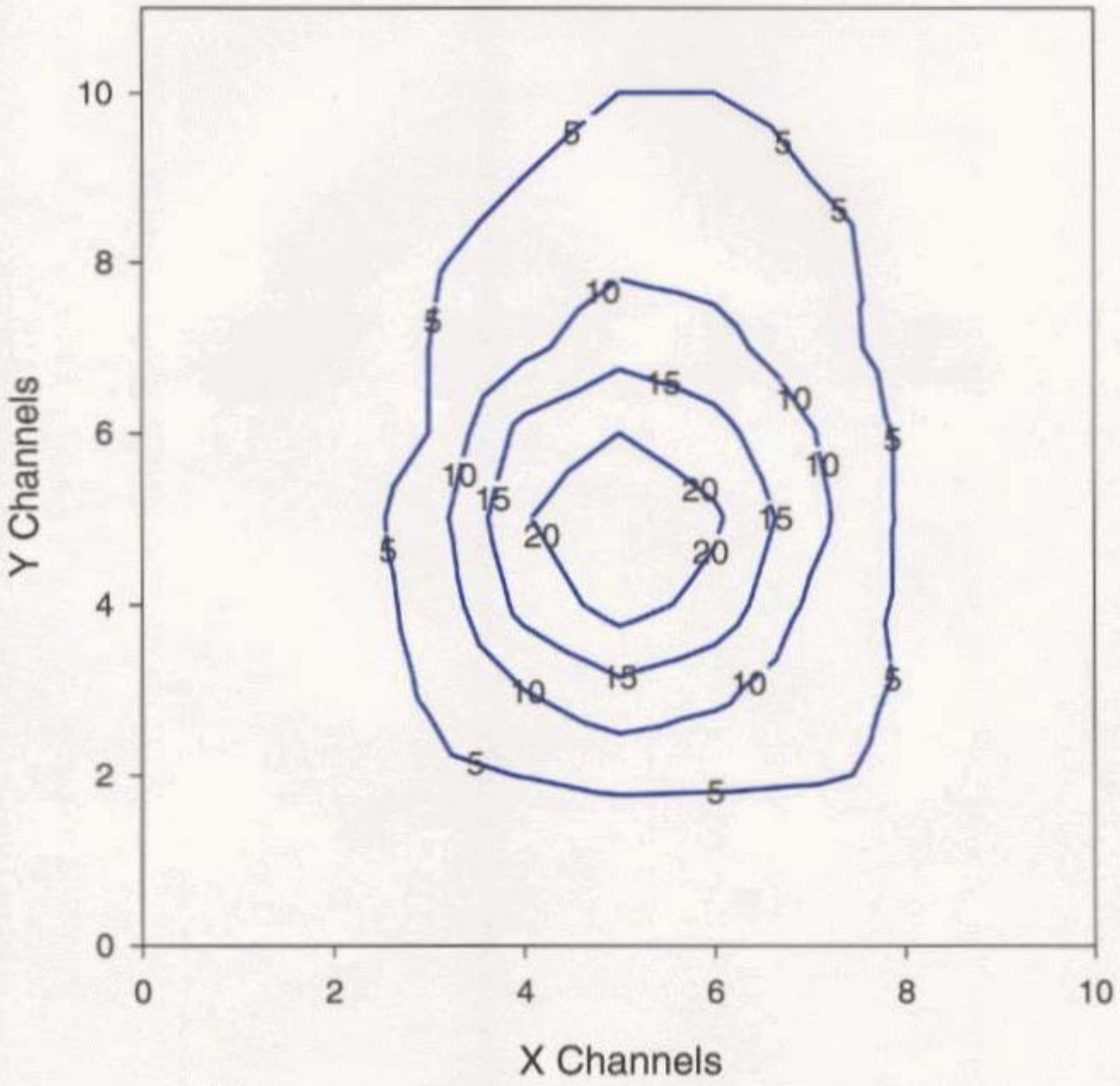

Fig. 28. Two-dimensional negative hydrogen ion beam contour profile.

7. Dependence of the negative hydrogen ions generation on plasma parameters

7.1 Magnetic field in the plasma grid area dependence

Conditioning coil 4 is used to reduce electron energy in the plasma grid area. It also changes the plasma drift root from production to confinement chamber. We tested how the conditioning coil 4 current (and the magnetic field strength in the plasma grid area respectively) affect the negative hydrogen ion production. Resulting beam profiles are summarized on Fig. 29. As we can see, magnetic field in the plasma grid (extraction) area causes beam deviation, because in this case the magnetic field of the filter in the extraction grid (60-200 G) superposes with the residual field of the coils system (0-30 G). Beam deviation moves from right to left while magnetic field is changed from negative to positive.

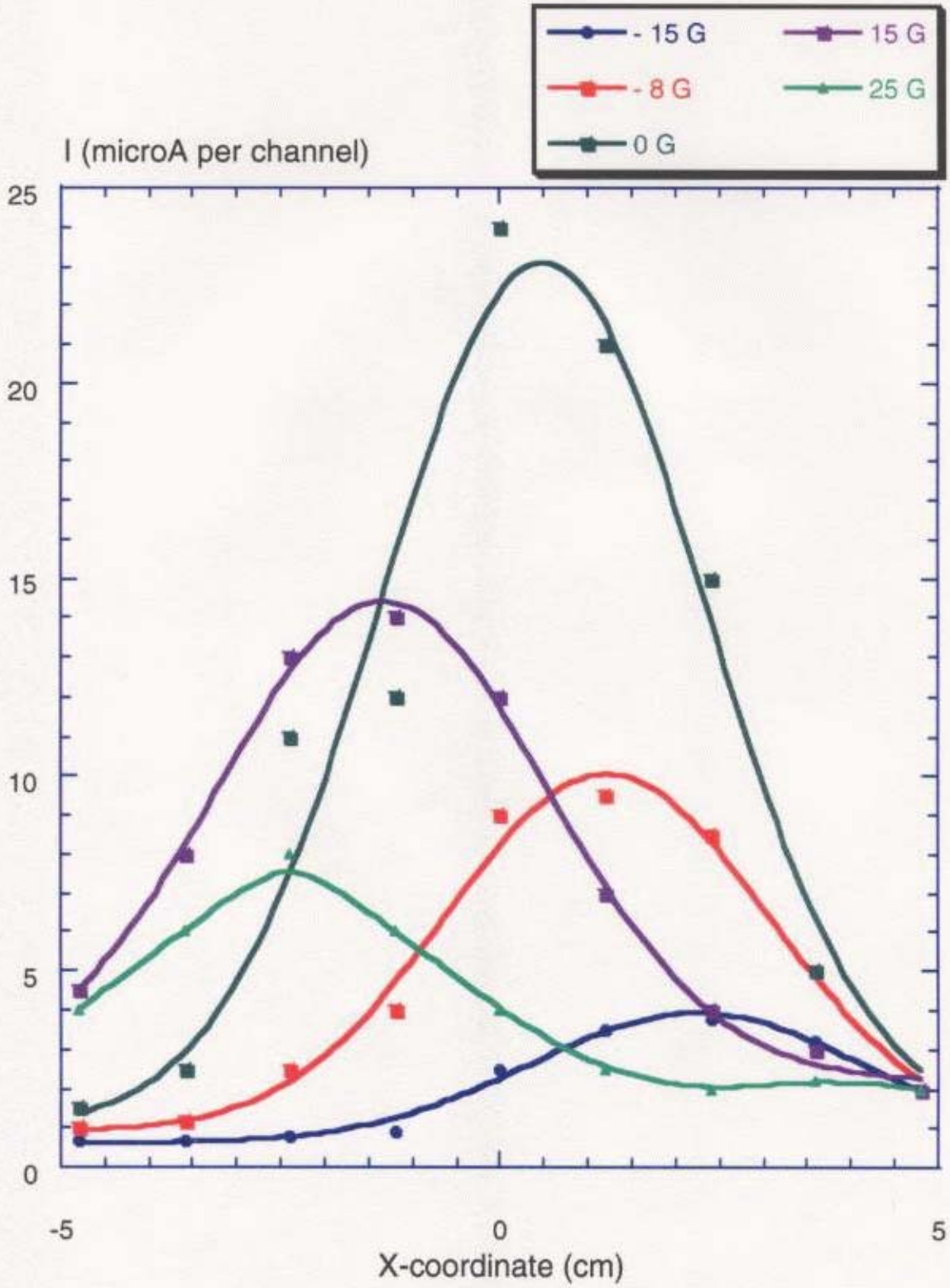

Fig 29. Beam profile dependence on the value of recidual magnetic field in the plasma grid area

To understand the reason of the beam deviation with the changing of the magnetic field in the plasma area, we need to take a look on the mutual orientation of the magnetic filters (Fig. 30). We can see that superposition of the residual magnetic field and the magnetic filter field gives asymmetric magnetic field lines structure.

We can consider that at the entrance to the acceleration region (Fig. 30 area (1)), negative ions have thermal speed. That corresponds to the ion temperature of $T_{H^-} \sim 0.03$ eV and $r_c(H^- 200G, T_{H^-}) = 1$ mm

After passing the magnetic filter negative ions region (Fig. 30 area (2)), energy turns to be 5 kVand $r_c(H^- 200G, 5keV) = 36$ cm

That means, H^- beam is affected by the magnetic field in the area (1) at the process of beam acceleration and is relatively unaffected by magnetic field after acceleration in the area (2).

If the magnetic field of the filter is symmetric, there is no big effect on beam deviation, but if the magnetic field has asymmetric behavior as a result of magnetic field superposition, then magnetic field behavior in the beam acceleration region defines beam deviation.

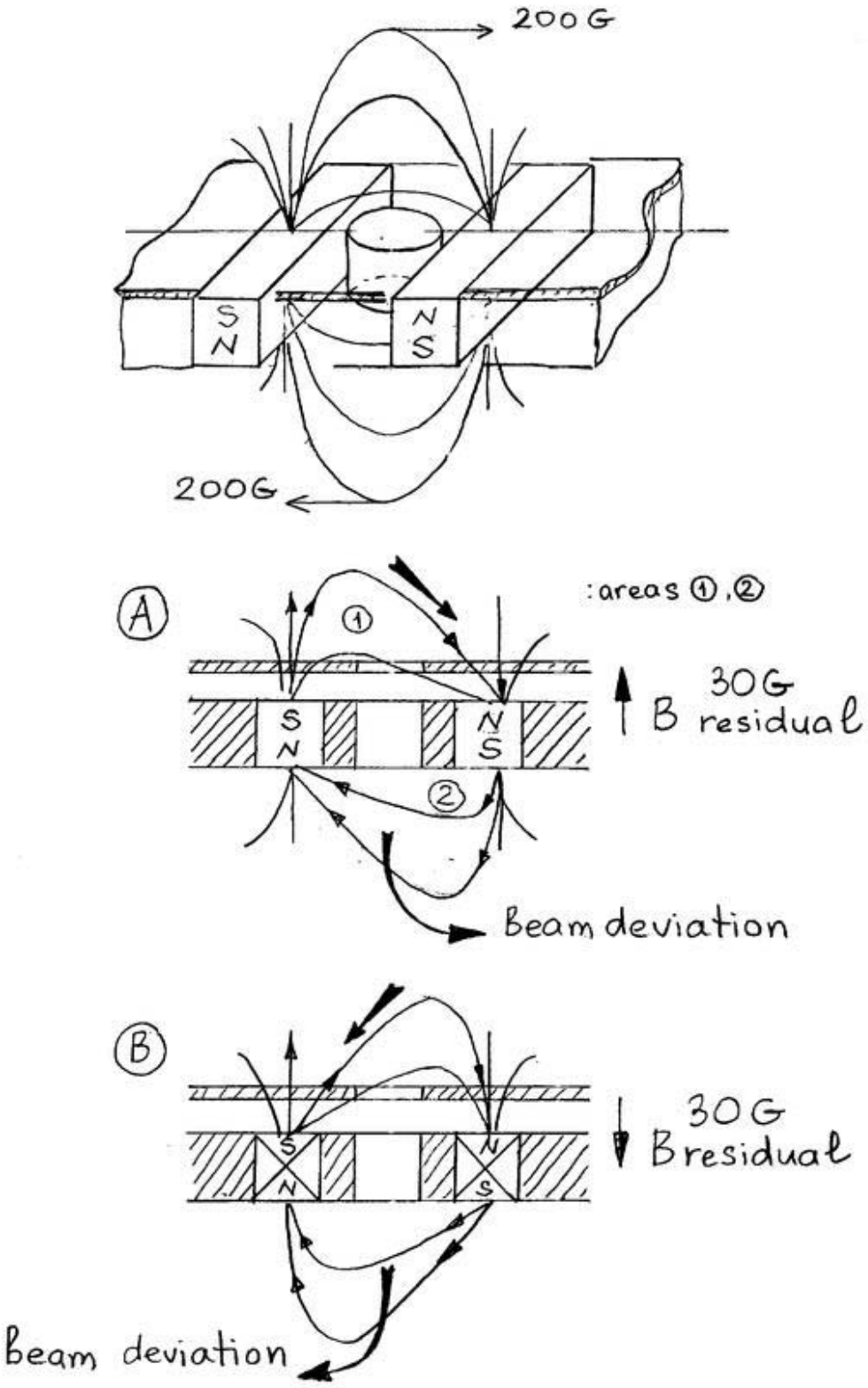

Fig. 30 Beam deviation

Left and right beam deviations are shown on fig. 30 (A and B) as a result of the residual magnetic field orientation.

Calculated negative hydrogen beam current is shown together with plasma parameters on Fig. 31-1. Negative hydrogen ions output is proportional to the plasma density, except for the left part of the graph, where electron temperature is high and H- current is decreasing faster than plasma density. This is obvious because several-eV electrons and residual high-energy electrons, which directly reach the plasma grid area, are efficiently destroying negative hydrogen ions. These results characterize the operation of the conditioning magnetic coil 4. With increase of the coil 4 magnetic field, B at the plasma grid area decrease and magnetic field lines leaving coils 1-3 are bent and end-up at the confinement chamber walls. When B=0 at the plasma grid region, there are almost no lines which end up on the plasma grid and therefore there is no direct flow of the high-energy electrons from the plasma production area. After graph is passing B=0 point there is no further decrease of the electron temperature. Further bending of the magnetic field lines results in longer diffusion path for plasma and more plasma losses to the wall and therefore decrease of the total plasma density

at the plasma grid area. From this point on (B>0, Te=2eV, constant), negative hydrogen ion production is proportional to the plasma density. This dependence is clear if we plot n_H/n_e ratio dependence on T_e (Fig.31-2). For the temperature about 2 eV H^- ratio in plasma is proportional to plasma density, but when electron temperature increases to 4 eV, n_H/n_e quickly decreases.

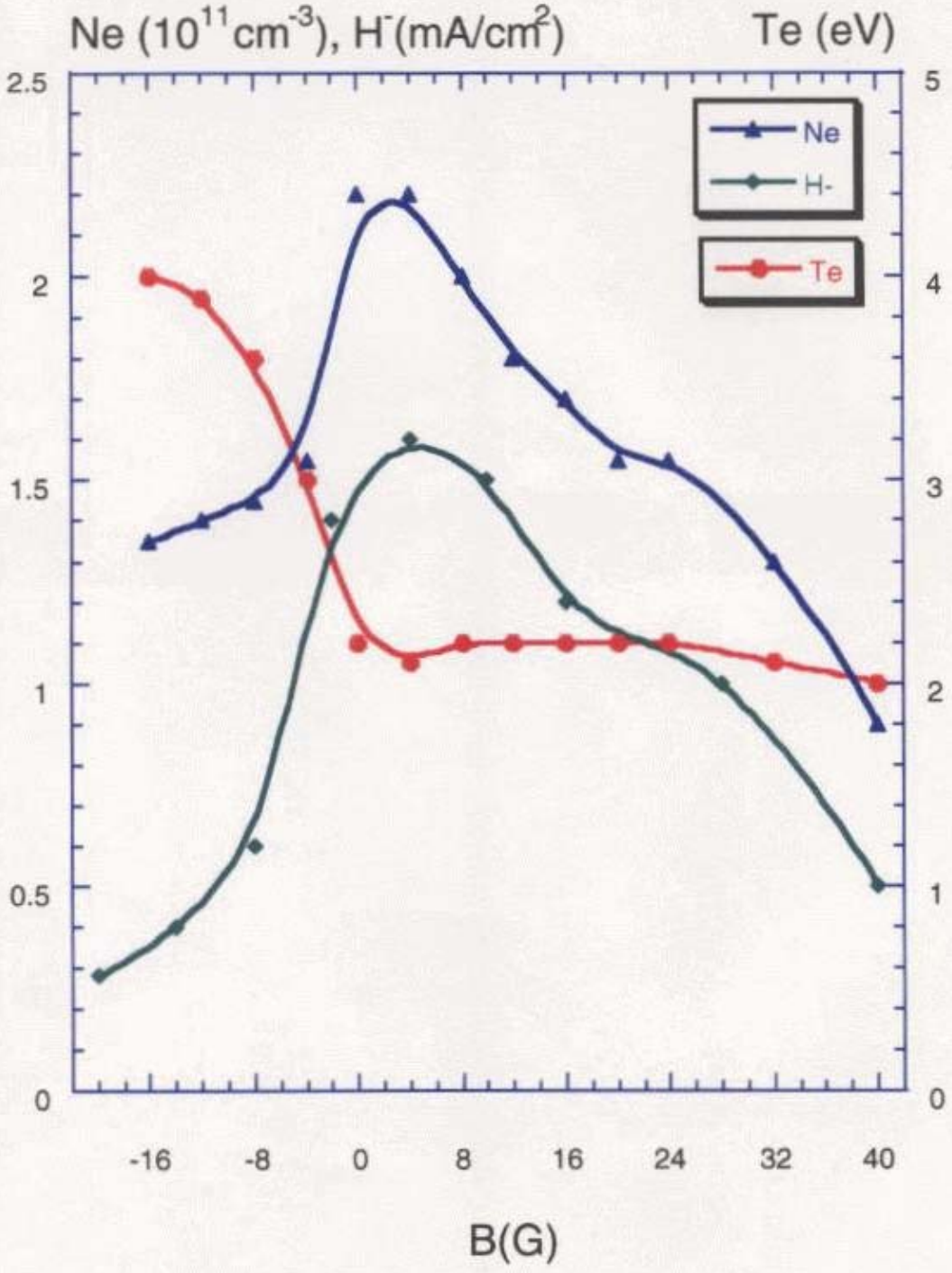

Fig. 31-1. Plasma parameters and the value of extracted negative beam in dependence on the magnetic field strength at the plasma grid (extraction) region.

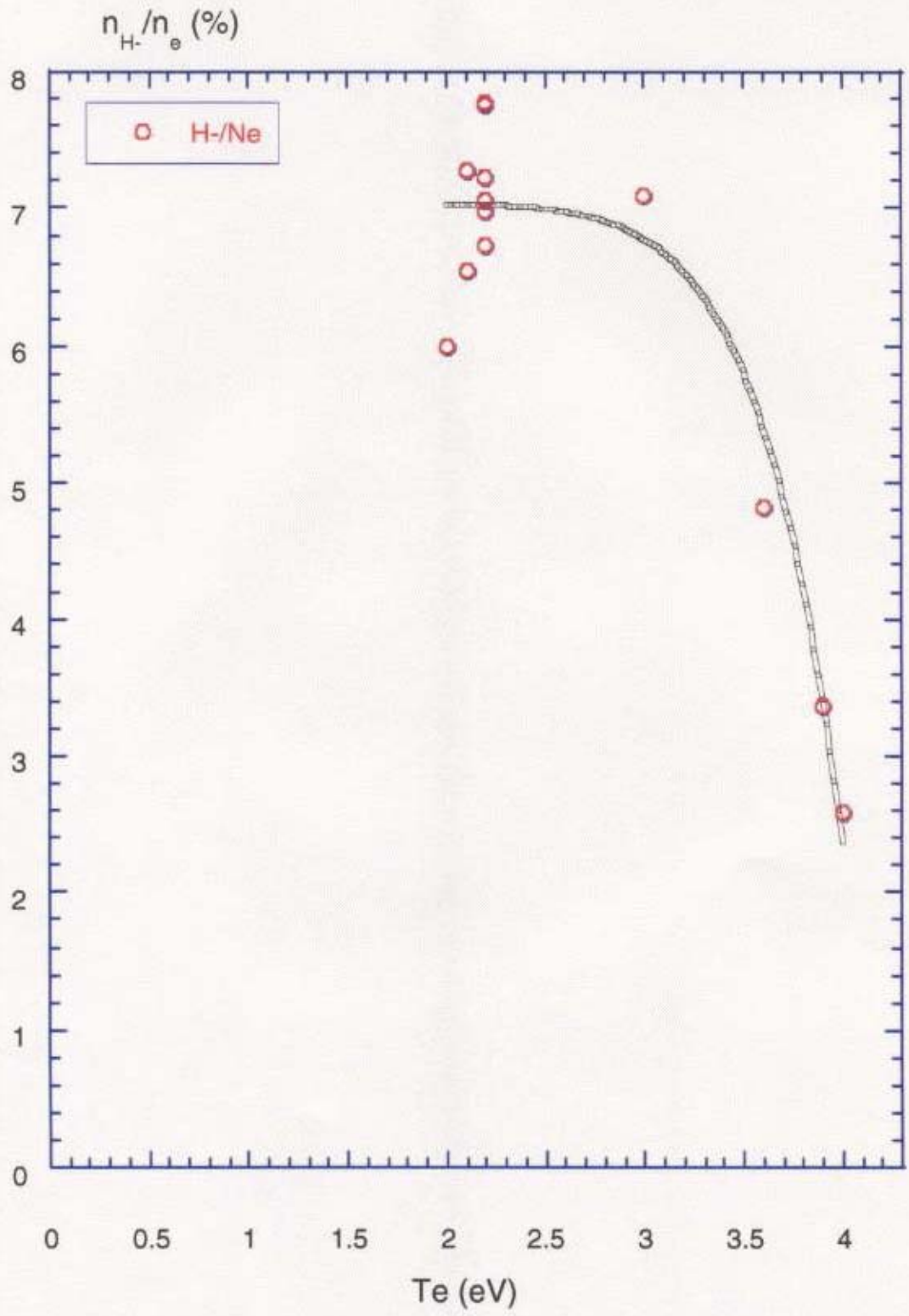

Fig.31-2. Dependence of the H^- /Ne (ions to plasma density) on the electron temperature Te.

7.2 Gas pressure dependence

Gas pressure dependence for the H^- beam profile is shown on Fig. 32 and the total beam current along with the other plasma parameters (plasma density and electron temperature) are presented on Fig. 33.

Distance between extraction unit and Faraday cup is 30 cm and we have to take into consideration negative ion stripping. The beam stripping loss-corrected value of H^- current is plotted along with the initialy measured value.

On a B-dependence (Fig. 31-1) we could clearly see that the negative ion current extracted is proportional to the plasma density near the extraction hole. In the case of pressure dependence collisional damping of the whistler wave with the increase of pressure results in decrease of the electron temperature (From 10 eV to 4 eV in our case) and therefore number of produced excited molecules is also decreasing.

Measurements of the electron temperature on the gas pressure were made with a specially designed U-probe (described later) and $T_e(P)$ gradually decreased from 8eV to 4 eV in the pressure range of 4-8 mTorr.

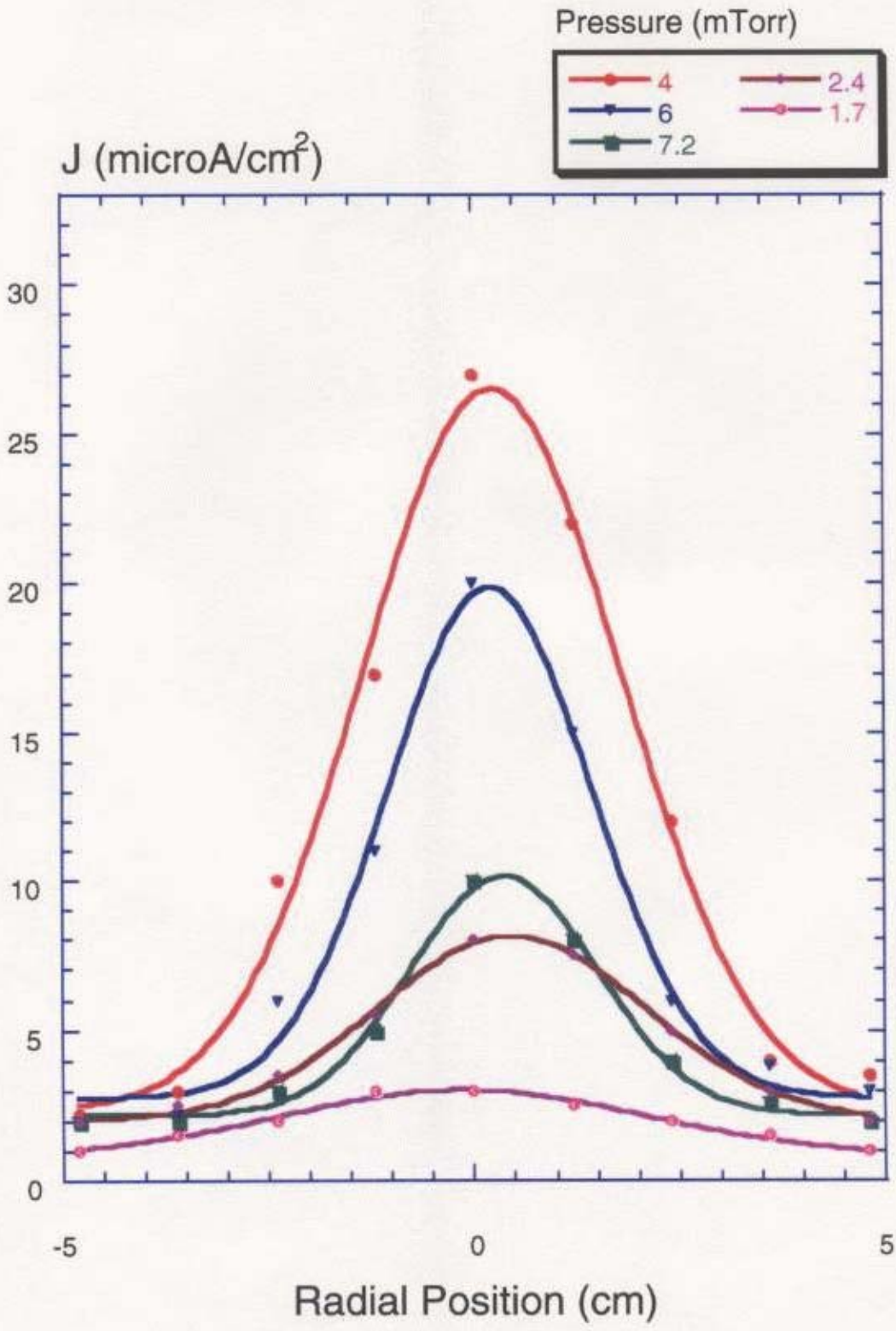

Fig.32. Beam profile dependence on the pressure of hydrogen.

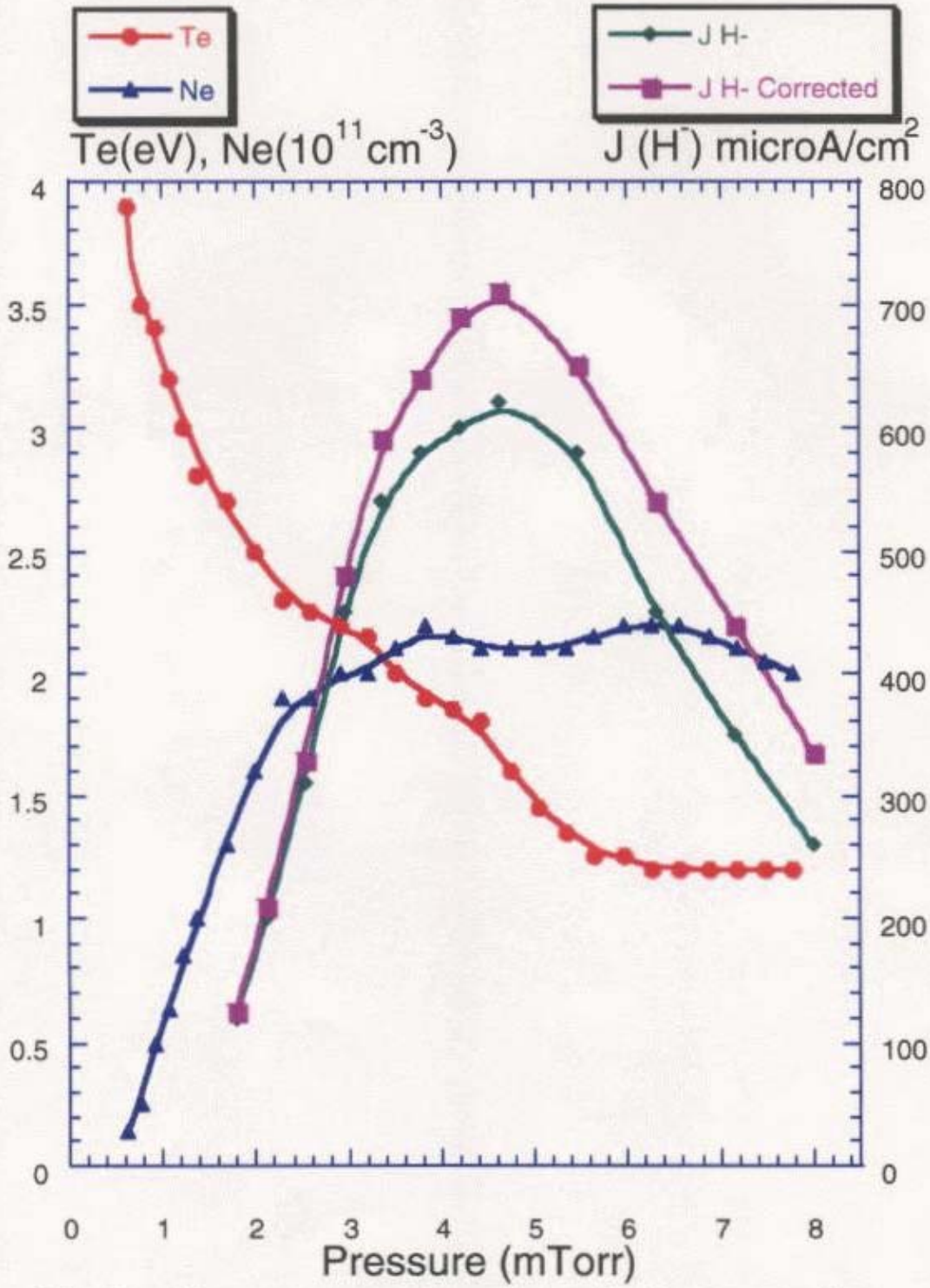

Fig.33. Plasma parameters and negative ions production dependence on pressure. Corrected H- data take into account ion losses through collisions with molecular hydrogen.

7.3 Further reduction of the electron temperature

During the experiments on MIXT-3 in Tokyo University, which were preceding the construction of this plasma source, the electron temperature in the plasma grid area has been reduced to 1 eV. Nevertheless we could not obtain temperature lower than 2 eV at the present experimental setup. The main difference between preliminary and present experiments in respect to magnetic field was that present confinement chamber was using soft iron plates to increase the field strength of the cusp magnetic field. These soft iron plates were partly shielding the correction field of the conditioning coil 4. After replacing these parts with aluminium plates, the absolute value of magnetic field at the plasma grid dependence on the current of the conditioning coil 4 never changed. However due to the changes in magnetic field lines distribution, it was possible to reduce T_e to 1eV in the plasma grid area. Pressure dependence for new configuration is shown on Fig.34.

Magnetic field strength dependence is shown on Fig. 35. With the removal of the soft iron, extracted beam profile (Fig. 36) and total beam

current (Fig. 37) did not change dramatically. These results are discussed in the next chapter.

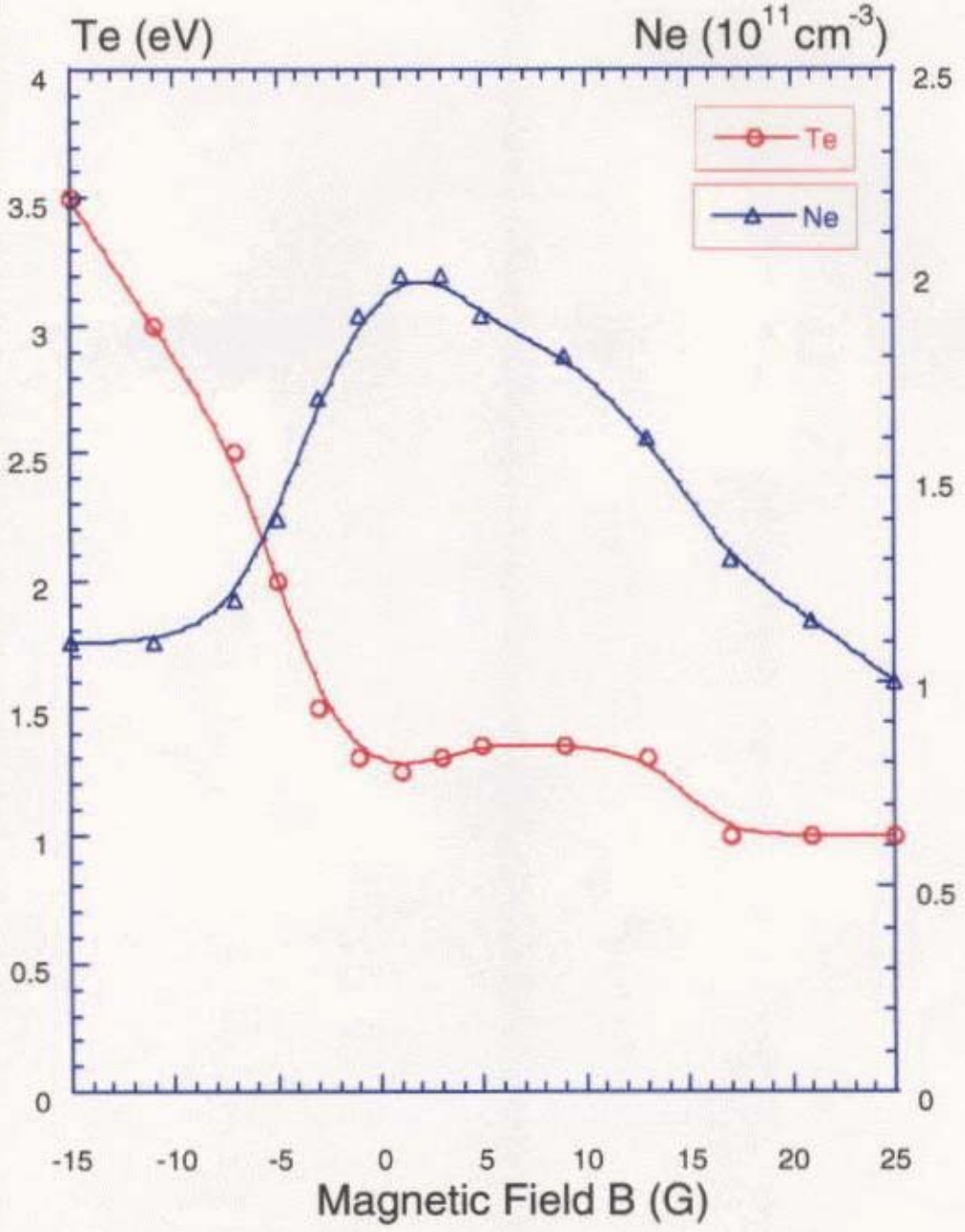

Fig 35. Hydrogen discharge parameters dependence on the magnetic field strength near the plasma grid with the soft iron parts of the confinement chamber removed.

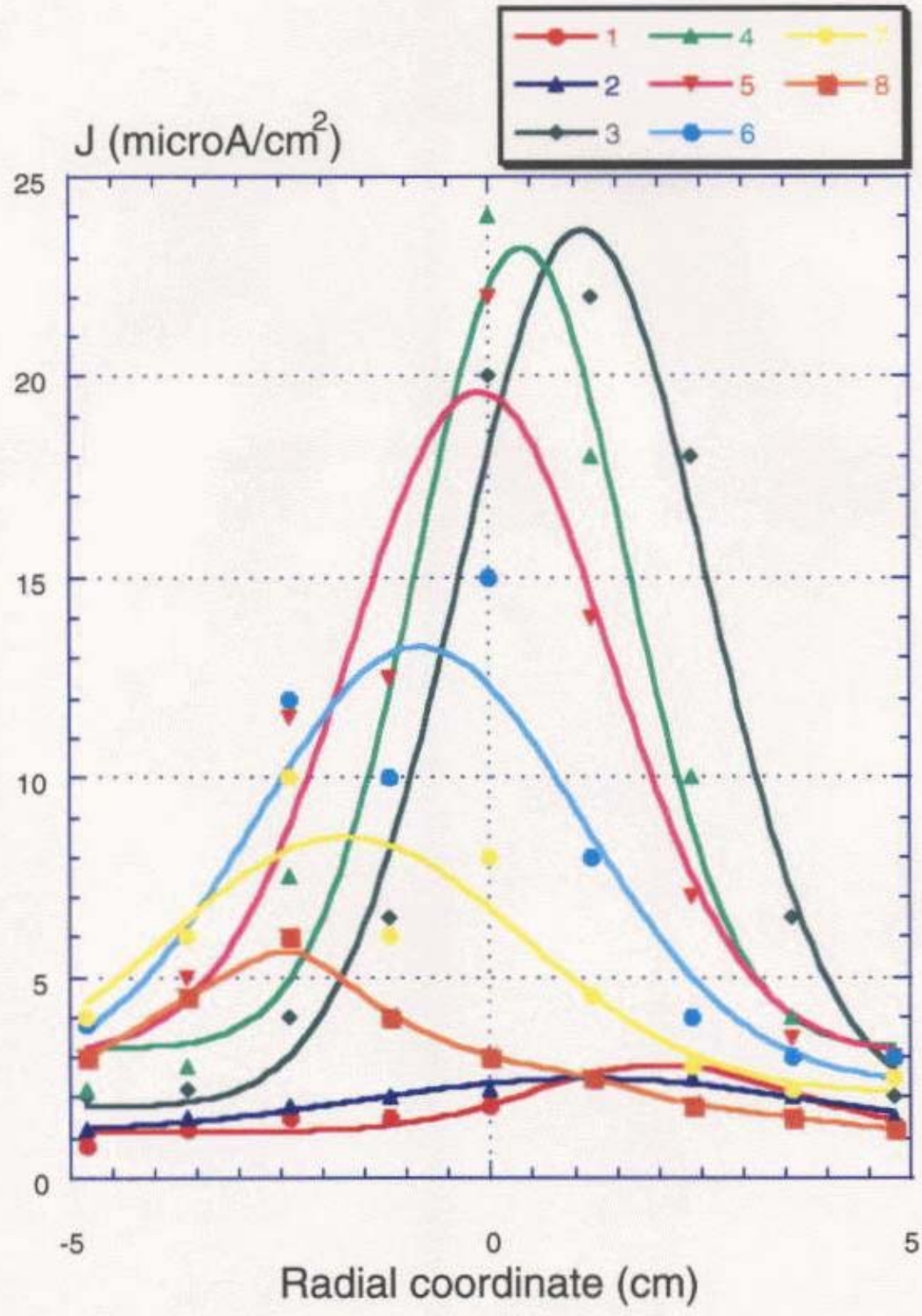

Fig 36. Beam profile variation with magnetic field change (1-8A configuration.

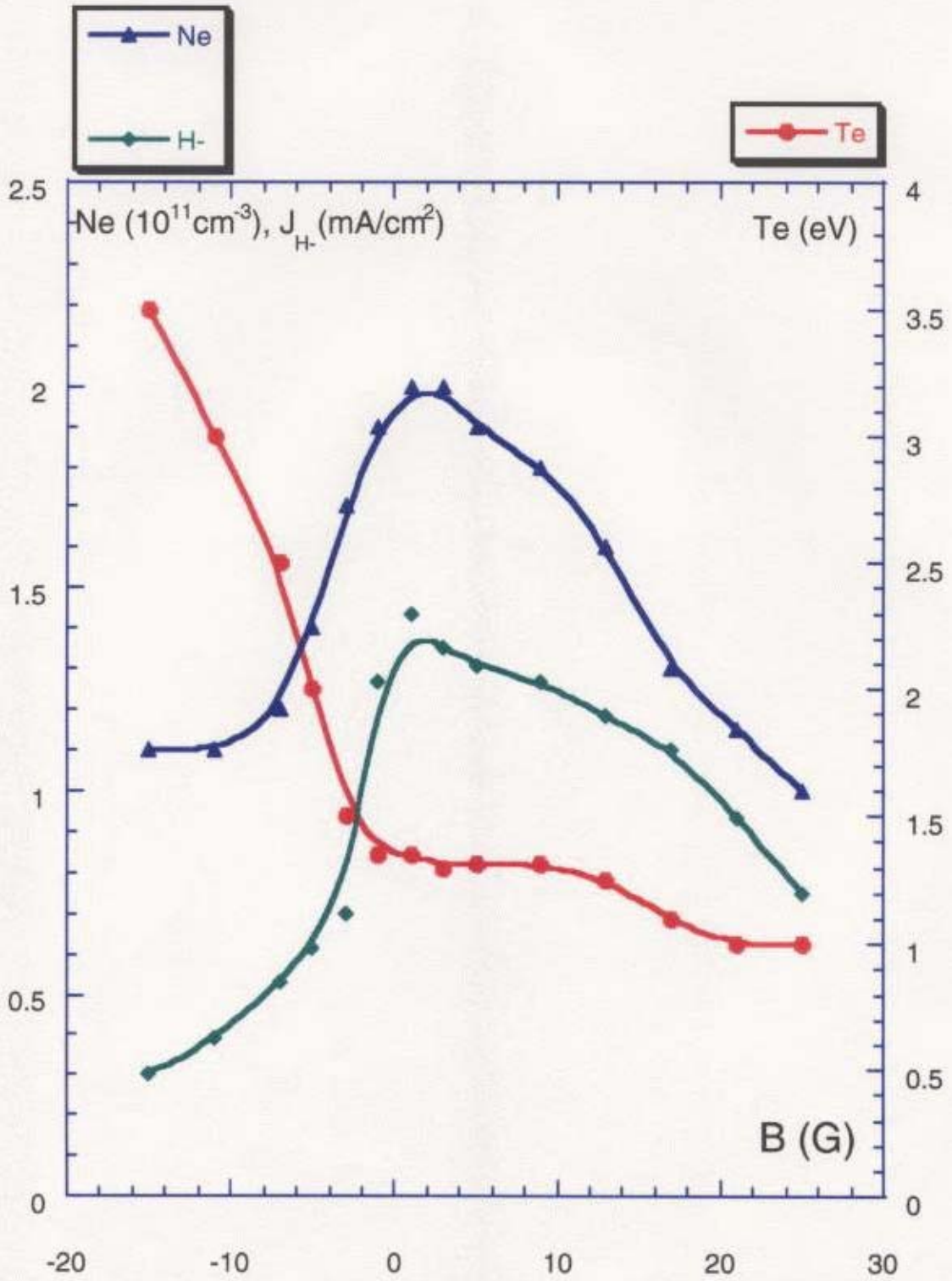

Fig. 37 Hydrogen discharge parameters and negative hydrogen ions production with soft iron removed.

7.4. Discussion

Plasma parameters and negative hydrogen ion beam density data for configuration with and without soft iron are represented on Fig. 38 for further discussion. As a result of soft iron removal it is possible to reduce electron temperature from 2 eV to 1 eV. Soft iron was used to strengthen the cusp magnetic field created by vertical rows of samarium-cobalt magnets surrounding the confinement chamber. With removal of soft iron the cusp magnetic field strength on the wall dorps from 2.5 to 2 kG. Decrease in the field strength results in the worse plasma confinement. We can see that plasma density slightly decreased.

It was expected that decrease in the electron temperature would result in increase of the negative hydrogen ion production, but this is not true in our case. Negative ion production dropped proportionally to the plasma density. In both cases at constant electron temperature negative ion production is proportional to the plasma density and with the increase of electron temperature the negative current drops rapidly.

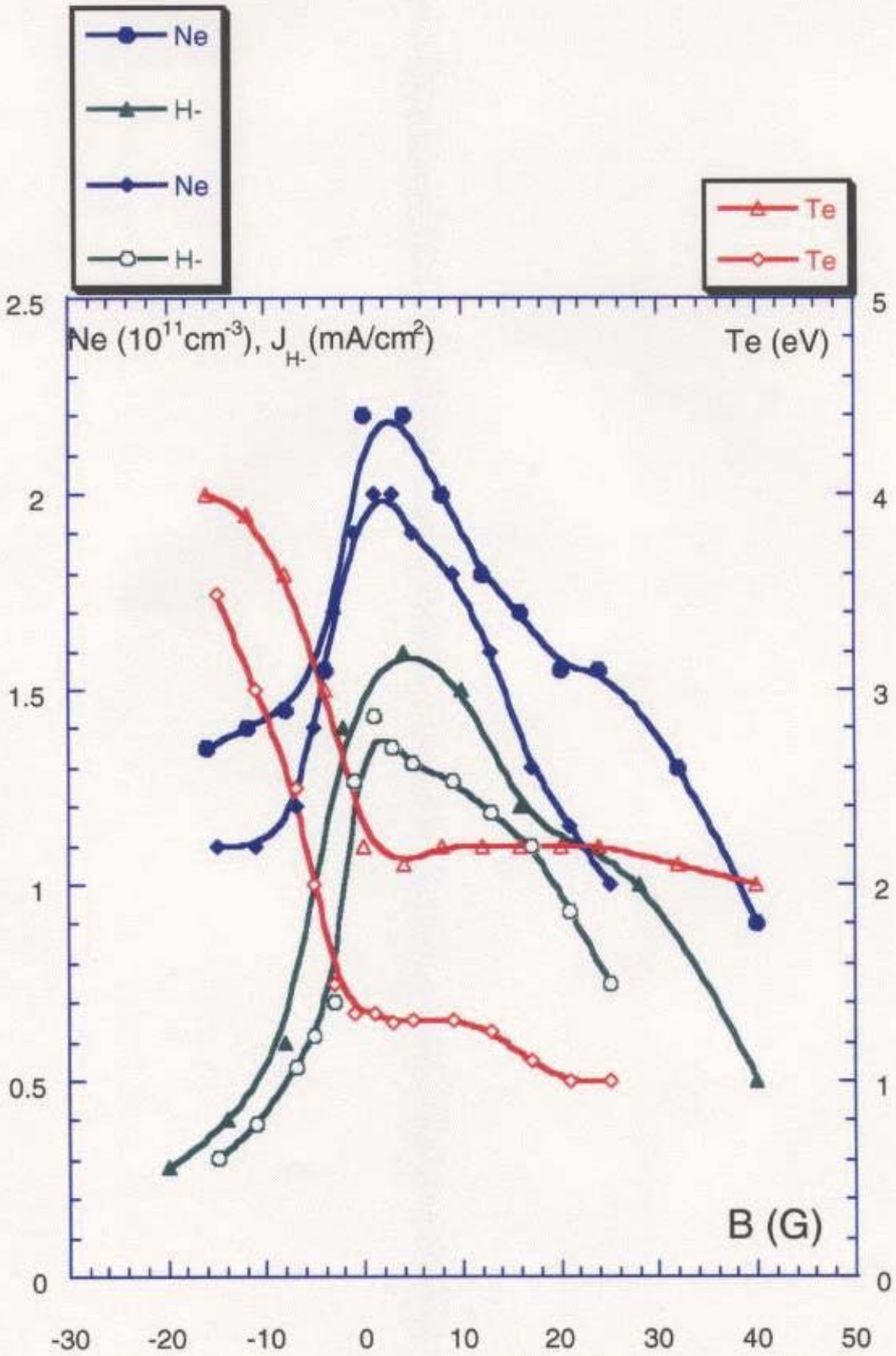

Fig.38 Joint graph for plasma parameters and negative ion production in cases with and without soft iron shielding.

This dependence shows that there is no big difference between the temperatures of 1 and 2 eV. Why then the negative ion production drops so rapidly when electron temperature reaches the value of 3-4 eV? The reason is not the absolute value of the temperature but the high-energy electron component that can reach the production plasma grid area directly from the production chamber without colliding with the confinement chamber wall first and passing multiple reflections from the cusp magnetic field.

The area of temperature increase corresponds to the presence of the residual magnetic field in the plasma grid area. That means, that some electrons directly reach the plasma grid area along the magnetic field lines. For that region the high-energy electron component of 8-10 eV was observed in the Langmuir probe volt-ampere characteristic (Fig. 40). On this figure in case a) of $I_{coil\ 4}$ =5A and residual magnetic field in the plasma grid area equal to zero one can see a clear volt-ampere characteristic with the slope of the logarithmic curve giving electron temperature of 2 eV. In case b) of $I_{coil\ 4}$ = 0 and residual magnetic field B = 15 G, the slope of the logarithmic curve breaks at a certain point and can be characterized by two very distinctive electron temperatures, 4 and 8.5 eV respectively. Presence of even higher energy electrons is also possible.

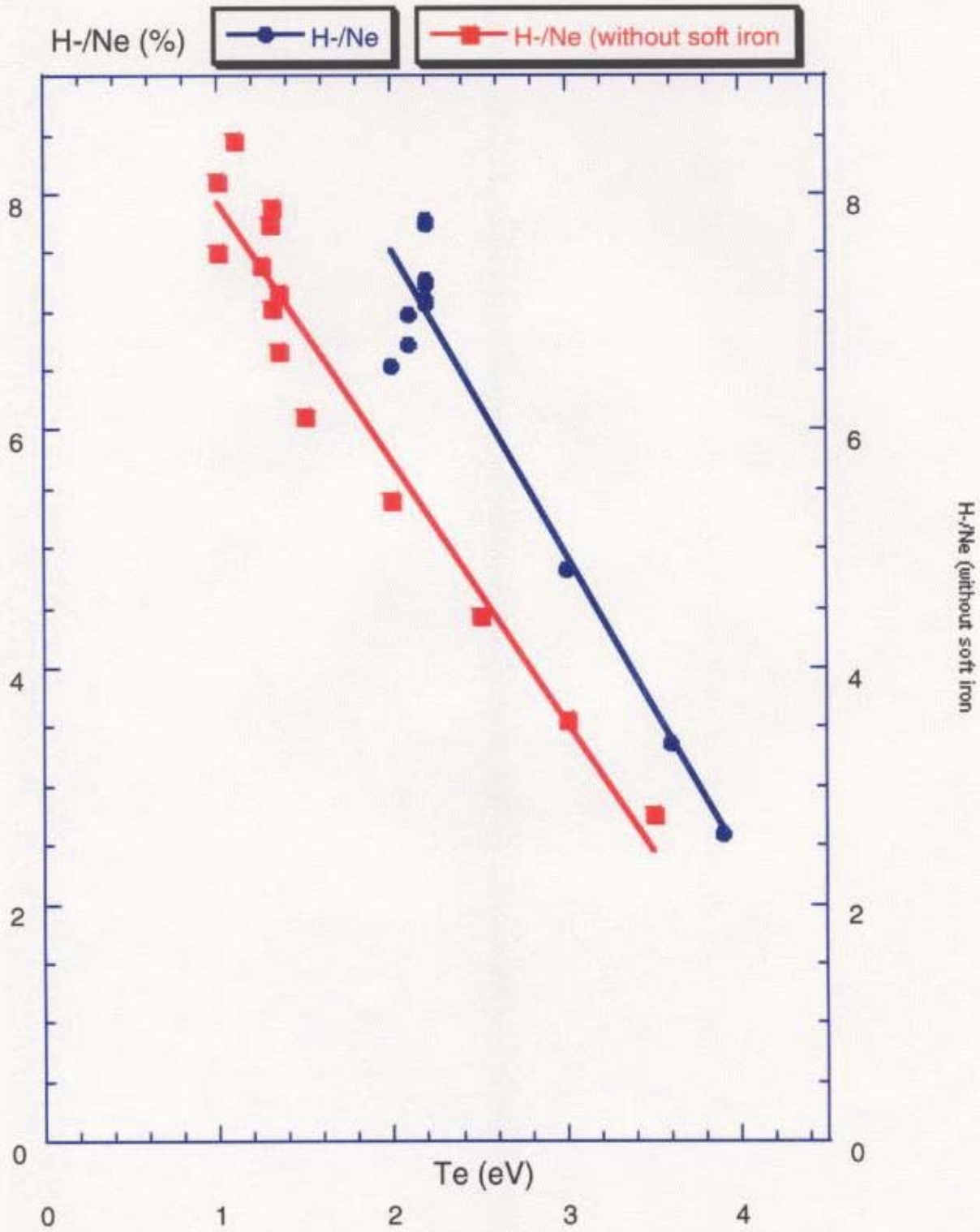

Fig. 39 Share of negative ions in the plasma, n_{H^-} / n_e dependence on electron temperature Te for 2 cases -with and without soft iron magnetic shielding.

It is obvious that the observed electron tail consists of electrons, which directly came from the production chamber along the field lines. As far as mean free path of electron in our conditions is about 1 cm, fraction of high energy electrons is small even in the case when no conditioning field applied.

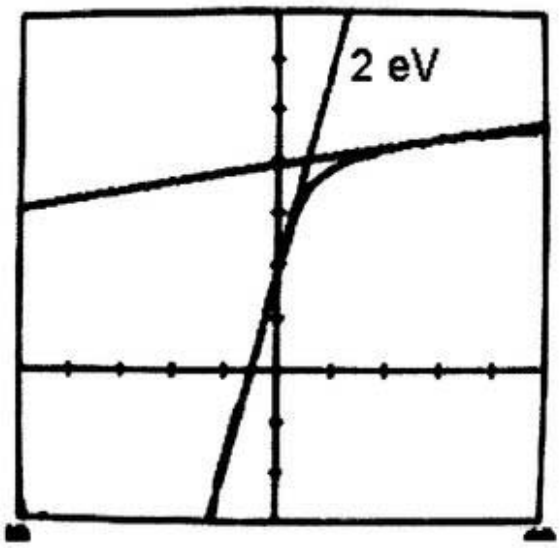

a. B=0 G at the plasma grid region

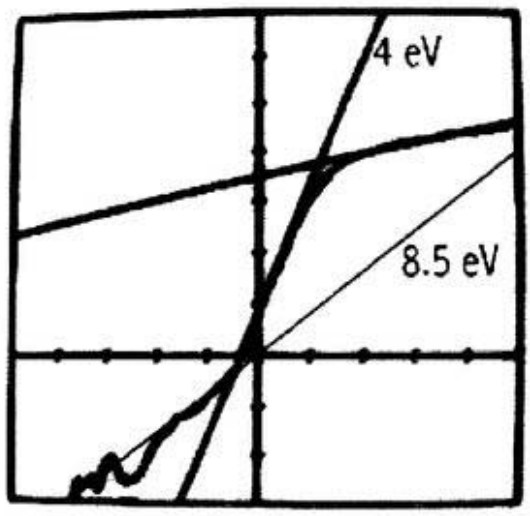

b. B=15 G at the plasma grid region

Fig. 40 Langmuir probe logariphmic volty-ampere characteristics for B=0 and B=15 G at the plasma grid region. (x-axis 10 V per division and y-axis in logarithm scale, one point per division)

From those Langmuir curves it is possible to calculate the percentage of the fast electrons which can reach the plasma grid area. By extrapolation of the fast electron branch it was found that the fast electrons fraction is about 0.3% of total electron density.

One can come to the conclusion that high-energy electron component destroys the negative hydrogen ions and it' s removal is resulting in the increase of the negative hydrogen ions production. Actually the crossection for the destruction of negative ions by fast electrons (10 eV) is only 2 times higher than that for the thermalized electrons (2 eV). Taking into account that the fraction of fast electrons is only 0.3%, the decrease of the negative ion beam current can not be explained only by growth of the fast electron fraction. Electron temperature at the outlet of production chamber have been measured and obtained electron temperature data show that with increase of gas pressure from 4 to 8 mTorr, electron temperature in the production chamber decreases from 9 to 4 mV. Vibrationally excited hydrogen molecules production also decreases and as a result less negative ions are produced in the plasma grid area.

8. Negative hydrogen ions production along the device axis

To analyze the negative ion production along the axis we should evaluate all the processes that lead to the H- generation and destruction.

Negative ions are formed as a result of the dissociative attachment and are destroyed mainly through collisions with electrons and positive hydrogen ions:

$$H_2(v'' > 6) + e_{slow} = H^- + H \quad (1)$$

$$H^- + e_{slow}\ (e_{fast}) = H + 2e \quad (2)$$

$$H^- + H^+\ (H_2^+, H_3^+) = 2H + e \quad (3)$$

I assume, that vibrational molecules are generated only in plasma production chamber with $T_e \sim 10$ eV. Negative ion concentration along z would be solved as one-dimensional problem with a source of vibrationally excited H_2 molecules at the point of z=0 and continuous generation and destruction of negative hydrogen ions along z.

All atomic and molecular reaction rates for the plasma with the same parameters are taken from the papers of O. Fukumasa[52,53]. From all the atomic processes two main processes with the highest reaction rates $\alpha(cm^3/s)$ were chosen:

1) $H_2(v'' > 5) + e\ (slow) = H + H,$ $\alpha_1 = 5.94 \times 10^{-9}\ (cm^3/s)$

2) $H^- + H^+ = 2H + e$ $\alpha_2 = 500 \times 10^{-9}\ (cm^3/s)$

As far as the source of H_2^* is at z= 0 and H_2^* are not produced along z, the solution of one-dimensional problem would be (Fig. 41):

$N_{H2^*} = N_{H2^*}(z=0) \exp(-z/\lambda)$

$\lambda_{H2^*} = n_e v_{H2^*} \tau_{H2^*}$

Where λ is a mean free path of H_2^*, v_{H2^*} is a thermal velocity and τ_{H2^*} is a lifetime of H_2^*.

Considering that $v_{H2^*} << v_e$, $\tau_{H2^*} = 1/n_e \alpha_1$ and

$N_{H2^*} = N_{H2^*}(z=0) \exp(-z\, n_e \alpha_1 / v_{H2^*})$

$\lambda_{H2^*} = 1/(n_e \alpha_1 / v_{H2^*})$

If we want to know the concentration of negative ions on the distance z from the entrance into the confinement chamber, we should sum all the negative ions produced along 0-Z line and take into account H^- attenuation through the collisions with H^+.

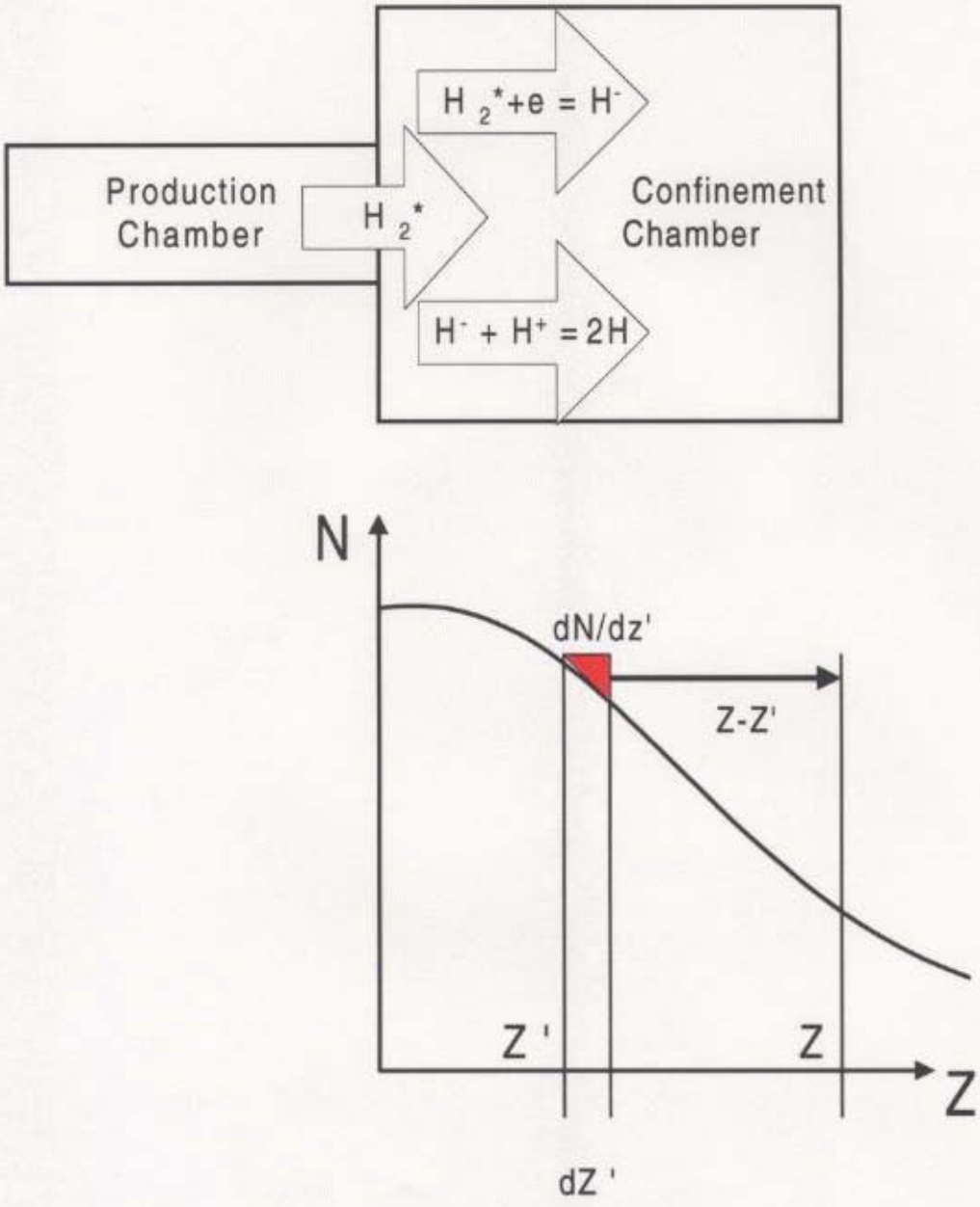

Fig.41. Negative hydrogen production along z (z - confinement chamber debth counting from chamber 1/2 connection)

At each point z' along the axis:

$dn_{H^-}/dz = - dn_{H2^*}/dz$

$= -(d/dz)\, N_{H2^*}(z=0) \exp(-z\, n_e\, \alpha_1 / v_{H2^*})$

$= N_{H2^*}(z=0)\, n_e\, (\alpha_1 / v_{H2^*}) \exp(-z\, n_e\, \alpha_1 / v_{H2^*})$

The attenuation of this amount $(dn_{H^-}/dz)dz'$ of H^- before it reaches coordinate z is described by the same formula:

$(dn_{H^-}/dz)dz'(z) = (dn_{H^-}/dz)dz'(z=z') \exp(-(z-z')\, n_{H^+}\, \alpha_2 / v_{H^+})$ (1)

$\lambda_{H^-} = 1/(n_{H^+}\, \alpha_2 / v_{H^-})$

I assume, that $n_{H^+} = n_e = n_p$, concentration of electrons and ions is equal to plasma density. Reaction rates for H- destruction by H_2^+ and H_3^+ are little less, but still this assumption is roughly valid. Velocities: v_{H^+} is calculated for $T_{H^+} = 0.5$ eV and v_{H^-} is calculated for $T_{H^-} = 0.05$ eV.

Finaly, integrating (1) from 0 to z we can find H- (z):

$$\int_0^z N_{H2^*}\, n_e\, (\alpha_1 / v_{H2^*}) \exp(-z'\, n_e\, \alpha_1 / v_{H2^*}) \exp(-(z-z')\, n_{H^+} \alpha_2 / v_{H^+})\, dz'$$

After performing the integration, we get:

$N_{H^-}(z) = N_{H2^*} \{(\alpha_1 / v_{H2^*}) / [(\alpha_2 / v_{H^+}) - (\alpha_1 / v_{H2^*})]\}$

$(\exp(-n_p(\alpha_1 / v_{H2^*})z) - \exp(-n_p(\alpha_2 / v_{H^+})z))$

For $n_p = 2 \times 10^{11}$ cm^{-3}, $T_{H^+} = 0.5$ eV and $T_{H^-} = 0.05$ eV,

$\lambda_{H2^*} = 1/(n_e \alpha_1 / v_{H2^*}) = 160$ cm

$\lambda_{H^-} = 1/(n_{H^+} \alpha_2 / v_{H^-}) = 2$ cm

Unfortunately, mean free path of the negative ion is too short and there is no considerable H^- accumulation on the long run. We can see that H^- concentration at any point is practically defined by the H_2^* concentration at that point. Calculated H^- concentration on z is presented at Fig. 47.

Talking about scaling along z, present depth of 30 cm is too big and as we see from Fig. 19-6, plasma uniformity and cooling down may be achieved at the depth of less than 10 cm (mark 200 cm on the plot, counting from present position of the plasma grid). As long as compared to the maximum H^- density is decreasing only 10%, there is no big correction to the experimental data of this work. However, distracting from one-dimensional model and taking into account particle losses on the wall, it is reasonable to make confinement chamber as short as possible. H^- density maximum at the depth of 8 cm might be an ideal point to place the plasma grid.

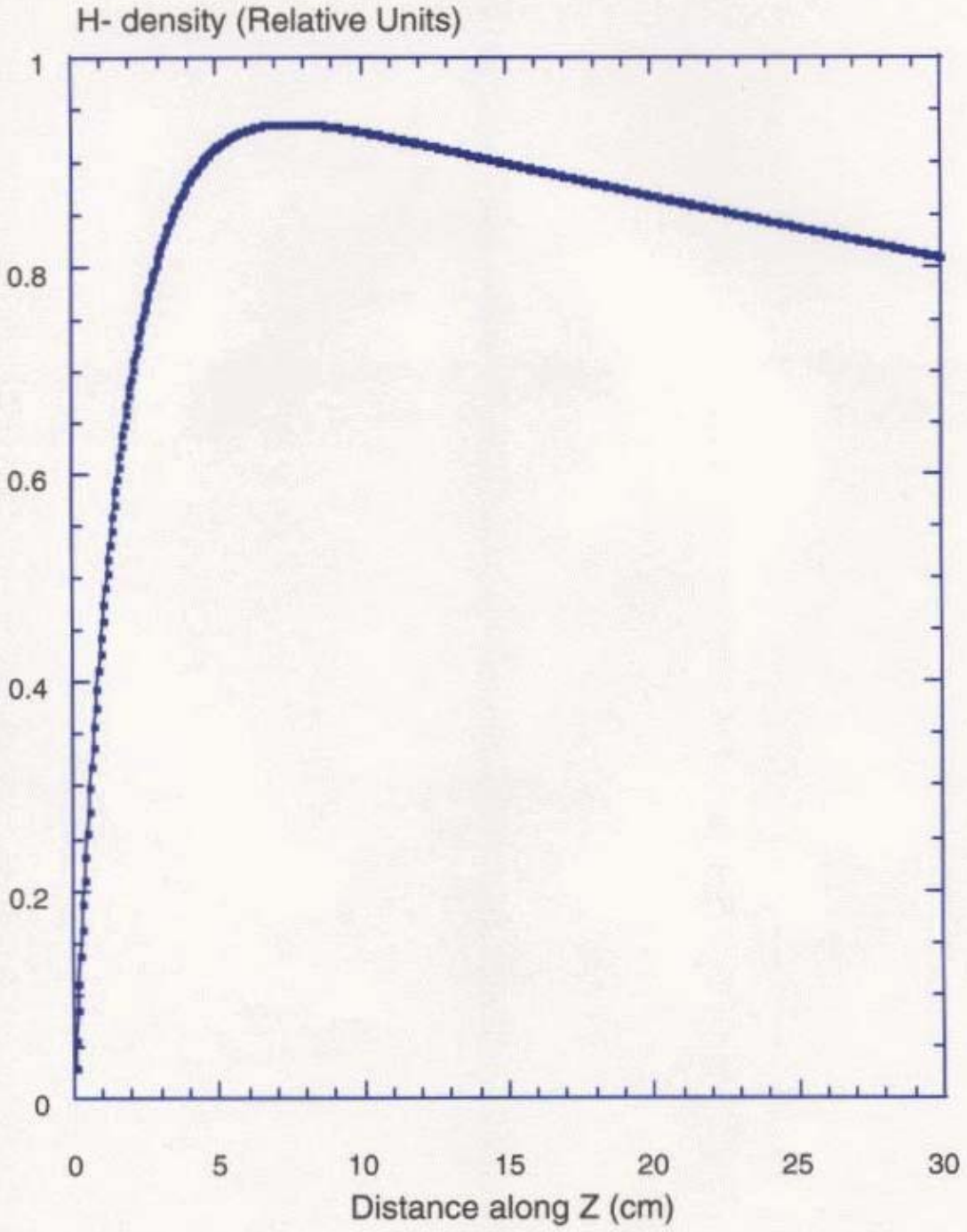

Fig. 47. Negative Hydrogen Ions density dependence along the confinement chamber axis.

9. Energetic Efficiency of the Source

9.1 Evaluation Criteria

The main evaluation criteria I used to estimate the efficiency of the constructed negative hydrogen ion source was a combination of the following parameters: Input Power P (kW), Extraction region crossection S (cm^2), Extracted negative hydrogen beam flux (H^- flux) J (mA/cm^2).

Resulting efficiency criteria is a total negative hydrogen current obtainable per 1 kW of input power and it would be calculated as:

Efficiency = J (mA/cm^2) x S (cm^2) / P (kW)

with a total dimension of (mA/kW).

For the case of the negative ion source under consideration, that would be:

Efficiency = 1.3 ma/cm^2 x 400 cm^2 / 5 kW = 90 mA/kW

9.2 Comparison with the existing sources

On the basis of the criteria described above, several wide-area ion sources constructed as prototype sources for the NBI system of the LHD (NIFS) are compared. Data are tabulated in the Table 1. In this case JxS/Power parameter represents actual source efficiency. As we can see, for the data taken without cesium injection, the energy efficiency of our source is better than that of the sources constructed before.

Cesium injection might improve H^- output and this is a next step in the development of the ion source presented in this paper.

At present ionization rate in the production chamber slightly exceed 1% and with further increase of the input power one might expect linear increase of the plasma density. There are several factors which can stop H- production growth with increase of the input power: plasma density saturation, weakness of the dielectric window to high power concentration and plasma impact, $n_{H^-}(n_p)$ saturation and limitation of the magnetron generator power. In this situation it is reasonable to apply the cellular method presently used for filament plasma sources. Situation would be more complicated than that for filament sources, because we have to take into

consideration the magnetic coils and have to coordinate their interaction. One of the possible geometrical solutions is shown on Fig. 48. We can utilize counter-currents of the compensation coils and thus reduce the coil 4 necessary power supply 2 times. It is possible to connect as many units as necessary to create a chessboard where black and white squares are characterized by the opposite current flow in all coils of the device.

Table 2. Comparison of the existing wide-area H^- ion sources for NBI

Plasma Source Type	Power Input P(kW)	Plasma Grid Crossection (cm)	Actual Plasma area $S(cm^2)$	Negative Hydrogen Ions Current density $J(mA/cm^2)$		JxS/Power	
				W/O Cs	With Cs	W/O Cs	With Cs
Arc	200	25x50	480	6	30	14	70
RF	20	30x30	580	2.7	4	80	120
Micro Wave	5	26x26	400	1.1	-	90	-

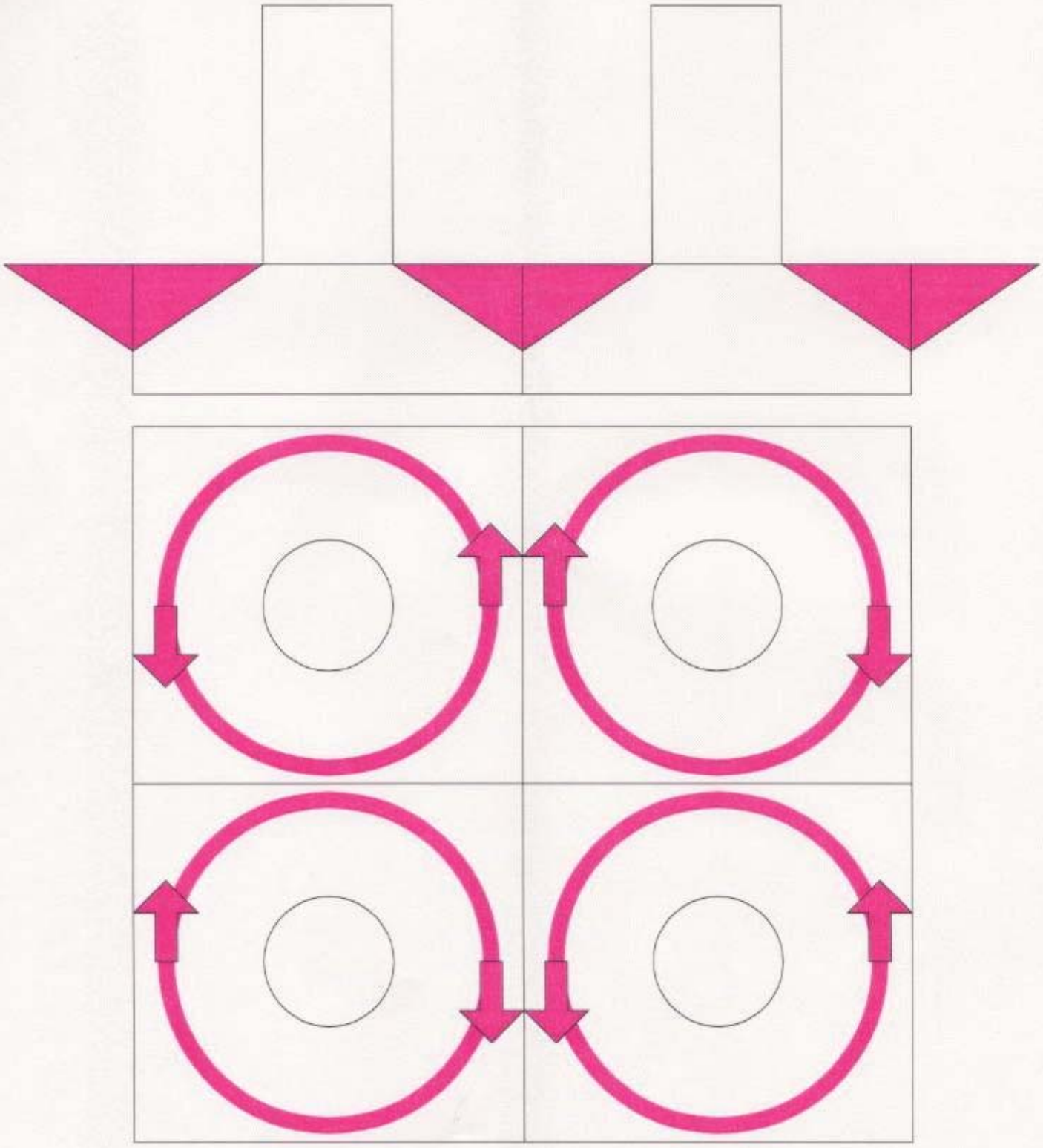

Fig. 43. Possible cellular design for the microwave plasma source. Conditioning coils of the neighbouring units are adjusted to help ieach other.

10. Conclusion

A tandem type microwave plasma production mechanism is applied in a new efficient negative hydrogen ion source. The produced high temperature high-density plasma is transformed by diffusion into wide-area uniform low-temperature plasma, which is appropriate for volume production of negative hydrogen ions. For the microwave power of 5 kW uniform hydrogen plasma density of $3x10^{11}cm^{-3}$ was obtained in the wide rectangular area of 20x20 cm. Electron temperature in the plasma grid region is reduced to 1 eV.

Negative ion source parameters were studied in details. Faraday cup array was used to measure the extracted negative ion beam. Pressure and magnetic field dependencies were taken. Axial and radial plasma parameters profiles were obtained for the whole volume of the plasma source.

Negative ion production is proportional to plasma density and rapidly decreases with increase of electron temperature over 2 eV. Pressure increase over 4 mTorr strongly affects electron temperature in the production chamber. With pressure increase from 4 to 8 mTorr, electron temperature in the production chamber decrease from 9 to 4 eV.

One hole extraction system have been used to produce negative ion beam. Orifice diameter is 1 cm and extraction voltage is 5 kV.

One mA of negative ion beam is extracted from a single hole of 1 cm in diameter, which corresponds to 1.3 mA/cm^2 of the negative hydrogen current density at the plasma grid area. Considering wide uniform plasma area and low input power, power efficiency of this ion source is higher than that of the conventional arc discharge and RF sources.

Present device construction proves to be successful. The above results for ion beam extraction without cesium seeding are encouraging to warrant further study of negative hydrogen ion production using tandem structure microwave plasma source and consider it as an alternative source for the Neutral Beam Injection (NBI) system.

Appendixes

1. Wavelength of microwaves in plasma and the cutoff size of the rectangular and cylindrical waveguide.

The transverse components of the field in a waveguide can be written as a sum of two parts, one derived from the longitudinal H ($H_z > 0$) and the other from the longitudinal E ($E_z > 0$)[54]. The first part is called a transverse electric field, abbreviated TE, and the second part is called a transverse magnetic, or TM field.

For every scalar solution of the two-dimensional wave equation, satisfying the condition that it vanishes on the boundary, we get a TM wave; and for every solution whose normal derivative vanishes, we get a TE wave[55]. The wave equation has an infinite number of solutions, which start with the largest cut-off wavelength and extend indefinitely toward shorter and shorter wavelengths. In a rectangular guide of dimensions a, b, the cut-off wavelengths are given[56] by the following formula:

$$\frac{1}{\lambda_c} = \sqrt{(m/2a)^2 + (n/2b)^2}$$

where m and n are integers. If the dimension *a* of waveguide is greater than *b*, the longest cut-off wavelength is given by m=1, n=0, and is equal to 2*a*. In some cases, the first mode has an infinite cut-off wavelength; this case is called a principal mode.

We should find a principal mode in the case of the rectangular wave guide if m and n are both zero; but in this case the field of the wave becomes zero identically. However, the principal mode exists if the wall of the wave-guide consists of at least two separated conductors, as in the case of a coaxial line.

Of all the modes of the guide, the one with the longest cut-off wavelength is the TE mode, for which m = 1, n = 0 (a > b). This is the mode used in common practice. In our device the same mode is used. For the frequency of 2.45 GHz we have

$$\lambda = c / \nu = 12.24cm$$
$$a = \lambda / 2 = 6.12cm$$

which defines the minimum dimension of the rectangular waveguide.

Production chamber is a cylindrical waveguide itself. At the transition from the rectangular waveguide to the cylindrical waveguide through the quartz window, the TE_{01} wave mode is converted into the TE_{11} wave mode. The cutoff wavelength for the cylindrical waveguide is defined by the formula:

$$\lambda_{c(mn)} = \frac{2\pi}{\chi(m,n)} R$$

where $\chi(1,1) = 1.841$ that gives for the $\lambda = 12.24$ cm the $R_{min} = 3.59$ cm, which means the currently used ϕ 7 cm chamber is just on the boundary or already below the cutoff diameter for the cylindrical waveguide.

d_{cutoff} (TE_{11}-mode) =7.19 cm

Attempts to create the compact ECR plasma source with below cutoff size chamber have been made previously. The cutoff size of the wave-guide filled with the dielectric material is inversely proportional to the square root

of the dielectric constant. Once the magnetized plasma, which is equivalent to a dielectric material with a high-dielectric constant, is excited in the below-the-cutoff size chamber, plasma becomes self-sustaining since microwaves enter the waveguide filled with plasma and are absorbed by the plasma. In this manner, ECR plasma can be excited in plasma chambers with the diameter smaller than a cutoff size.

To evaluate the possibility of using this principle in Chamber 1 of the MIXT-3 Plasma Source, operation plasma parameters were considered:

$n_e = n_i = n_p = 2 \times 10^{12}\ cm^{-3}$

$w = 2 \pi \nu = 1.54 \times 10^{10}$ rad/sec

Ion Plasma Frequency:

$w_{pi} = (4 \pi n Z^2 e^2 / m_i)^{1/2} = 1.32 \times 10^3 Z (n_i)^{1/2} = 1.9 \times 10^9$ rad/sec

Electron Plasma Frequency:

$w_{pe} = (4 \pi n e^2 / m_e)^{1/2} = 5.64 \times 10^4 (n_e)^{1/2} = 8 \times 10^{10}$ rad/sec

Ion Gyro frequency:

$w_{ci} = ZeB/m_ic = 958 \;\; B = 2 \times 10^6$ rad/s

Electron Gyro frequency:

$w_{ce} = eB/m_ec = 1.76 \times 10^7 \;\; B = 3.5 \times 10^{10}$ rad/s

In these conditions the ratio between frequencies is the following:

$w_{pe} > w_{ce} > w_{pi} \cdot w_{ci}$

The dispersion relation can be approximated[57] by the formula:

$$n^2 = 1 - \frac{4 \cdot \pi \cdot n_0 \cdot e^2}{m_e w(w - e \cdot B / m_e c)}$$

Wavelength will be:

$$\lambda = \frac{c}{w}(1 - \frac{4 \cdot \pi \cdot n_0 \cdot e^2}{m_e w(w - e \cdot B / m_e c)})^{-1/2}$$

As we can see, in a wide range of magnetic field strengths at the entrance of the chamber, wavelength drops below 10 cm for the plasma density over 10^{11} cm^{-3}. If in the beginning of the wave propagation we can

create plasma of the appropriate density, the microwave can be introduced into the waveguide of the diameter even less than 1 centimeter.

Incoming microwave power of 5 kW is large enough to cause a microwave breakdown even in the absence of the magnetic field. In the presence of a magnetic field of the magnitude $B > B_{ce}$ only 20-50 V/cm of microwave electric field are required for plasma excitation[58]. For the cavities several centimeters in diameter these electric fields correspond to 10-20 W of microwave power. Considering the data of plasma density in an operating regime and a value of magnetic field at the junction of the waveguide and production chamber, the smaller diameter production chamber of 6cm was used. This decrease power consumption by coils on the creation of a magnetic field in a wide area, miniaturize the size of the plasma source and improve gas efficiency. All the above are very important for practical applications.

This is called a Whistler wave, or a W-wave.

On the contrary, when $p^2 << 2k_0^2K_{II}$, then equation 1 becomes:

$$k^2 = -p^2 (K_1 /K_{II}) = -p^2 w^2(w^2 - w_p^2 - w_c^2)/(w^2 - w_p^2) (w^2 - w_c^2) \quad (3)$$

and this mode is called Trivelpiece mode, or T-mode.

From equation 1 we can get dispersion relation:

$$c^2k^2/2 = w^2(w^2 - w_h^2)(w^2 - w_\bullet^2)/(w^2 - w_p^2) (w^2 - w_c^2)$$

where $w_h^2 = w_p^2 + w_c^2$, $w_\bullet^2 = w_p^2 + w_{co}^2$, $w_{co} = cp/\sqrt{2}$

It was shown, that $p^2 << 2k_0^2K_{II}$ in the dense plasma ($w_p > w$) is equivalent to

$$w < \sqrt{(w_p^2 - w_{co}^2)}, w_p \qquad (4)$$

and is the condition of W-wave propagation (T-wave can not propagate).

For the cylindrical waveguide $p = j_{01}/R$, where $j_{01} = 2.40$ – the first root of the zero-order Bessel function. Then $w_{co} = w_{co} = c\, j_{01}/\sqrt{2}\, R$

$$w_{co}(R=3) = 1.7 \times 10^{10} \text{ rad/sec}$$

$$w_c = 1.76 \times 10^7 \text{ B (rad/sec)} = [B=2000G] = 3.5 \times 10^{10} \text{ rad/sec}$$

$$w = 2 \pi \nu = 1.54 \times 10^{10} \text{ rad/sec}$$

$$w_p = (4 \pi n e^2 / m_e)^{1/2} = 5.64 \times 10^4 (n_e)^{1/2} = 8 \times 10^{10} \text{ rad/sec}$$

$(4) \Leftrightarrow 1.54 < \sqrt{(64 - 2.9)}, 8$

As far as condition (4) is satisfied, we have W-wave and don't have T-wave.

2.2 Whistler wave absorption

Let us consider dispersion relation and special damping of Whistler waves propagating in the plasma column having relatively high electron density and moderate electron temperature.

The dispersion relation in the Mawellian plasma is given by:

$$\left(\frac{ck}{w}\right)^2 = 1 + \frac{w_p^2}{\sqrt{2}wkv_T} Z(\zeta), \ldots \zeta = \frac{w + iv - w_c}{\sqrt{2}kv_T} \qquad (1)$$

where $Z(\varsigma)$ is the usual dispersion function, $v_T = (kT_e/m)^{1/2}$ and ν is an effective collision frequency of electrons.

The least-damped root of eq. (1), $k_1 = \mathrm{Im}(k)$ is due to cyclotron damping only when $\nu = 0$ and is due to cyclotron damping plus collisional damping when $\nu \neq 0$. In general k_1 can only be obtained numerically and an asymptotic expression does not exist.

In the region far from the resonance eq. (1) reduces to the dispersion relation in the cold plasma theory:

$$\left(\frac{ck}{w}\right)^2 = 1 + \frac{w_p^2}{(w_c - w - iv)} \qquad (2)$$

2.2 Whistler wave absorption

Let us consider dispersion relation and special damping of Whistler waves propagating in the plasma column having relatively high electron density and moderate electron temperature.

The dispersion relation in the Mawellian plasma is given by:

$$\left(\frac{ck}{w}\right)^2 = 1 + \frac{w_p^2}{\sqrt{2}wkv_T} Z(\zeta), \ldots \zeta = \frac{w + iv - w_c}{\sqrt{2}kv_T} \qquad (1)$$

where $Z(\varsigma)$ is the usual dispersion function, $v_T = (kT_e/m)^{1/2}$ and ν is an effective collision frequency of electrons.

The least-damped root of eq. (1), $k_1 = \text{Im}(k)$ is due to cyclotron damping only when $\nu = 0$ and is due to cyclotron damping plus collisional damping when $\nu \neq 0$. In general k_1 can only be obtained numerically and an asymptotic expression does not exist.

In the region far from the resonance eq. (1) reduces to the dispersion relation in the cold plasma theory:

$$\left(\frac{ck}{w}\right)^2 = 1 + \frac{w_p^2}{(w_c - w - iv)} \qquad (2)$$

Collision frequency is composed of the electron-neutral collisions and Coulomb collisions given by:

$$\nu_{ei} = 8\pi ne^4 \ln\Lambda / m^{1/2}(3kT_e)^{3/2} = 4.2x10^{-6}(n/T_e^{3/2})\ln\Lambda, \ sec^{-1}$$

we have gas density $n = 1.4x10^{14}$ cm^{-3}, $T_e = 10$ eV, and

$\nu = 5.3 \times 10^8$ sec^{-1} ,

$w_c = 1.76 \times 10^7$ B (rad/sec) = [B=2000G] = 3.5×10^{10} rad/sec

$w = 2 \pi \nu = 1.54 \times 10^{10}$ rad/sec

then:

$\nu/w_c = 1.5 \times 10^{-2}$

$w/w_c = 0.45$

Comparison with the numerical solutions of the equation (1)[62] gives completely collisional absorption mechanism for the values mentioned above.

Microwaves are converted to the Whistler waves, which are absorbed through the collisional damping mechanism.

Acknowledgements

I wish to express my gratitude to Professor T. Kuroda, who made my participation in this research program possible and whose help and cooperation during these years have been invaluable. I also want to express my gratitude to Professor O. Kaneko for his help and guidance during this program and especially in the final stage of this work.

I want to express my special thanks to Dr. Y. Oka for many useful discussions and participation in some experiments, Dr. Y. Takeiri, Dr. K. Tsumori, and Dr. M. Osakabe for discussions, help with experimental equipment and advise, Dr. T. Takanashi, Dr. T. Kawamoto for technical help and assistance. My thanks are also extended to the following very helpful colleagues: E. Asano for technical advice and Mr. Mizusawa for his cooperation and help in the creation of numerous components for the experimental device. I am also grateful to Dr. M. Tanaka for microwave-related discussions and some ideas of the antenna probe design.

Test experiments preceding the creation of this device were held at The University of Tokyo, Faculty of Engineering, Professor Inoue laboratory. I want to thank Professor Inoue for giving me such an

opportunity and Dr. Nihei for participating in these experiments and many useful advises concerning design of the microwave source.

I want to thank also Dr. A. Gavrilin for his help and advice in calculation of the spatial field of the magnetic coils system.

References-

[1] K. Ehlers, J. Vac. Sci. Technol., A1, p. 974 (1983)
[2] A. Iiyoshi and K. Yamazaki, Phys. Plasmas, Vol.2, pp. 2349-2356 (1995)
[3] O. Kaneko et al., Fusion Engineering and design, vol.26, pp. 455-462, (1995)
[4] T. Mutoh et al. Fusion Technology, Vol.1, pp.552-556, (1989)
[5] A. Ando, Y. Takeiri et al. Rev. Sci. Instrum. 66(12) pp. 5412-5418 (1996)
[6] Y. Takeiri et al., Rev. Sci. Instrum. 67(3) p. 1021 (1996)
[7] Y. Takeiri et al., Rev. Sci. Instrum. 66(3) p. 2541 (1995)
[8] M. Tanaka et al., IEEE Transactions on plasma science, 25,6, p. 1412 (1997)
[9] M. Hamabe, Rev. Sci. Instrum, 69, p. 944 (1998)
[10] T. Takanashi et al., Rev. Sci. Instrum., 67 (3), p. 1024 (1996)
[11] T. Takanashi et al., Jpn. J. Appl. Phys. 35 pp. 2356-2362 (1996)
[12] K. Leung at al., Rev. Sci. Instrum. 62, p. 100 (1991)
[13] S. Wells, Y. Takeiri at al., Rev. Sci. Instrum, 63, p. 2735 (1992)
[14] G. Dearnaley et al., Ion Implantation (North Holland, Amsterdam, 1973)
[15] C. McKenna, Nucl. Instrum. Methods Phys. Res. B 37/38, p. 449 (1989)
[16] K. Miyake and K. Ohashi, Jpn. J. Appl. Phys., 32, L120 (1993)
[17] Y. Ono et al., J. Vac. Sci. Technol.,A4, p. 788 (1986)
[18] N. Sakudo, Nucl. Instrum. Methods Phys. Res. B 21, p. 33 (1987)
[19] G. Hellblom and C. Jacquot, Nucl. Instrum. Methods A, 243, pp. 255-259 (1986)
[20] J. Willis at all., Rev. Sci. Instrum. 67(3), pp.1227-1229 (1996)
[21] M. Tanaka and K. Miyake, at al., Rev. Sci. Instrum.,66 (10), p. 4911 (1995)
[22] K. Hashimoto, Fusion Engineering and Design 26, pp. 495-500 (1995)
[23] M. Bacal et al., J. Appl. Phys. 52(3), p. 1247 (1981).
[24] J. Wadehra, Physics Rev. A 29, p. 106 (1984)
[25] D. Skinner et all. Phys. Rev. E 46, p. 2122 (1993)
[26] M. Bacal et al. J. Appl. Phys. 52, p. 1247 (1981)
[27] J. Hiskes and A. Karo J. Appl. Phys. 56 (7), p. 1927 (1984)
[28] M. Bacal and F. Hillion, Rev. Sci. Instrum, 56(12), p. 2274 (1985)
[29] H. Nihei, J. Morikawa, D. Hagahara, H. Enomoto and N. Inoue, Rev. Sci. Instrum. 63(3), p. 1932 (1992)
[30] Y. Takeiri et al., Rev. Sci. Instrum. 66 (3), p. 2541 (1995)
[31] M. Hopkins et al., J. Appl. Phys. 70, p.2009 (1991)
[32] M. Hopkins, Phys. Rev. Lett., 65, p.1207 (1994)
[33] H. Nihei et al., Rev. Sci. Instrum. 63 (3), pp. 1932-1938 (1992)
[34] H. Nihei, Jpn. J. Appl. Phys. Vol. 34 pp. 277-284, (1995)
[35] Y. Takeiri et al., Rev. Sci. Instrum, 67(3), p. 1021 (1996)
[36] M. Bacal et al., Rev. Sci. Instrum. 50, p. 719 (1979)
[37] M. Bacal and G. Hamilton, Phys. Rev. Lett. 42, p. 1538 (1981)
[38] P. Devynck et al., Rev. Sci. Instrum. 60(9), p. 2873 (1989)
[39] M. Bacal, Plasma Sources Sc. Technol. 2 pp.190-197,(1993)
[40] L. Friedland et al., Physical Review E. 49, 5, p.4353 (1994)
[41] M. Tanaka et al., Journal of the Physical Society of Japan, 60, p. 1600 (1991)
[42] R. Hidaka, M. Tanaka et al., Journal of the Physical Society of Japan, 32, p. 174 (1992)
[43] M. Tanaka et al., Journal of the Physical Society of Japan, 32, p. 1818 (1993)
[44] N. Hirotsu, M. Tanaka et al., Journal of the Physical Society of Japan, 33, p. 2712 (1994)
[45] E. Alexov et al., Jpn. J. Appl. Phys. 33, p. 2730 (1994)
[46] K. Okhubo and S. Tanaka, Journal of the Phys. Society of Jpn, 36, 2, p. 572 (1974)
[47] K. Okhubo and S. Tanaka, Journal of the Phys. Society of Jpn, 36, 3, p. 843 (1974)
[48] K. Okhubo and S. Tanaka, Journal of the Phys. Society of Jpn, 41, 1, p. 254 (1976)

[49] M. Mozjetchkov et al., Rev. Sci. Instrum. 69 (2), pp.2533-2540 (1998)
[50] Y. Takeiri et al., Rev. Sci. Instrum. 65 (4), p. 1198 (1994)
[51] M. Bacal, C. Michaut, L. Elizarov and F. Balghiti, Rev. Sci. Instrum. 67(3), p.1138 (1996)
[52] O.Fukumasa, J. Phys. D: Appl. Phys. 22 (1989) pp.1668-1679
[53] O.Fukumasa, J. Phys. D: Appl. Phys. 22 (1989) pp.1931-1934
[54] Rabindra N. Ghose, Microwave Circuit Theory and Analysis, McGraw-Hill Book Company, Inc. (1963)
[55] D. M. Kerns, R. W. Beatty, Basic theory of waveguide, Pergamon Press
[56] John C. Slater, Microwave Electronics, D. Van Nostrand Company, Inc. (1950)
[57] Thomas H. Stix, The theory of plasma waves, American Institute of physics, (1992)
[58] B. Lax, W. P. Allis, J. Appl. Phys. 21, p. 1297 (1950)
[59] B. Wieder, Phy. Of Fluids 7 (1964), p.964
[60] J. C. Lee, Int. J. Electronics 26 (1969) p.537
[61] W.P. Allis, et.all., Waves in Anisotropic Plasmas, (M.I.T. Press, 1963) p. 165
[62] K. Ohkubo, S. Tanaka J. Phys. Soc. Japan 36 (1974) p. 843